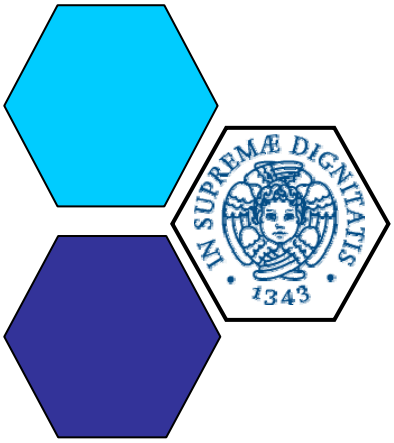

Università di Pisa

Corso di Dottorato di Ricerca in

Ingegneria Meccanica

Development of a Residual Lifetime Prediction Methodology for Creep and Fracture Behaviour of Ferritic-Martensitic Steels using Small-Punch Testing Technique

Allieva:

Ing.Phys. **Darina Todorova BLAGOEVA**

Tutori:

Prof. **Roger C. HURST** - JRC - Institute for Energy, EC

Prof. **Leonardo BERTINI** – D.I.M.N.P., Università di Pisa

Prof. **Marco BEGHINI** – D.I.M.N.P., Università di Pisa

VII Ciclo
Anno 2009

SOMMARIO

Lo scopo principale della tesi consiste nel dimostrare l'applicabilità delle prove di "Small-Punch" (SP) per la stima della vita residua di materiali metallici operanti ad alta temperatura. La mancanza di normalizzazione di questa tecnica e dubbi sulla correlazione dei dati con quelli ottenuti da test di scorrimento viscoso convenzionali, giustifica l'utilizzazione del "Code of Practice for SP Testing" (CEN/WS 21). Il lavoro presente e' in particolare dedicato ad investigare le proprieta' di scorrimento viscoso delle saldature di acciao P91 alla temperatura di 600^{o}C assieme con proprieta' di frattura a basse temperature. Dischi sottili, di 8 mm di diametro e 0.5 mm di spessore, sono stati fabbricati estratti da diverse zone di un componente in P91 contenente una saldatura: metallo base (BM), materiale esposto all'ambiente (SE), saldatura (WM), zone termicamente alterate sia a grana fine che a grana grossa (FG-HAZ & CG-HAZ). I risultati delle misure di scorrimento viscoso sui dischi, ottenuti a 600^{o}C sotto differenti carichi consistentemente secondo il "Code of Practice", si possono correlare con i dati ottenuti attraverso prove standard di scorrimento viscoso. Le misure di SP dimostrano di fornire un metodo solido per descrivere il comportamento di queste leghe e saldature e il modello di scorrimento viscoso derivato, utile per predizione di vita residua, che potrebbe essere anche dimostrato attraverso FEA per la stima delle deformazioni da scorrimento viscoso dei dischi. Addizionalmente, il metodo SP dimostra alto potenziale per la valutazione delle proprieta' di frattura per saldature P91, in particolare per stimare la temperatura di transizione fragile-duttile e la resistenza alla frattura.

ABSTRACT

The main aim of the thesis is to demonstrate the suitability of Small Punch (SP) testing for lifetime prediction of metallic materials operating at high temperatures. The lack of standardisation of this technique and doubts about the correlation of the data with that obtained from conventional creep tests, supports the need to exploit the recently launched Code of Practice for Small Punch Testing (CEN/WS 21). The present work is specifically concerned with investigating the creep behaviour of P91 steel weldments at 600^{o}C along with low-temperature fracture behaviour. Thin discs, 8mm in diameter and 0.5mm thick, were manufactured from different zones of a component containing a P91 welded joint: base metal (BM), service exposed material (SE), weld metal (WM), fine-grain and coarse-grain heat affected zones (FG-HAZ & CG-HAZ). The results of SP creep tests on these disks, performed at 600^{o}C under different loads carefully following the Code of Practice, could be correlated with standard creep data. The SP test is shown to be a reliable method to depict creep behaviour of this alloy and its weldments and a creep model derived, useful for life time prediction, could also be demonstrated through FEA to predict the creep deformation of the SP discs. Additionally, the SP testing method shows potential to evaluate the fracture properties of P91 weldments, in particular the ductile-to-brittle transition temperature and fracture toughness estimations.

Acknowledgments

The author is grateful to Prof. R. HURST from the Joint Research Centre (JRC) - Institute for Energy (IE) EC, Prof. L. BERTINI and Prof. M. BEGHINI from D.I.M.N.P. (Mechanical Department) of the University of Pisa for their fruitful constructive guidance and helpful advice; to Dr. G. DE SANTI , Director of JRC-IE for providing facilities; to Dr. L.DEBARBERIS and Dr. N.TAYLOR from JRC-IE for the collaborative management support; to Prof. P. HAEHNER, Dr. F. Di PERSIO, Dr. E. PAFFUMI from JRC-IE, Dr. Y. LI from KEMA (Netherlands) and Dr. Ph. Tipping from HSK (Switzerland) for their consultative cooperation; and to Dr. F. HUKELMANN, Ph. MINNEBO, R. Ch. RAMOS, J. MENDES, R. VAN DER AAT, S. RIPPLINGER, F. HARSKAMP, R. SMIT, A. PFRANG, E. CONCEICAO and M. WALLENDORF for the good teamwork, collaboration and technical support.

CONTENT

ABREVIATIONS

AC1	Lower Critical Transformation Temperature
AC3	Upper Critical Transformation Temperature
ASME	American Society of Mechanical Engineers
ASTM	American Society for Testing and Materials
BM	Base Metal
BML	Base Metal LICON
BMI	Base Metal INTEGRITY
CT	Compact Tension
CEN	European Committee for Standardization
CG-HAZ	Coarse Grain Heat-Affected-Zone
CWA	CEN Workshop Agreement
CoP	Code of Practice
CVN	Charpy V-Notch
DBTT	Ductile-to-Brittle Transition Temperature
EC	European Commission
ECCC	European Collaborative Creep Committee
EPERC	European Pressure Equipment Research Council
EU	European Union
FATT	Fracture Appearance Transition Temperature
FE	Finite Element
FG-HAZ	Fine Grain Heat-Affected-Zone
F/M	Ferritic/ Martensitic
HAZ	Heat-Affected-Zone
HB/ HV/ HRC	Hardness Brinell/ Vickers/ Rockwell
HTR	High Temperature Reactors
IC-HAZ	Intercritical Heat-Affected-Zone
IE	Institute for Energy
JRC	Joint Research Centre
LSE	Lower-Shelf Energy
LVDT	Linear Variable Differential Transformer

NDT	Non-Destructive Testing
NPP	Nuclear Power Plant
PWHT	Post Weld Heat Treatment
SE	Service Exposed
SEM	Scanning Electron Microscopy
SP	Small Punch
SPC	Small Punch Creep
SPF	Small Punch Fracture
TE	Transition Energy
USE	Upper-Shelf Energy
UWS	University of Wales Swansea
WM	Weld Metal
WMI	Weld Metal INTEGRITY
WML	Weld Metal LICON

NOTATIONS

A	Elongation
E	Young's modulus
ν	Poisson's ratio
σ	Stress
$\sigma_{0.2}$	Yield stress defined at 0.2% plastic strain
UTS	Ultimate tensile strength
δ	Deflection in SPC test
R	Radius of the disc receiving hole
r	Radius of the punch indenter
h_o	Initial disc thickness
h_f	Final disc thickness
t	Thickness of the gauge-block
$\dot{\varepsilon}_s$	Creep strain rate
$\dot{\delta}_s$	Creep deflection rate
t_r	Time to rupture
k_{SP}	Ductility factor

M	Monkman-Grant constant
n	Stress exponent in the uniaxial creep test
n*	Force exponent in the SP creep test
$\Psi = n/n^*$	Stress/ force exp ratio
p	Time exponent in uniaxial test
p^*	Time exponent in SP test
$\Phi = p/p^*$	Time exp ratio
ε_{pl}	Plastic strain
J_{IC} (K_{IC})	Fracture toughness
E^{SP}	SP fracture energy
ε_f (ε_{qf})	Fracture strain
u_m	Maximum deflection (displacement) in SPF test
u^*	Displacement at fracture in SPF test
F_m	Maximum force in SPF test
σ_f^{SP}	Fracture stress in SPF test
T_{SP}	DBTT measured by SPF test
k, J_o, C	Empirically determined constants

1. INTRODUCTION

There is an increasing worldwide demand in the power-generation, metals and chemical process industries for efficiency improvements, together with safe, economic and reliable operation, and this forms the primary focus in today's rapidly evolving energy market. As a consequence, in the last two decades, there was a need for the service pressure and temperature of components for advanced power plants to be increased significantly and more severe requirements on strength, corrosion resistance and creep properties were imposed on high temperature steels. Such higher working temperatures and pressures allow increased thermal efficiency thereby lowering fuel consumption and environmental impact. Unfortunately elevated operating temperatures and pressures tend to accelerate material degradation of the working components.

During the exploitation period a number of degradation mechanisms such as temper embrittlement, creep, hydrogen attack and hydrogen embrittlement can impair plant integrity. The damage subsequently may lead to initiation and propagation of defects into cracks and eventual failure. Creep is a common degradation mechanism when high temperatures are employed, e.g. HTR (high temperature reactors), boilers, piping, steam generators, gas turbine engines, oil refineries and petrochemical plants. All these systems possess some components that will experience creep. An understanding of high temperature materials behaviour is beneficial in mitigating failures in these types of systems.

Many industries are faced with an increasing array of ageing plant and equipment, in many cases close to or even beyond original design life. The capacity, efficiency and safety of plants depend critically on the integrity of the components and materials employed. Thus, it is crucial to evaluate the degradation processes due to long-term service exposure with higher accuracy in order to ensure integrity of the power plants and further to extend their life. Possibility of failure and remanent life-time assessments are critical issues in the safety analysis of the current industrial plants. Besides the safety, another important aspect is the economical advisability to extend the life time of the existing components beyond their design life rather than to build new plants. This requires increasing innovation in material testing and research to provide improved remaining life analysis.

Initially the design life was based on some empirical assumptions and experience in materials and technologies developments, implementing an appropriate safety factor. As a generality, the design of plant components and safety performance assessment of materials used for high temperature applications in the power generation, nuclear, petrochemical, chemical process and other such industries is currently based on their tensile and creep rupture strength. Service experience has shown that the present design codes are very conservative. The conservatism in the design, the use of more sophisticated procedures/codes and careful husbandry of components may reduce the safety factor while maintaining safety and frequently allows life to be extended beyond that originally intended.

At the same time however, the question concerning the uncertainty in the evaluation and monitoring of the residual life of plant components is of great importance for the industry. Some uncertainty comes from using the nominal properties of the materials instead of their residual mechanical properties, due to lack of enough experience and knowledge. The historical recording of use is the basis for reliable assessment of the remaining value and reuse possibilities of technical equipment and tools. In addition, residual lifetime prognosis helps to fix guarantee terms for reused components. Obtaining information on the mechanical condition of service exposed components however can be problematic because of the need to sample significant quantities of material for testing direct from the component. The traditional destructive testing methods require large specimens that would violate the structural integrity of the working components.

The shortage of enough material to be sampled non-invasively rarely permits material evaluation by conventional and well standardised test techniques. In this case Non-Destructive Testing (NDT) is applicable in order to identify damage and irregularities in materials. NDT often provides the only method of obtaining information about the current 'health' of process plant. To address this problem, various non-destructive or miniaturised specimen innovative testing techniques have been developed over the past two decades.

The small punch (SP) technique is considered an almost non-destructive technique, requiring a small amount of material, easy to carry out and relatively inexpensive. The SP method, proposed by Manahan et al. [1], enjoys an increasing interest lately and can be applied for studies of creep [37, 38, 191] and fracture properties [174], as well as fatigue, ageing embrittlement, hydrogen embrittlement [213] and irradiation damage [104]. The small specimen size of this test technique – discs of 0.3-1mm thickness and 5-10mm diameter, can eliminate the need for large amount of material removal, while at the same time permitting measurement of properties in key local areas of components.

Beyond the considerable success and promising results, however, there is no doubt that technical limitations still exist for the SP technology. Such limitations are the reduced specimen size, and thereby potential oxidation effects, and how non-representativeness of the sampled material could influence the test results to a much stronger extent than is the case for conventional creep testing. The ability of the “small-scale” tests to reproduce data from full sized specimens and their range of applicability is still open for discussion. These aspects remain a concern and much work needs to be done in order to convince industry to have the necessary trust to heed the results of such testing. In spite of this, interest in the technique is on the increase and an effort for possible wide adoption by industry is timely. The late efforts on standardisation and some doubts about the correlation of the data with that obtained from conventional creep tests, provide strong arguments for further investigations in this direction.

A ferritic-martensitic steel 9Cr-1Mo, standardized as Grade P91 in ASTM in the early 80’s, and its weldments have been investigated in the thesis. Because of the excellent creep rupture strength values of this steel it is used worldwide by many engineering companies, boiler builders, piping companies and utilities. P91 steel is

a candidate material for Generation IV nuclear power plants (in-core and out-of-core applications), as well as for fusion applications. Thin discs, 8mm in diameter and 0.5mm thick, produced from different zones of a full repair weld between P91 fresh and P91 service exposed material, were tested following the Small Punch Testing Code of Practice for creep and fracture properties evaluation. All tests were performed following tightly the guidelines given in the Code of Practice (CoP) for SP testing or CEN Workshop Agreement CWA 15627 [2], published in December 2006.

Why is this work timely and topical?

- Several authors published results on the SP creep testing of P91 base metal. However, the accumulated results are not sufficient and most of them are based on accelerated short-term test that could be a source of discrepancy and inaccuracy. Moreover, mainly empirical correlations between the SP results and those obtained by conventional creep tests were developed. The thesis proposes a linear relationship between the stress [MPa] applied in the conventional uniaxial creep test and the load [N] applied in the SP method; thus, offering a direct correlations between the SP creep results and the conventional creep results over an extended test duration (up to approximately 4300h).

- Very limited data are reported in the literature on SP creep testing of P91 weldment material, particularly the coarse- and fine-grain heat-affected-zone, known to be the most critical zone in the weldment. The research conducted compares the SP creep strength values obtained from homogeneous HAZ material with the creep strengths of the other zones of the weldment: BM, WM and SE material.

- Variety of specimen geometries and testing equipment is used by different researchers for SP creep testing. The work conducted here tends to unify the results acquired from different equipments, particularly the puncher radius, the radius of the receiving hole where the disc lies, and the sample thickness, by comparing the thesis results with results obtained by other authors. All these quantities participate in the relationship establishing the stress/load ratio, proposed in the CoP. Additionally this relationship takes into account also the ductility of the material, which turns out to be an important issue when a broader stress interval is applied. In this sense, the stress/load relationship has not only a purely empirical, based on testing geometry, but also a physical meaning depending on the material itself and the testing condition. Hence, the study is also to support the published CoP for the SP testing.

- Published results on low temperature SP testing used for fracture properties evaluation, particularly the ductile-to-brittle transition temperature and fracture toughness, are incomplete or simply missing. Although it was not the main subject of the thesis, an important progress has been achieved in conducting SP fracture tests over a wide

temperature range, down to cryogenic temperatures, establishing correlations between the SP data and the data obtained by conventional Charpy and fracture toughness test and, as well as, recommendations for future work in this direction.

In conclusion, the present thesis tends to prove that the SP testing methodology can be a promising method for the evaluation of creep properties and that in future it might be used as “stand alone” method giving the opportunity for creep strength measurements, especially for very small areas of the components where using conventional creep samples is not an option.
As far as the fracture properties are concerned, it could be said that the thesis provides preliminary but pioneering results in this research sphere, which can be used as a basis for future investigations.

2. LITERATURE REVIEW

The literature review introduced below, aims to provide a comprehensive background to the subject treated in this thesis work, namely: applicability of the Small Punch testing methodology for predicting the long-term creep-rupture behaviour of advanced ferritic/martensitic (F/M) steel, in particular P91 steel. Reference to the current industrial needs and future requirements, especially with regards to the high temperature production processes, will be made in the present review. An overview on the life time assessment techniques and creep damage from a physical point of view, as well as the evolution of the ferritic/martensitic steels for high temperature applications will follow. Finally an introduction to the state of the art of the Small Punch testing technique and its potential as a reliable non-destructive integrity assessment method will be presented and objectives of the current study will be formulated.

2.1 Creep damage: An industrial problem

There is an increasing worldwide demand in the power-generation, aircraft, metals and chemical process industries for improvements in the efficiency, utilisation and longevity of high-temperature components, which may be subjected to creep, fatigue and creep-fatigue loading and environmental attack, leading to the degradation of their material properties over an extended period of time. Improvement of the thermal efficiency of power generation Plants is an important issue from the viewpoint of energy saving, environmental conservation (carbon dioxide emissions) and economy. This can be achieved by elevating operating temperatures and pressures, which would however accelerate material degradation of high-temperature components. It is crucial to evaluate their degradation due to long-term service exposure with higher accuracy to ensure integrity of the power plants and further to extend their life.

Creep and stress rupture is one of the root cause failure mechanisms for industries associated with high temperature operations such as HTR (high temperature reactors), boilers, piping, steam generators, gas turbine engines, oil refineries and petrochemical plants. All these systems possess components that experience creep.
An understanding of high temperature materials behaviour is beneficial in evaluating failures in these types of systems. The damage subsequently leads to initiation and propagation of defects into cracking and eventual failure. Failure of a component indicates it has become completely or partially unusable or has deteriorated to the point that it is not dependable or unsafe for normal sustained service which could then lead to unwanted damages in terms of human life and economics. Low failure rates of components, vehicles, plants, and any technical object are highly important for human lives, environment and capital invested. At the same time, strong international competition compels the reduction of life-cycle costs of products.
In order to reduce the down time and increase the overall efficiency of the plant, it is essential to look into the mechanics of failure and its after effect on the life to failure. Though a well-planned maintenance programme can prevent catastrophic

failures there is still considerable interest in the development of techniques for assessing the remanent life of critical components.
Nowadays, the European Commission together with other representatives of the universities, industry and research and technology organizations are putting more and more efforts in developing unified European Codes treating component design and plant integrity assessments. Developing of one such Code of Practice [2] for plant integrity assessment using small punch creep testing requires high level technical input but once it is developed and becomes standardised and routine, it is economically worthwhile. This emerging technology is to be promoted by standardisation in order to become a widespread tool for a variety of industrial equipment owner/operators and maintenance and integrity assessment service providers that presently have the problem of choosing between complex expensive techniques, or inexpensive yet poor NDT methods in routine work.

2.2 Creep

2.2.1 An introduction to creep

Creep is the term given to the material deformation that occurs as a result of long term exposure to levels of stress even below the yield strength. The rate of this damage is a function of the material properties and the exposure time, exposure temperature and the applied load (stress). Depending on the magnitude of the applied stress and its duration, the deformation may become so large that a component can no longer perform its function.

The evaluation of creep behaviour is one of the most important factors to assess the integrity of elevated temperature structural components. Creep is usually a concern to engineers and metallurgists when evaluating components that operate under high stresses and/or temperatures. Creep is not necessarily a failure mode, but is instead a damage mechanism. Rather than failing suddenly with a fracture, the material permanently strains over a longer period of time until it has to be replaced or finally fails. Creep does not happen upon sudden loading but the accumulation of creep strain in longer times causes deterioration of the material. This makes creep deformation a "time-dependent" deformation of the material.
Creep deformation can be obtained in rather rapid time frames under very high temperatures, i.e. temperatures around half of the melting temperature. Plastics and low-melting-temperature metals may creep at room temperature (cold flow), and virtually any material will creep upon approaching its melting temperature. Since the relevant temperature is relative to melting point, creep can be seen at relatively low temperatures depending upon the alloy. This deformation behaviour is important in systems for which high temperatures are endured, such as conventional and nuclear power plants, jet engines, heat exchangers etc.

2.2.2 Stages of creep

The test techniques which serve to evaluate the creep properties of materials generally are based on uniaxial test loading parallel to the longitudinal axis of a cylindrical or plate specimen. The basic parameters recorded are the dependence of the creep strain ε (or rather extension) versus time. The load is constant and it is applied to a tensile specimen maintained at a constant temperature. Strain is then

measured over a period of time. Experimental studies of creep behaviour have produced strain-time curves exhibiting four characteristic segments, as illustrated schematically in Figure 2.1.

- Instantaneous strain due to loading, ε_o
- Primary or transient creep - stage I – deformation takes place and the resistance to creep increases until stage II - decreasing strain rate to a steady state level.
- Secondary or steady-state creep - stage II - it is this regime that is most well understood. The "creep strain rate" is typically the rate in this secondary stage. The stress dependence of this rate depends on the creep mechanism.
- Tertiary creep - stage III - occurs when there is a reduction in cross-sectional area due to necking or effective reduction in area due to internal void formation. The tertiary stage onset is marked by exponential increase in the strain rate ultimately leading to rupture.

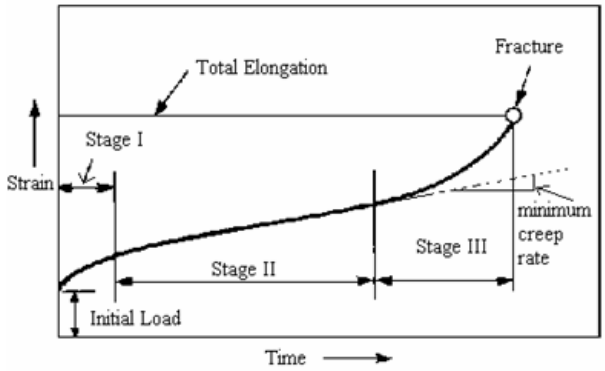

Fig.2.1 Schematic representation of a creep curve

2.2.3 Mechanisms of Creep Deformation

There are several different creep regimes, depending mainly on the temperature, where different mechanisms are applied. The temperatures between which creep deformation mechanisms are operating are usually expressed as a fraction of the melting temperature T_M, expressed in degrees absolute. The different regimes roughly cover the temperature ranges 0-0.5 T_M, 0.5-0.9 T_M, and 0.9-1.0 T_M:

- Lower range creep regime: $T < 0.5\ T_M$

It includes the so-called "*logarithmic creep*" so named due to the nature of the equation describing the creep strain accumulated at low temperatures [3].

$$\varepsilon = \alpha_1 \log_e(\alpha_2 t+1) \qquad (2.1)$$

where α_1 and α_2 are constants and t is time.

- Upper range creep regime: $T > 0.9\ T_M$

In this high temperature range the factor controlling the creep rate is mainly linked to diffusional flow of vacancies. Creep by diffusion of vacancies (*diffusion creep*) is somewhat similar to flow in liquids. Vacancies are point defects, and they tend to

favour grain boundaries that are normal, rather than parallel, to the applied stress Vacancies tend to move from regions of high to low concentrations.
Diffusional flow can occur at low stresses but, usually, it requires high temperatures. In this temperature range and at stresses too low for dislocation processes to be significant, a mechanism known as Nabbaro-Herring creep operates [4].

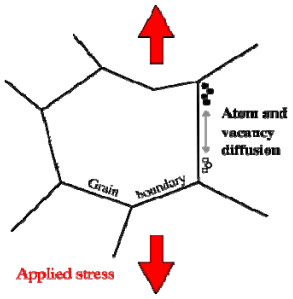

Nabarro-Herring (N-H) creep is a process by which dimensional changes of the material are caused by atom-vacancies or defects exchange through the lattice. This form of creep is also known as bulk diffusion.
However, vacancy diffusion involving stress directed vacancy flow through the grain matrix and along preferred paths, such as grain boundaries, has also been reported at lower temperatures and is known as Coble creep (Figure 2.2).

Fig.2.2 Diffusional creep

- Intermediate range creep regime: 0.5 Tm <T< 0.9 Tm

This is the temperature range in which most engineering materials operate and in which creep may cause concern to the engineers. At high stresses creep is controlled by the movement of dislocations. This is the so called *"dislocation creep*". Dislocations are line defects. They may move in a conservative fashion, retaining their length, or they move in a non-conservative fashion - increasing their length through atomic diffusion. The former process is known as 'glide'. Typically dislocation glide is opposed by obstacles – other dislocations, solute atoms or precipitates, grain boundaries, etc. The later process is known as 'climb' (Figure 2.3).

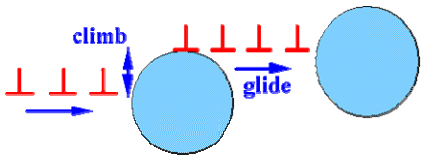

Fig.2.3 Dislocation creep

The different creep deformation mechanisms can combine. A Deformation Mechanism Map is schematically presented in Figure 2.4.

Grain boundary sliding is sometimes considered as a separate mechanism which also contributes to the creep deformation.

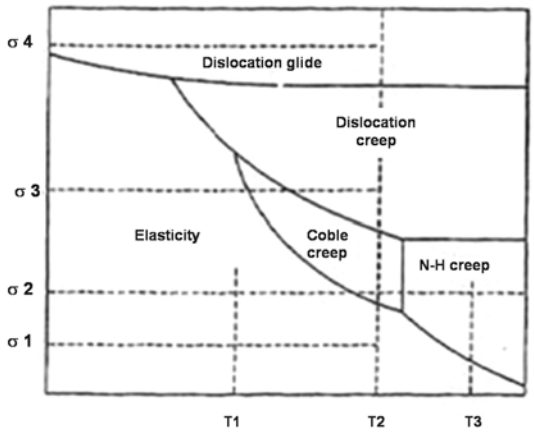

Fig.2.4 Deformation mechanisms map

2.2.4 Power law approach

The creep at intermediate temperatures is often explained in the literature as a process, involving competing strain hardening and thermal recovery processes, commonly known as "recovery creep". In the recovery creep theory, the steady state creep is assumed to be a major part of the plastic creep deformation process and $\dot{\varepsilon}_s = d\varepsilon/dt$ value is used to describe the curve as a whole and can be calculated from the slope of the secondary stage in the time-strain creep curve (Figure 2.1). The onset of the secondary creep stage is characterised by thermally driven dislocation annihilation processes, which initiate the effects of strain hardening. Permanent plastic strain rate is reached at the point of equilibrium between these two processes.

Temperature, together with the stress, are fundamental factors influencing material deformation under creep conditions. The steady state creep rate can be expressed as:

$$\dot{\varepsilon}_s = f(\sigma,T) \qquad (2.2)$$

This can be rewritten as

$$\dot{\varepsilon}_s = u(\sigma).v(T) \qquad (2.3)$$

where u(σ) describes the variation of έs with stress at constant temperature and v(T) describes the variation of $\acute{\varepsilon}_s$ with temperature at constant stress. Thus, the stress dependence of the secondary creep rate at intermediate stresses and at the same temperature can be expressed in terms of a power law:

$$\dot{\varepsilon}_s \propto \sigma^n \qquad (2.4)$$

where “n” is a stress exponent, obtained from plotting “log σ” against “log $\acute{\varepsilon}_s$”.
This is often called "Norton's Law". Values of “n” in the intermediate stress range can be ~ 4-5 for a pure metal and between 5 and 40 for more complex materials [5,6].

The temperature dependence is no surprise, since it is quite clear that creep is a thermally activated phenomenon and variation of $\dot{\varepsilon}_s$ with temperature at the same level of stress can be expressed in terms of an Arhenius rate type equation. The Arhenius model predicts failure acceleration due to temperature increase. This empirically based model takes the form:

$$\dot{\varepsilon}_s \propto -(Q_c/RT) \quad (2.5)$$

where Q_c is the activation energy for creep and R is the gas constant (= 8.314 J/mol K). For pure metals and single phase alloys Q_c is approximately equal to the activation energy for self diffusion. In more complex polycrystals and alloys, Q_c values twice that of self diffusion activation energy values have been reported [7,8]. These equations can be combined to give a simple power law approach applicable at temperatures and stresses to be found in common engineering applications.

$$\dot{\varepsilon}_s = A\sigma^n \exp -(Q_c/RT) \quad (2.6)$$

where A is a constant and T denotes the temperature measured in degrees Kelvin (273.16 + degrees Celsius) at the point when the failure process takes place.

The rupture time is inversely proportional to the creep rate:

$$t_r \ (\propto 1/\dot{\varepsilon}_s) = A'\sigma^{-n}\exp(Q_c/RT) \quad (2.7)$$

2.2.5 Mechanisms of creep fracture

As it was discussed above, at high temperatures, the application of a stress leads to a creep deformation resulting from:

- Motion of dislocations (dislocation creep);
- Mass transport by diffusion (diffusion creep) - dominant at lower stress levels; or
- Grain-boundary sliding process.

These processes in turn lead to a distribution of internal stresses that may relax on removal of the stress. In the metals it is associated with the un-bowing of pinned dislocations, rearrangement of dislocation networks, and local grain-boundary motion.

Creep rupture can be considered as a consequence of the following process:

- Damage accumulates in form of internal voids (cavity nucleation);
- Voids appear on grain boundaries normal to the tensile stress;
- Atoms diffuse from the void surfaces into grain boundaries and voids grow (formation and growth of stable cavities);
- Voids grow faster and faster, until they link, leading to creep fracture (initialization of discrete cracks).

2.2.5.1 Cavity nucleation

When a metal is loaded to a stress level below the yield stress, it undergoes immediate elastic deformation but, initially, does not deform plastically because the dislocations in the metal are pinned by a variety of obstacles. The obstacles include dislocation pile-ups, grain boundaries, precipitates, twin boundaries, alloy and impurity atoms and other microstructural defects in the metal lattice. Further, the metal may make plastic adjustments by dislocation motion in regions of stress

concentrations and high interstitial concentrations (stage 2). These regions include grain boundaries, the metal adjacent to inclusions, precipitates and second phase particles and lattice regions near microscopic cracks and notches.
During tertiary creep (stage 3), damage accumulates in the form of internal voids on grain boundaries normal to the tensile stress. Atoms diffuse from void surface into grain boundaries, and voids grow at an increasing rate inside the material until they link, leading to creep fracture (Figure 2.5).

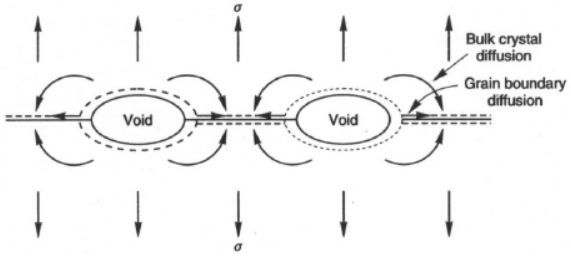

Fig.2.5 Diagram showing voids growing and coalescence

2.2.5.2 Cavity growth

Early concepts of cavity growth and development were proposed at the beginning of the 90s [9,10]. Although these models are now known to be inaccurate, they highlighted the early need for models of cavity behaviour. Initial models of cavity growth based on the continued sliding of grain boundaries were not popular as they predict that the cavity shape will be irregular. Work on creep cavity growth has shown cavities to be rounded or ellipsoidal in appearance, which suggests that diffusion processes contribute to cavity growth [11].
Numerous theories have proposed that cavities on boundaries experiencing a tensile stress may grow by the direct absorption of vacancies generated in a similar manner to diffusional creep [12-14].
Early work by Hull and Rimmer [12] showed that the activation energy for grain boundary diffusion was half that of the activation energy for lattice self diffusion. This was considered evidence for diffusion mechanisms occurring in cavity growth. They concluded that grain boundary cavity growth was due to the diffusion of surface atoms to the surrounding grain boundaries under the action of an applied stress. This Hull and Rimmer model was refined by other workers who found that the finite diffusion rate of the atoms at a cavity tip was no longer sufficient to maintain a rounded cavity if the stress levels, and thus deformation rates, were sufficiently high. Thus, while diffusional growth models may be applicable at low stresses, the broad based acceptance of diffusion models has now lessened.
Current models are based on the generally accepted premise that creep cavity growth is controlled by the creep rate. Models range from cavity growth associated with localized deformation in grain boundary regions [15] to those assuming growth by vacancy absorption but with the growth rate constrained by the deformation rate in the surrounding material [16,17]. This constrained cavity growth model depends on the fact that the ability of a grain boundary to cavitate not only relies on its orientation to the tensile axis but also on the properties of the boundary itself i.e. low or high-angle boundaries. Thus, cavitation may occur on a boundary but the adjacent boundaries may be undamaged, surrounding the grain with a 'shell' of un-

cavitated boundaries [18,19]. Now the voids can only grow on cavitated boundaries at a rate governed by the creep rate of the surrounding grains [20-22].
It is also possible to link the deformation rate of a material to the growth of creep cavities. Within the material, a dislocation moving along its glide plane is stopped when it reaches a grain boundary which doesn't contain its glide plane. If the applied stress is maintained, the dislocation can continue moving by a combination of glide and climb. The resulting non-conservative climb events emit vacancies. The role of these emissions will depend on the normal stress causing climb as well as the shear stress causing sliding. The result of an injection of vacancies at the grain boundary is that the cavity opens and grows. The dislocation also may have crossed the grain interior by a glide mechanism, thus contributing to the grain deformation as it went. It can be seen from these processes that the arrival of dislocations from the lattice to the grain boundary can govern the processes involved in cavity growth. Thus the growth of cavities can be linked to the deformation rate of the material instead of diffusional processes. The motion of dislocations within the lattice as seen in creep controlled mechanisms can be used to explain the dependence of rupture life on creep rate, known as the “Monkman-Grant relationship” [23].

$$M = \acute{\varepsilon}_s.t_f \tag{2.8}$$

where M is a constant.

It is generally agreed that the creep fracture of low alloy Cr-Mo steels is the result of grain boundary cavity and inter-granular crack formation, and this has been shown over a wide range of testing conditions [24-27].
However controversy exists as to when in the creep life of a two phase alloy the creep cavities contribute to the acceleration of the creep rate. Some workers have reported the formation of cavities during the initial stages of creep [28], while others have claimed an incubation or threshold for cavity nucleation [28, 29] and that the time at which cavities first appear can be at any stage during the secondary or tertiary creep regimes. Other more recent work [24] on low alloy steel has found intergranular cavities to be absent during secondary creep, except in regions near the specimen surface. This effect was clearly visible in large specimen where it could be distinguished from general cavitation. Further evidence from ex-service low alloy components has shown creep cavitation damage of the type which has led to service failure to develop only late in the service life under service conditions [30, 31].

Work by Cane on low alloy steels [25,32] performing tests with failure lives of ~1000 hours showed that failure occurred as a result of high localised strains in the vicinity of carbide particles. This work was later expanded to conclude that the nucleation of these creep cavities occurred mainly at grain boundary particles, specifically sulphides and that the carbides remained coherent [24,30].
Failure can occur by one of two mechanisms, first proposed by McLean [33], depending on the applied stress. At low stress levels, the fracture is due to inter-granular cavitation linkage. At higher stresses, the stress level is high enough to produce stress concentrations and so initiate triple point cracking. This change in mechanism was reported by Cane to be linked to a change in rupture mode from a low ductility 'brittle' inter-granular form at low stress to high ductility failure at high stresses involving considerable plasticity of the matrix material [26]. This work

would seem to be supported by the findings of Parker and Wilshire who observed mechanical instability and necking in high stress creep tests on low alloy steels [24].

2.2.5.3 Initialisation of discrete cracks

The development of wedge type cracks and cavity nuclei during creep is illustrated in Figure 2.6. Wedge or triple point cracking is the result of sliding on grain boundaries experiencing shear stresses which lead to a stress concentration sufficient to develop cracks on the boundary normal to the tensile axis (Figure 2.6(a)). A minimum applied stress is required to initiate the triple point crack. Thus this cracking mode is only observed at relatively high stresses.

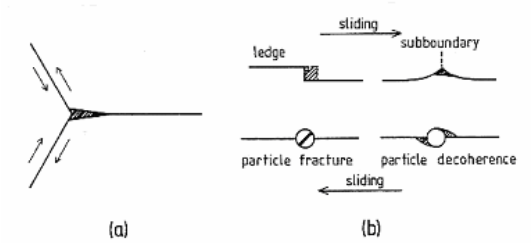

Fig.2.6 Diagram illustrating the development of: a) Wedge cracks; and (b) Four types of cavity nucleation

The nucleation of cavities at lower stresses is generally agreed to be as a result of grain boundary sliding being impeded by a range of grain boundary irregularities (Figure 2.6(b)):

- The interaction of a slip band with a grain boundary- sliding then produces a ledge;
- The interaction of a sub-grain with a grain boundary- sliding then produces a cusp;
- Particle fracture or de-coherence of particles sat on grain boundaries.

2.3 Ferritic / Martensitic (F/M) steels for elevated temperature applications

In the last two decades the service pressure and temperature of components for advanced power plants increased significantly and more severe requirements on strength, corrosion resistance and creep properties were imposed on high temperature steels. These are the factors that typically determine the thermal efficiency of the unit. Higher working temperatures allow increased thermal efficiency that lowers the fuel consumption and environmental impact [34]. Thus, an important aspect in current energy production is to find a compromise between the most economical and environmentally friendly solutions to keep plants competitive in the market. To comply with the requirements for improved efficiency for operation up to 650°C and higher steam pressures than used in the past and reduced CO_2 emission, the classical materials must be replaced by the new high-Cr progressive creep resistant steels, whose development and verification are still ongoing [35-44]. These materials are predominantly martensitic, with varying amounts of retained delta-ferrite. Materials with F/M microstructures are preferred

because of their favourable physical properties such as good thermal conductivity and low coefficient of thermal expansion coupled with higher resistance to thermal shock. These are some of the advantages over austenitic stainless steels. For these reasons there has been a great demand for high strength and heat resistant chromium ferritic and F/M steels which has resulted in the development and application of several variants.
The difference in the mechanical properties of different steels: martensitic and F/M, ferritic, ferritic-austenitic, austenitic; is perhaps seen most clearly in the stress-strain; tensile & creep strength curves below (Figure 2.7):

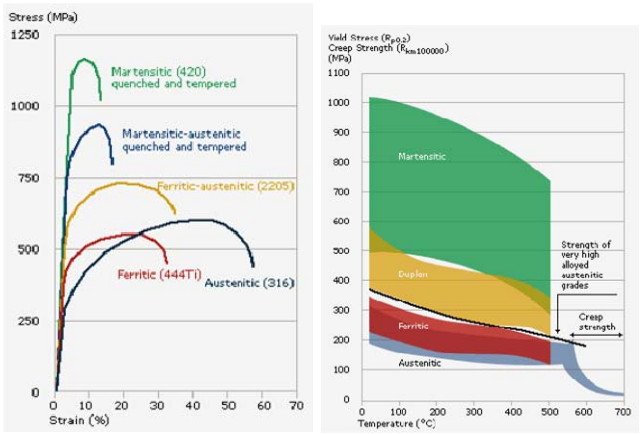

Fig.2.7 Stress-strain curves, tensile & creep strength curves for various steel grades

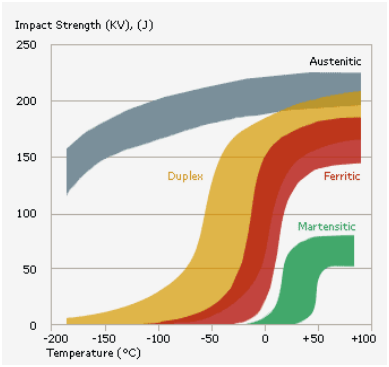

The toughness of the different types of stainless steels shows considerable variation, ranging from excellent toughness at all temperatures for austenitic steels to the relatively brittle behaviour of martensitic steels (Figure 2.8). Toughness is dependent on temperature and generally improves with increasing temperatures. Martensitic, ferritic and ferritic-austenitic steels are characterised by a transition in toughness, from tough to brittle behaviour, at a certain temperature, the transition temperature.

Fig. 2.8 Fracture toughness curves for various steel grades

2.3.1 Power Generation Industry applications

The first Cr-Mo steels were used for conventional power-generation applications in the 1920s. The 2¼Cr-1Mo designated by ASTM as Grade 22, was introduced in the 1940s and is still widely used today. Along with Grade 22, 9Cr-1Mo (T9) was in early development - the additional chromium added for corrosion resistance. Since then, there has been a continual push to increase operating temperatures of conventional fossil-fired power-generation systems. This led to the development of

several “generations” of steels with improved elevated-temperature strengths (Table 2.1). The evolution of steel compositions, which began with T22 and T9 (zeroth generation) with 100,000 h creep-rupture strengths at 600ºC of about 40 MPa, has allowed for increased operating steam temperatures and pressures [45-48].
Three generations of steels have been introduced since the introduction of T22 and T9, and a fourth generation is in the development stage. Steels beyond the zeroth generation contained mainly 9–12% Cr for improved corrosion and oxidation resistance for elevated temperature operating conditions.
The first generation, in addition to increased chromium, involved primarily the addition of the carbide formers vanadium and niobium to T22 and T9 compositions to add precipitate strengthening. In some cases, a small tungsten addition was made for further solid solution strengthening, in addition to that provided by molybdenum. These steels, introduced in the 1960s for applications to 565ºC, included 2¼Cr-1MoV, HT9, HT91, and EM12. These steels allowed to increase the 10^5 h rupture strengths at 600ºC up to 60 MPa.

Generation	Years	Steel Modification	10^5 h Rupture Strength, 600°C (MPa)	Steels	Max Use Temperature (°C)
0	1940-60		40	T22, T9	520-538
1	1960-70	Addition of Mo, Nb, V to Simple Cr-Mo steels	60	EM12, HCM9M, HT9, HT91	565
2	1970-85	Optimization of C, Nb,V, N	100	HCM12, T91, HCM2S	593
3	1985-95	Partial Substitution of W for Mo and Add Cu, N, B	140	NF616, E911, HCM12A	620
4	Future	Increase W and Add Co	180	NF12, SAVE12	650

Table 2.1 Evolution of F/M Steels for Power-Generation Industry

For the second generation, developed in 1970–1985, carbon, niobium, and vanadium were optimized, nitrogen was added, and the maximum operating temperature increased to 593ºC. The new steels included modified 9Cr-1Mo grade P91/T91 and HCM12, which has a duplex structure (tempered martensite and δ-ferrite). These steels have 10^5 h rupture strengths at 600ºC of about 100 MPa. Of these latter steels, P91/T91 has been used most extensively in the power-generation industry throughout the world [45-48].
The third generation of steels was developed based on the previous generation, primarily by the substitution of tungsten for some of the molybdenum, although boron and nitrogen were also utilized. They were developed and introduced in the 1990s for 620ºC operation with 10^5 h creep rupture strengths at 600ºC of 140 MPa.
Finally, the next generation of steels is being developed at present, where the intention is to push operating temperatures to 650ºC. These fourth-generation steels, SAVE12 and NF12, differ from the previous generation primarily by the use of up to 3% cobalt; they have projected 10^5 h creep-rupture strengths at 600ºC of 180 MPa [45-48].

2.3.2 Nuclear applications

The expected increasing world-wide demand for energy in the XXIst century has spurred international cooperation to consider ways to meet energy needs while maintaining and improving the environment. This has led naturally to nuclear energy, since it can be produced without the environmental effects that accompany the use of coal or petroleum products. Although renewable energy sources offer the possibility of clean energy, there are concerns about economic efficiency and reliability, whereas the economic reliability of nuclear energy has been demonstrated by the reactors operating today. Rather than relying on the present generation of reactors, an international collaboration is directed toward developing a new generation (Generation IV) of reactors that will produce abundant, reliable and inexpensive energy. For several Gen IV reactors concepts, because of the high temperatures envisioned (up to 650ºC and higher), F/M steels are contemplated as possible structural and/or cladding materials. The primary emphasis is on the high-chromium (9–12% Cr) steels.

Although there are uncertainties concerning the long-time stability and creep properties of the third and fourth generation of the 9–12% Cr Martensitic steels, there appears to be no question that there are significant improvements over the first- and second-generation steels, at least for ≈100,000 h based on present experimental data from which lifetimes are extrapolated. Given the increased operating temperatures of the new reactor designs, steels with increased elevated-temperature strength will be required if the advantages of F/M steels are to be available to the reactor designer. It should be noted that for some in-core applications (e.g. cladding) the service lifetimes are very much less than the ≈300,000h envisioned for conventional power plants.

2.4 P91 steel

The modified 9Cr-1Mo steel was chosen for the thesis. This steel generally costs less than austenitic alloys so the economic incentive to use this material can be significant depending on the specific application. The enhanced properties like lower thermal expansion coefficient, higher thermal conductivity, and improved oxidation resistance at intermediate temperatures, would enable steam-plant components to be manufactured with thinner walls, thus they would minimize thermally induced stresses. With the addition of niobium, vanadium, and nitrogen, the “standard” 9Cr-1Mo also exhibited a substantial increase in creep-rupture strength, compared to traditional steels, thus giving birth to the known today “modified” 9Cr-1Mo – Grade T91 for tubing and Grade P91 for headers and piping. Modified 9Cr-1Mo containing niobium and vanadium, was developed in the USA [49] and standardized as T/P91 in ASTM in the early 80s. The advantages of this material have been recognized in many countries by engineering companies, boiler builders, piping companies and utilities with the result that grade 91 is being installed in many power stations worldwide. P91 steel is a candidate material for Generation IV nuclear power plants (in-core and out-of-core applications), as well as for fusion applications. The excellent creep rupture strength values allow the optimum use of this material in the temperature range from 540^{o}C to 600^{o}C.

Compared with the conventional material (T/P22) considerable wall thickness and weight reductions are possible and have been realized in many cases.
The creep properties of 9% Cr steels have been widely investigated in Europe, USA and Japan by very long tests in the range 550-650^{o}C [50]. However, P91 steel has been in use, in a limited number of plants, since the late 80s /early 90s, and that although the steam temperatures in most of these older units were between 540 - 565°C (below the maximum design temperature of 600^{o}C for this steel), there have been some disturbing reports about P91 failures [51]. These failures are a matter of concern especially because they occurred at lower temperatures than the maximum design temperature of 600°C for such steels and the present operating temperature of up to 590°C in some of the new higher efficiency European and Japanese plant where 9Cr martensitic steels have been introduced more recently [51-55].
The grade 91 material can also be used with substantial technical and economical advantages in the case of refurbishment of old piping systems by the new material. By the end of this decade, hundreds of power plants will be built or refurbished. Whether old or new, much of the pipe that carries the high-pressure steam to the turbines is now made from a newer alloy. This newer grade, 9Cr-1Mo (P91) steel, offers a much better strength-to-weight ratio than "the old standby" P22 steel.

2.5 Microstructural evolution of P91 steel and its weldments

For the long term application of the new steels, it is necessary to evaluate the microstructure changes that are likely to occur during service and to assess the effect of such changes on the high-temperature creep behaviour. Evaluation of the microstructural changes in service exposed material is fundamental for a correct characterisation of material condition and predicting the service extension terms. For ferritic steels the main aspects of the microstructural evolution relevant to the creep exposure period are:

- Microstructural phase evolution;
- Formation of microvoids at grain boundaries;
- Carbide evolution;
- Interparticle spacing.

The phase evolution aspect is related mainly to the temperature effect and not so strictly connected to the load application. It can be expressed as: tendency to martensite spheroidization; coarsening of precipitates in the ferritic matrix and at grain boundaries; and broadening of denuded zones (no precipitates) along grain boundaries [56]. Formation of micro-voids at grain boundaries is based on the fact that creep damage mechanisms are related to the appearance of cavities some time before the rupture occurs. These cavities gradually form micro-cracks by interlinkage that leads to rupture initiation. The size and density of the cavities increase as creep progresses from secondary to tertiary. Material type also influences the cavities' size significantly, however it is in the microns range – the reason they are called "micro-voids" or "micro-cavities".
Many studies have been carried out on the evolution of carbides present in the steels during creep exposure. Separation and coarsening of carbides is in general an index of material degradation due to damage progress. Presence of different classes of carbides in steel is related to the global composition and thermal

process applied in manufacturing. Some studies [57] revealed the possibility to establish a correlation between carbide composition and exposure time for defined temperature. However, because of the large scatter of the microstructural related parameters, these equations in theory can be applied for residual life time estimation, but they are not standardised yet.

Interparticle distance concept is related to the carbide coarsening phenomena and grain boundary area denudating. Creep curve calculation theoretical models based on interparticle distance and carbides coarsening have been developed in the early eighties and compared to the experimental creep test data [58,59]. These models are based on changing of creep rate (tertiary creep) due to particle coarsening.

2.5.1 Microstructural phases in P91 base material

The modified 9Cr-1Mo alloy is an advanced material whose mechanical properties depend on the creation of a precise microstructure, and the maintenance of that microstructure throughout the component's service life. The optimum chemical composition with its low carbon content results in good fabricability and weldability (Table 2.2).

	C	Si	Mn	P	S	Cr	Mo	V	Nb	Ni	N
wt,%	0.1	0.27	0.53	0.007	0.01	9.0	0.91	0.2	0.04	0.35	0.0038

Table 2.2 Chemical composition of P91 steel

The superior properties of P91/T91 hinge on a precise addition of vanadium (V), niobium (Nb) and nitrogen (N), and a carefully controlled normalizing process to produce a complete phase transformation from austenite into martensite. This produces hard steel with high tensile strength at elevated temperatures and high creep resistance. Next, a controlled tempering process must follow, to allow the V and Nb elements to precipitate – as carbides and carbon nitrides – at defect sites in the microstructure. This serves to anchor or "pin" the defect sites, thereby holding the microstructure in place. Most recently the importance of the V and Nb additions and their precipitating action was reported by Takashi Onizawa [60] and others, at the ECCC Creep Conference, held in September 2005 in London by the European Collaborative Creep Committee. Mo is a solid-solution strengthening element; Cr is to increase the corrosion resistance, and N is a carbo-nitride precipitates former.
The microstructure of P91 steel – tempered martensite formed during a final normalizing and tempering heat treatment is presented in Figure 2.9. After normalising at 1050^{o}C air cooling leads to martensitic transformations due to the chromium content. Tempering in the range 730-780^{o}C leads to improved ductility and toughness, and induces formation of carbides and carbo-nitride precipitates (strengthening precipitates). Secondary microstructural phases identified in P91 steel are: $M_{23}C_6$ Cr-carbides and MX (V, Nb)-nitride particles (Figure 2.10) that precipitate in the steel during tempering, on prior austenite grain boundaries, ferrite subgrain boundaries and on dislocations inside subgrains (Figure 2.11). Further particles precipitation like intermetallic $(Fe,Cr)_2(Mo)$ Laves phase might be

observed when the steel is put into operation in power plant at temperatures below the final tempering temperature.

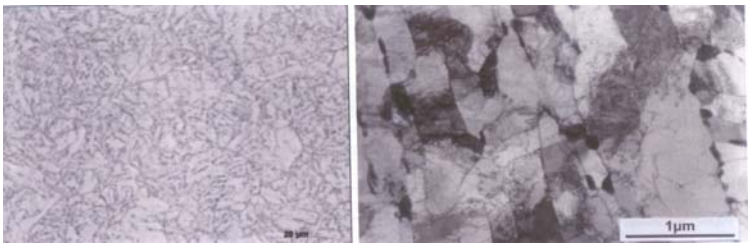

Fig.2.9 P91 microstructure – base material (optical left, TEM micrographs right) [61]

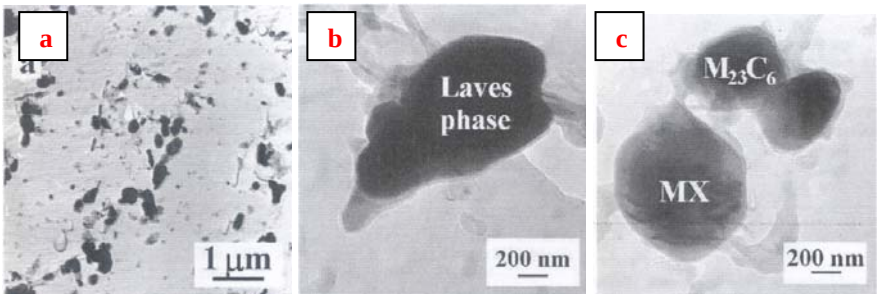

Fig.2.10 Phases identified in P91 steel: (a) Morphology and distribution of secondary phase particles, (b) TEM-micrograph of Laves phase, carbon extraction replica, and (c) TEM-micrograph of M23C6 and MX particles, carbon extraction replica [62]

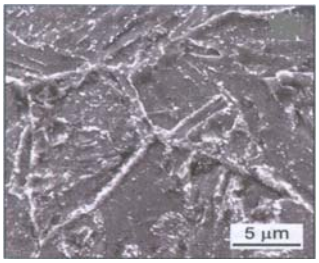

Fig.2.11 SEM micrograph showing microstructure of P91 steel – tiny precipitates both on grain/ subgrain boundaries and on former martensitic laths [63]

2.5.2 Thermal processing of P91 steel

"Thermal processing" is an important issue and refers to any heating process that has the potential to alter the microstructure of the material. Problems that can significantly impair the creep-rupture strength of these alloys are over-tempering, under-tempering, and exposure to temperatures in the intercritical region.
Over-tempering causes a coarsening of critical precipitates, with a corresponding loss in creep-rupture strength because of the loss of the restraining influence of these precipitates. Under-tempering also can endanger the high-temperature

properties, since the required precipitation does not go to completion, and the precipitates either are absent or are of insufficient size to stabilize the structure.
Other complications associated with under-tempering – such as the risk of brittle fracture and stress-corrosion cracking - also must be considered.

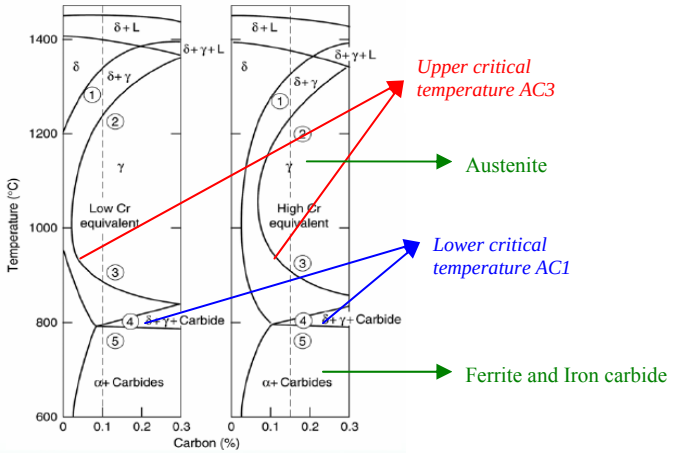

Fig.2.12 Phase diagram for high- and low- Cr Steel

Perhaps the most common problem with Grade 91 is post-production exposure to temperatures in the intercritical region – above the temperature where the tempered martensite begins to transform back into austenite (referred to as the lower critical transformation temperature or AC1) and below the temperature where phase transformation is complete (the upper critical transformational temperature, AC3). When Grade 91 is heated into this intercritical region, the material partially re-austenitizes, and the resulting structure will have substantially reduced creep-rupture strength (Figure 2.12). In the worst case, this material will have lower creep-rupture strength than that of traditional Grade 22.
Thus, the two important parameters for Grade 91 components are:

- Lower critical transformation temperature (AC1), above which the alloy's phase transformation from martensite back into austenite begins, which was found between 800°C and 830°C (depending on the chemical composition) , and
- Upper critical transformation temperature (AC3), above which the phase transformation to austenite is complete, which was found between 890°C and 940°C.

2.5.3 Creep behaviour and related microstructural changes for P91 steel

The foreseen life for a power plant may be 40 years as the average creep rate is about $10^{-11}s^{-1}$. However to make an extrapolation to this rate from rates measured in the standard laboratory creep testing is risky and we need to understand the physical processes involved. At low rates of creep deformation (low stresses – up to about 100MPa) the transport of matter occurs by migration of vacancies rather than by the glide of dislocations. These creep processes are usually classified as viscous creep [64, 65].

The technically applicable stresses and temperatures for creep testing for P91 steel are in the range 300MPa/500°C – 50 MPa/650°C. The rupture times with loading conditions in this range are between 100 and 300,000 hours and the minimum creep rates – between 3.10^{-6} and $5.10^{-12}s^{-1}$. In the author's opinion [61] in this stress/temperature range the creep mechanism is dislocation creep. Generally speaking, the combination of pressure and high temperature makes the dislocation based creep process the dominant damage mechanism. Creep deformation sources are the migration of dislocations and sub-grain boundaries [66,67].

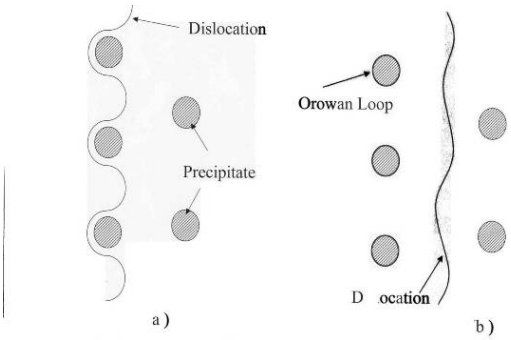

By alloying the creep properties are improved with precipitation of stable carbides and nitrides. These particles will obstruct moving dislocations and will slow down the creep rate. At lower temperatures the Orowan mechanism (Figure 2.13) can be used to explain the strengthening of hard impenetrable particles.

Fig.2.13 Orowan mechanism: a) bowing between particles;
b) Bypassing the particles, thus leaving dislocation loop surrounding each one

In this mechanism, the dislocation bends between the particles leaving a dislocation ring about each particle (Figure 2.13). At higher temperatures the particle strength according to Orowan will overestimate the contribution since the increase in dislocation climb mobility at high temperatures allows climb across particles. A model for dislocation climb around particles has been developed in [68, 69].
Thus, the improved creep strength of P91 steels, as for all 9-12% Cr steels, is due to the mechanisms which retard the migration of the dislocations and sub-grain boundaries, and consequently delay the accumulation of creep strain with time.

Such mechanisms consist of:
1) Solid solution strengthening due to formation of solute atoms clouds around the dislocations; and
2) Precipitate strengthening due to interactions with particles.
The solution strengthening effect often is referred to the presence of Mo. During high temperature creep exposure at 600-650°C, most of the Mo in the steel precipitates as intermetallic Laves phase and thus the solution will become poor in Mo. The dominating opinion is that forming of Laves phase would cause creep instability in the steel, since the precipitation strengthening effect from Laves phase was believed to be insignificant.
However, it has been made clear recently that long-term microstructure stability is not influenced significantly by the solid solution strengthening from Mo. The most important strengthening mechanisms for 9-12% Cr steels including P91 steel is believed to be precipitation hardening by pinning of dislocations and sub-grain boundaries. Thus the microstructure stability under creep load will be equivalent to precipitate stability [70,71]. Precipitates are known to retard recovery and

recrystallisation [72-74]. Further more it is recognised that altering the particle distribution by varying the heat treatment procedure can have a marked effect on the creep properties of these alloys. As a result, several theories have been proposed to predict the effects of variations in particle size and spacing on creep behaviour [75-77]. Threadgill and Wilshire [78] proposed that during creep of precipitate hardened alloys with constant volume fractions of precipitates, small particles are sheared so that the work done in cutting each particle increases and the creep rate decreases with increasing particle size.
In P91 steel, unlike the low alloy ferritic steels operating in the creep regime, the more easily visible changes such as spheroidisation and break down of the microstructure at a scale that can be seen under an optical microscope does not occur in P91. This means that much more costly transmission electron microscopy (TEM) has to be used to identify changes in the microstructure. Even then the changes may not be visible to a non-specialist, as it is mainly the changes in the precipitates and dislocation density that adversely affect the life of these steels.

2.5.4 P91 weld material

Manufacturing fabrication of weldments are standard procedures in a production process of large castings for power plants components. The knowledge of the behaviour of welds during long term service of the castings is of great importance. For acceptance in practice and successful application, the weldability and long time behaviour of the newly developed materials is one of the most important aspects.
The welding operation leads to several changes in the mechanical properties of the resulting structure that may have dramatic influences on the creep strength.
More generally, several problems can be related to the welding operation:

- The solidification of the weld metal may lead to the formation of cracks especially for very thick components;
- The solidification is accompanied by a metal contraction leading to stress concentrations that may be significant. As a consequence a post weld heat treatment (PWHT) is performed to relax residual stresses;
- Local heating of the base metal induces phase transformations and several microstructural and mechanical properties changes in the so called heat affected zone.

Because at least ten years have passed since the first P91 practical applications, there have been growing concerns about age degradation in the mechanical properties at elevated temperatures for structural components manufactured from this steel. Therefore, much research has been conducted to predict the creep life and residual life of base metal of P91 steel [79-82]. After long term service at elevated temperature, fracture occurred not in the base metal but mainly in the weldments of the components, where the rupture strength can be lower than that of the parent material. A weld joint of dissimilar materials under external stress usually represents a critical point in many technical solutions involving elevated temperatures. Material damage, cracking and failure in high temperature plant are often related to the welded areas - weld metal and its associated heat affected zone. This accounts both for F/M and austenitic materials and dissimilar welded joints. The consequence is weld repair or even replacement of the component, resulting in significant outage time costs.

The weld deposit composition is designed to be as close as possible to the parent P91 steel consistent with achieving optimum properties, weldability and microstructure. In order to achieve the optimum balance of creep properties and toughness, the weld metal compositions differ from the parent alloy as follows:

- Reduced niobium for improved weld metal toughness;
- Nickel is beneficial in improving toughness properties;
- Manganese is generally controlled at a higher level than the parent material to promote deoxidation and ensure a sound weld deposit;
- Silicon is an essential deoxidant and in conjunction with chromium it contributes to the alloy's oxidation resistance. Even a low level of Si benefits weld metal;
- Vanadium, Carbon, Nitrogen - all have a minor influence on toughness, as incorrect balance may lead to ferrite formation, and weld metal ranges and values are essentially the same as the parent alloy to maintain good creep performance.

The weldment microstructure of F/M steels is shown in Figure 2.14.

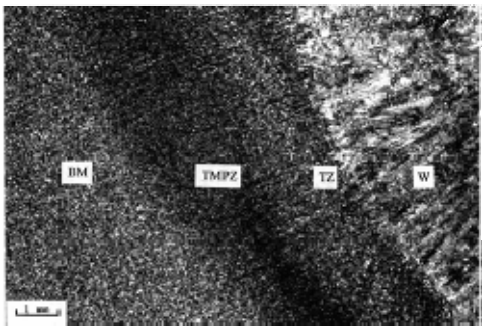

BM - base metal
TMPZ - tempered zone (fine grain zone)
TZ - transformation zone (coarse grain zone)
W - weld metal

Fig.2.14 Weldment microstructure of F/M steel

F/M steels are more difficult to weld than austenitic stainless steels – pre-heat and post-weld heat treatments are required. These types of thermal treatments are generally required in order to ensure suitable weld integrity and will typically prevent or remove undesirable characteristics in the completed weld. Properly done, post weld heat treatment reduces residual welding stresses and softens hard metallurgical micro-constituents that form in both weld metal and base metal heat-affected zones. The minimum required PWHT temperature according to the ASME codes is 704^{o}C. However, P91 is relatively resistant to tempering, and higher PWHT temperatures are generally needed to reduce hardness in weld heat-affected zones and to develop the necessary toughness in weld deposits [83]. P91 steel normally transforms completely to martensite during air cooling [84].
Creep properties of P91 steel weldments at different PWHT conditions have been investigated in [85]. The PWHT temperature, however, should not exceed the lower critical temperature for the ferrite-to-austenite transformation, AC1, otherwise austenite will be reform in the microstructure. This "fresh" austenite will then partially or completely transform to martensite on cooling from the PWHT temperature, and it will result in untempered martensite in the final microstructure.

Another important factor is the handling of weldments between completion of welding process and PWHT. If prior to PWHT weldments are cooled to room temperature, they will transform more completely to martensite than weldments that are maintained at or above minimum preheat temperature. Consequently, weldments that are cooled to room temperatures are less likely to contain untempered martensite after PWHT. However, maintaining preheat temperature prior to PWHT is essential for minimising the probability of hydrogen cracking in weld heat-affected zones.

2.5.5 P91 weldment under creep conditions

The creep properties of the weld metals for high temperature applications, i.e. for the welded components of power plants with higher steam temperatures and pressures, are extremely important. These materials exhibit prominent change in their microstructure when subjected to high-temperature service conditions, which predetermines their residual creep life. Experience has shown that the first cracks always appear in the welded joints – different creep strain rates are generally observed in the different regions of the weldment under external stress and this leads to the generation of increased mismatch stresses and earlier failure.
Like the low alloy ferritic steels before it, P91was introduced on the basis of the performance of its base metal strength and it is only in the last eight years or so that attention has moved to the performance of its weldments, the weakest link in the chain. In the case of weld joint applications at elevated temperatures, the mechanical properties can be related to chemical concentration and phase transformation processes in the diffusion-affected zone (transformation zone) [86]. Information on the time evolution of both the phase and the element redistributions at a given temperature treatment is therefore very important. The main factors that influence the stability or instability of the weld joint of steels are [87, 88]:

- Carbide nucleation;
- Phase transformation;
- Rate of diffusion;
- Carbon depletion dependence on temperature.

These factors in weld joints of multi-component alloys have become very complex due to the high degree of freedom of the multi-component system [89,90]. The diffusion fundamentally affects the rate of phase transformations at elevated temperatures and the changes in chemical potentials of the elements are consequently the cause of phase precipitations, growth, phase dissolutions, and/or phase boundary replacement in the weld diffusion zone [91].

In many cases, regions parallel to the initial weld interface are formed in the diffusion-affected zone, with different microstructures having different mechanical and corrosion-resistant properties. In order to evaluate long-term mechanical/microstructure stability of weld joints it's necessary to investigate the relationships among the element/phase redistributions, the microstructure at various points across the weldments, and local mechanical properties [92].
Purmensky et al. [93] explain the reason why the creep rupture of welded joints at high temperatures is often observed in the heat affected zone, especially in the so called intercritical zone (IC-HAZ). They found that with increasing interparticle spacing of secondary phases ($M_{23}C_6$ and nano-particles of MX), which determine the precipitation strengthening the proof stress and creep rupture strength

decreases, while creep rate increases. The interparticle spacing of secondary phases in the HAZ is found to be much higher than in the base material. Therefore the proof stress and hardness as well as the creep rupture strength of HAZ is much lower (about 20%) than that of the base material.

The creep properties of a welded joint can be measured by extracting cross-weld specimens. Recently creep failure in uniaxial cross-weld tests for high Cr steel welds, including P91 welds, has been reported [94-100]. Creep failure involves complex interactions between zones and the observed weld uniaxial test failures of plane bar specimen geometry are, however, highly artificial. Still some micro-mechanisms ongoing in particular zones of a welded joint cannot be identified for certain. Thus, it is important to develop a testing methodology to characterise local properties of a welded component. Micro-tensile testing, although not standardised yet, may be used for this purpose [101-103].

2.6 Miniaturized Testing Technique

2.6.1 Current industrial needs

The possibility to estimate the extent of properties degradation of the alloys in service and predict the remanent life time is a big issue in the industry that becomes possible by testing of small scale specimens. Additionally, many advanced materials are often in limited supply and the use of small test pieces can accelerate the production of useful data. Therefore, the needs for miniaturised testing methods may be summarised as follows:

- A need for minimally invasive assessment of structures, especially for thick components of plants where Small sections can be taken from working components and tested to assess bulk homogeneous material degradation without affecting the performance – almost non-destructive testing;
- A need for evaluation where the zone to be investigated is localised:
  When mechanical characteristics for a given component are not known, nominal properties are used. For the critical locations in working components (most stressed, more damaged ones) the local material properties could be very important for quantitative evaluation of the residual life. Specimen miniaturisation is extremely desirable therefore for limited sampling material from thick walled components, i.e. by using non-invasive or even locally invasive methods which exert no detrimental influence for the component;
- A need for failure analysis of a wide range of components and products where the available material is restricted;
- Another need is the availability of mechanical properties on samples from service exposed parts of infrastructures for failure analysis purposes. Machining the conventional (large) specimens for the standard tests might not be compatible with the dimensions and shapes of the available parts. In other cases, the damaged region to be investigated must be assessed by highly localised sampling, involving small volumes for the tests;
- A need for an analysis of thin components: measurements from miniature samples are needed for assessing not only the local damage in massive steel components, but also for thin parts, only few mm thick. In such cases,

the zone to be characterised is very small and a traditional (large) specimen is poorly representative of the surface damaged region;
- A need for weldment assessment including weld material and heat affected zones within the parent metal, coatings, claddings etc.

The analysis of such critical zones would need sampling of regions with a thickness less than 1 mm. Here the important characteristics for evaluating damage and residual life are: creep strength, ductility, impact fracture toughness and fatigue resistance. In this case neither uniaxial, nor impact tests using conventional Charpy specimens can be miniaturised enough. There is an obvious need to scale down the specimens' size in order to fulfill such thickness requirements.

2.6.2 Miniature specimen design

The current range of "sub standard" specimens is considered here. Many of these designs have been created for the needs of the nuclear industry: its construction costs, its need for identification of radiation effects on materials and stringent safety requirements create a strong requirement for small specimen testing which can be readily justified economically. Thus, there can be a "spin-off" to more conventional industry for the use of such mini techniques.
The miniature specimen design can be categorised as:

- Miniature specimens similar in shape and form to the conventional specimens but scaled down in absolute size;
- Miniature specimens of innovative design specifically developed to take advantage of the smaller dimensions.

2.6.2.1 Miniature specimens similar in shape and form to the conventional specimens but scaled-down in absolute size

A typical geometry for a specimen for *tensile testing* used worldwide has a 50mm gauge length and a 10mm diameter. A similar but smaller specimen design is illustrated in figure 2.15 [104]. It has only a 20mm gauge length and is 3.2 mm in diameter. Much smaller micro-tensile specimens with only 9mm gauge length and 2mm diameter are used by Ceyhan et al. in [105] to characterise local properties of a welded component, see Figure 2.16.

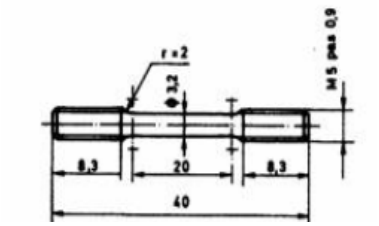

Fig.2.15 Typical 20 mm gauge length tensile sample [104]

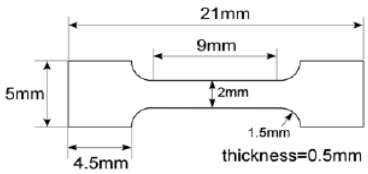

Fig.2.16 Microtensile specimen of 9 mm gauge [4]

Other authors using micro-tensile testing across the weldments are Sekhar, Cam et al. in [106,107]. Thus it is also useful for in-service material characterisation that might possibly be compared with other test methods as small punch testing [108].

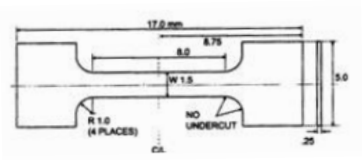

Fig.2.17 A typical sample design, plate, for gauge lengths of the order of 8 mm [114]

Small-scale "conventional" *creep testing* is essentially a scaled down version of conventional testing utilising specimens of similar geometry loaded in a similar manner to produce creep rates equivalent to those obtained from larger specimens. Several different techniques are known, for instance in [109-113].

Other typical designs of the smaller forms are generally formed from "plate" and are flat rather than round specimens. Ranges of sizes have been used, typically 2-3 mm thickness, and although the specimen itself is quite small, the total length can be fairly large and in excess of 20mm. Smaller sizes, such as those with a width of 1.5mm, a thickness of 0.25mm, an 8mm gauge length and a total length of around 17mm, are the next size option, see Figure 2.17.

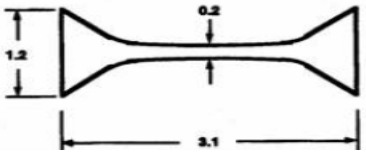

Fig.2.18 The smallest conventional specimen design found in the literature [116]

Some authors [115] are using flat type specimens with square section of 3mmx3mm and 25mm gauge length. However, the smallest conventional shape form found in the literature is shown in Figure 2.18. The specimen has length of 3.1mm and a thickness of 0.2mm [116].

As can be seen, a full range of sizes has been used over the years. As the specimen size is reduced, it increases the degree of difficulty for manufacturing, handling, testing and interpretation of the results. Indeed, it is pointed out that the test methods and handling are not trivial for such small samples.

Toughness testing, using the simple Charpy impact energy approach generally uses 10mm square bars of 55mm length with a notch machined at centre of one edge. There are constraints placed on data validity, dependent on material strength and ductility, in using such type specimens. Such effects are more pronounced as the bar size is reduced. However, the advantages are using limited amount of material for alloy development or for operating components that can only provide limited material or for radiation reasons. A range of sizes has been exploited and tested in notched bars from 10mm square to the small 1.5mm square bar section, see Figure 2.19a [117]. The smallest notched sample can be cut from a failed half Charpy, Figure 2.19b.

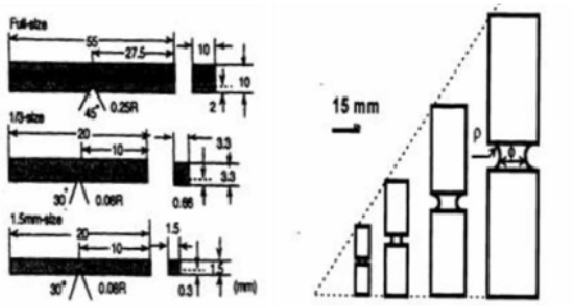

a) b)

Fig.2.19 a) Typical size ranges of Charpy impact samples, many of them capable of removal from failed halves of conventional Charpy samples [117];
b) Typical range of notched bar samples which allow the samples to be cut from failed Charpy samples [118]

2.6.2.2 Miniature specimens innovatively developed in order to take advantage of the small size

The main specimen geometry used by different researchers is a disc, cut from material whose properties are required [119-123]. In general there are two typical disc diameters, 3mm, referred to as a TEM disc [124] (it can be prepared using the same principles as the conventional disc for TEM examination) and 6.5 – 10mm diameter size and up to 0.5mm thick, often utilised in Europe for high temperature studies. Rectangular, rather than round "discs", are used by some researchers- 10x10x0.3/0.5/0.25mm [125-127].
Special attention to the devices used for extraction of such small specimens, as well as the problems that can arise during the sampling process is detailed in [128]. A view of the SP sampling equipment is shown in Figure 2.20.

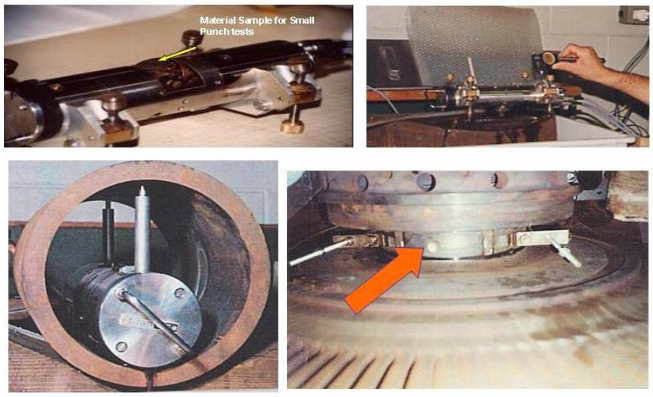

Fig.2.20 Small Punch sampling equipment

The specimens of this design are quite small, therefore techniques and appropriate testing equipment have been developed for handling and testing such samples,

which is not trivial task. The discs are loaded by a central rod, in a small jig that can fit either on the conventional test machines or special testing rigs designed for small scale specimens. The loading itself can be from a flat ended cylinder or a hardened steel hemisphere or ball with a diameter from 1mm to 2.5mm, depending on the disc size, normally referred to as a small punch or bending test. Variations in the loading system used and reported in the literature can be summarised as:

- Changes in the ball or cylinder diameter;
- Modifications of the clamping of the disc during loading;
- Use of different shapes punches - annular [129]; elliptical [130].

Two classes of use for such indentation tests can be envisaged; in the first one the deformation is enclosed within the thickness of the sample, and in the second ones the test is taken to failure. The former is generally referred to as *indentation testing* and usually is used to define the yield stress and work hardening in plasticity and the secondary creep rate in constant load high temperature creep testing.
The second relates to penetration of the indentor to failure. The larger deformation class separates into two main punch forms: shear punch [120] and bulging type tests [131,132]. The latter can use either cylindrical or ball punches whereas the former is restricted to cylindrical or sharp edged punches. With cylindrical punches the contact area is fixed and constant during the indentation (shear punching) with deformation and damage focused into the narrow ring of material sheared between the punch and the hole edge. The alternative bulge test can use any shape indentor, although generally this is a hemispherical ball. Here the loading initiates at the disc centre line and the contact area will change with indentation depth. The resulting specimen will have a pronounced bulge and the deformation and damage will be more evenly spread over the deformed area. The deformation distribution is complex and will be influenced by material ductility.
These indentation type samples can have an important input in property measurements testing if suitable interpretation of the test data is possible. Their size allows them to meet the general requirements for miniaturized samples: localisation within specific microstructural constituents, small enough to allow uniform radiation damage, ability to be taken from operating plant. However, the preparation and testing require careful consideration [119-121,133] as the techniques are not trivial. Due to their reduced thickness, these types of specimen require:

- Special surface preparation, similar to that applied for TEM disc samples;
- Detailed procedures for testing;
- Development of testing modules that can be fitted into conventional test equipment; or
- Designing special equipment for testing small geometry specimens.

Investigations on the machine compliance [134] and loading system geometry [135] have been conducted and reported. It turns out that the effect of the test jig geometry can be significant for the testing results. The uncertainty of measurements can rise not only due to different testing equipment employed, but also when different materials or different shape specimens are tested. To avoid all these uncertainties, in order to have robust and repeatable results it is strongly recommended that efforts to establish solid guidelines and testing procedures for conducting small scale testing be continued. The key feature of all these specimen designs is their small size and a major question is whether the properties

measured from them are relevant or compatible with those measured from conventional designs.
The quoted specimen designs have been developed over the last twenty years to meet required commercial objectives. The data interpretation in most cases has either reached an acceptable stage for specific materials important for the industry or approximate methods are available, currently being refined. As a future work, optimisation of the test procedures for small specimen testing needs to be improved, as more experimental test data become available for verification, as well as standardisation of the experimental methods to ensure accurate and reproducible tests, confirmed by Round Robin experiments.

2.6.3 Indentation techniques

The *indentation methods*, as mentioned above, have been extensively employed to measure technological characteristics and to estimate mechanical properties of materials. The reasons for the application of the hardness test for material qualification are several:

- Relatively simple, well established and low cost procedure;
- The possibility to be applied on a small sample or a small area in a larger sample such as a coating, weldment heat affected zone etc.;
- Non-destructive test, applicable also on in-service components.

This area has been reviewed or considered in detail in [136-140].

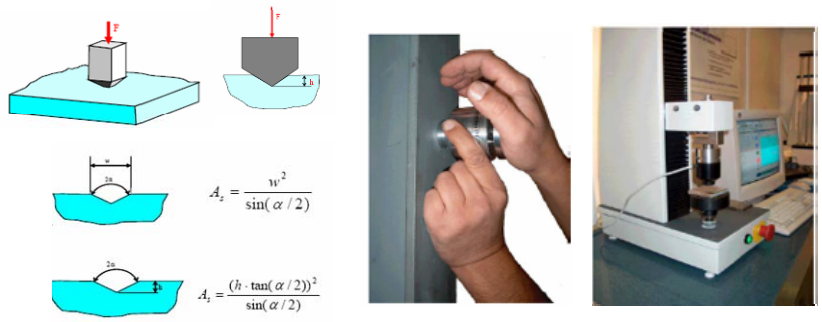

Fig.2.21 Instrumented indentor –stationary application in laboratory as well as mobile for ambulant testing of components

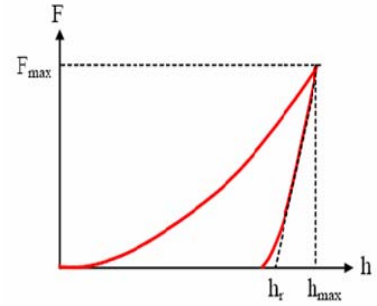

In particular, the hardness is obtained by dividing the maximum force applied during the indentation by the extension of the residual crater produced on the surface of the sample (Figure 2.21). The measured indentation hardness is scalable to other hardness parameters such as HV, HB, HRC. The curve registered during the indentation test is shown in Figure 2.22.

Hardness = Force F / Indentation surface area A_s

Fig.2.22 Indentation curve – applied force versus penetration depth

Parameters such as E-modulus, ultimate / yield strength, residual stresses, strain hardening, rate effects can be evaluated through this technique. Several authors are using the indentation test for direct correlations of the hardness with yield and tensile strengths [141-145]. The disadvantage of the proposed correlations is that they are valid only for specific classes of materials and this makes the use of the hardness properties a procedure lacking in accuracy and not generally appropriate for evaluating the main material strength parameters.

Beghini, Bertini and Fontanari [146] are using the spherical indentation test in order to deduce the stress-strain uniaxial properties of the investigated material. Tipping and Schindler [147] also apply an indentation technique to obtain material parameters such as the Meyer hardness number, the work hardening related index, the Meyer constant and estimated true stress-true strain tensile behaviour on a different metal weld between austenitic and ferritic steel.

The introduction of the instrumented indentation testing machines made many details of the indentation process available and stimulated a great effort to develop more refined procedures for acquiring more accurate estimates of the elastic-plastic properties [148-151]. The indentation method is quick, convenient, sensitive and a non-destructive way to physically characterise metallic materials before and after service conditions and can complement the more traditional ways of obtaining data from materials undergoing degradation in NPP environments.
Where creep properties are concerned, so called "impression creep", the indentation at high temperatures is utilised to produce a constant deformation rate from which a creep strain rate can be derived. Technical details of the technique can be found in [141,152-155].

2.7 SP testing method background

In recent years, interest has increased in developing a new "small punch (SP) test" technique, developed over the past 20 years, with the aim of restricting the volume of the test material by creating miniature samples. The SP technique is a powerful method capable of providing direct values for mechanical properties of materials (tensile, toughness and creep strength data) in contrast with indirect measurements using X-rays, metallographic, ultrasonic or magnetic techniques. Compared to large-scale testing, the SP-test is relatively non-destructive and allows mechanical property changes to be determined locally in materials using fairly small disc specimens. It may serve as a useful tool in assessing structural component integrity, for instance in weldments and high stressed regions, which requires strength, toughness, and ductility properties. It has the potential to estimate creep behaviour for materials in high-temperature service. The main advantages can be summarised as follows: compact geometry, relatively easy sampling (sampling operation removes only a modest amount of material from the component surface and in most cases no repair is needed afterwards), relatively easy sample preparation & handling; small geometrical inhomogeneity effects; the test itself is rather simple to perform and inexpensive. In addition the SP method is useful for characterising coated components, claddings, welding zones of components and other critically weak regions where cutting of standard specimens is not possible.

Originally it has been developed with the objective of measuring the *ductile to brittle transition temperature (DBTT)* [156-168], and estimating *fracture toughness* in a range of low temperatures [124,167,169-180]. Later on, the *creep properties* also started to be the object of investigation, looking mainly at the potential of the SP technique for revealing the effects of creep [34, 37, 38, 55, 59, 63, 214, 215 etc.], thermal ageing, fatigue, ageing embrittlement, hydrogen embrittlement [212, 213] and irradiation damage [104, 156, 163, 184]. Isselin et al. [181] are using the SP method to evaluate the environmentally assisted cracking effect using very small specimens – 3mm in diameter and only 0.25mm thickness in a water environment.

When the SP technique is used to evaluate the degradation of creep properties and/or degradation due to thermal aging, it supports the maintenance of structural integrity in high-temperature components. Small punch creep testing uses a punch arrangement to deform flat disc specimens to failure at high temperature, producing a deformation curve similar to that of a conventional creep test. The SP technique is well documented in the literature. Refs [125-127,182-192,113] reported that the method provided useful information on the evaluation of high-temperature strength for components. Klevtsov, Dedov et al. [193, 194] use SP test method to assess the ultimate tensile strength and yield strength of power plant steels, and Campitelli et al. [195,196] for assessment of the stress-strain relationship.

One of the key aspects is the interpretation of the test data obtained from mini specimens and developing standards for small scale specimens. At present a number of theories and test techniques are under development for the purpose of applying the small punch creep test to the residual creep life assessment of in-service high temperature components [155,191,192,197]. However, these methods all depend on uniaxial creep results and can not be extended to study life assessment only using small punch creep data.
Some authors proposed empirical relationships in an attempt to correlate the response of SP tests directly with the results from conventional tests for high temperature creep [109, 127, 183, 192, 189, 199, 125, 200, 207-210] and for fracture mechanics properties [124, 156-179, 201-206]. This makes the analysis of SP creep results simple and practical, but unsuitable for seriously quantifying the remaining creep life fraction of in-service components. Actually, the failure time in SP creep tests is not the only important parameter. The way in which the SP specimen is deforming and the thickness is reducing in the necking area is more critical and meaningful.

Other papers introduced models that help the interpretation of the SP results in terms of stress and strain. The definition of the stress state within the SP specimen appears to be the more complex problem, although the membrane-stretching mode has been accepted as a basis for a valid model. Yang [190] and Dobes [192] present a simplified solution taken from the works of Chakrabarty [182] and Timoshenko [211] and adapted for the SP creep testing technique. However, in both cases, the SP-load/uniaxial-stress ratio found by the authors was lacked of physical meaning. Komazai [127] and Mao [124] present the more complete strain model for the high temperature SP creep and for the SP tensile test. Also in this

case, the models come from the work of Chakrabarty. The thickness reduction was evaluated and directly measured on interrupted tests and directly linked with the strain. Furthermore, Mao [123] together with Yang [190], introduced a simplified finite element model for the strain, finding an unequivocal relationship between the calculated strain and the measured central deflection. Finally, a detailed stress-strain analysis of the SP tensile test was made by Byun [129] which tried to correlate the deformation regime with the stress and strain state within the SP specimen.

2.8 Code of Practice for Small Punch Testing

The recent progress in Europe of SP creep testing is presented by Hurst, Bicego and Foulds in [198]. A major development is the CEN Workshop Agreement, CWA 15627, "Small Punch Test Method for Metallic Materials" comprises two parts, Part A: A Code of Practice for Small Punch Creep Testing, and Part B: A Code of Practice for Small Punch Testing for Tensile and Fracture Behaviour [2]. Each part contains an appendix that describes various aspects of application, including field sampling, sample location selection, test specimen configuration and preparation, the apparatus, test procedures applied, interpretation of the test results etc.
This workshop agreement is proposed to find a consensus solution to the problem of materials analysis of components of engineering equipment, as required for testing of equipment at several moments during their operational life (integrity assessment and residual life evaluation).

To get reliable results, samples must be taken from actual operational components and not from new casts. Conservative lower-bound curves published in the design codes and material manufacturer specifications also should not be used to get material characteristics during operation of the components. Such data are not specific to the particular material under study, the properties of which may also be changing during long term service. All this would lead to a large uncertainty in the integrity analysis.

The existing standardised solutions specify particular test sizes that require removal of an amount of material that may result in damage of the actual component, rendering its continued operational use impossible.
The development of improved procedures such as SP testing to support integrity assessments needs to be addressed on a European or even global, level, rather than at national or even individual organizational level. This reflects the increasing importance of EU legislation on one hand, and on the other hand the international nature of business.
Although some limitations on SP applicability still exist (mainly concerning the interpretation of the data), in general it seems to be promising technique for material properties determination.

2.9 Conclusions from the literature review

Many power and petrochemical plants are currently approaching, or are already operating beyond, their design life. These industries are then strongly interested in developing and using a reliable method for residual lifetime assessment to justify their maintenance costs. The traditional destructive testing methods require large specimens that would violate the structural integrity of the working components. Various non-destructive or miniaturised specimen testing techniques have been developed over the past two decades. The SP technique seems to be a promising method for determining mechanical properties of metals, considered an almost non-destructive technique, requiring a small amount of material, easy and inexpensive.

The small specimen size not only eliminates the need for large amount of material removal, but at the same time permits measurement of properties in local most critical areas of components. It is obvious that there is a genuine need for small specimens to meet technical rather than just economic objectives. Thus, the specimen design, development and interpretation has been strongly user driven for at least 20 years period with individual research projects, industrial user projects, collaborative projects involving both companies and the European Commission (for example in Europe), as well as validation / round robin projects. From the literature review it is clear that there is no "perfect" design specimen, but that each design or family of designs aims to meet the objectives of a specific work area.

The SP technique, proposed by Manahan et al. [1], enjoys an increasing interest lately and can be applied for studies of creep and fracture properties, as well as fatigue, ageing embrittlement, hydrogen embrittlement and irradiation damage. The current status of the testing methodology in question is presented (at European level), as well as some preliminary investigations to show the suitability of the SP testing technology for application as a lifetime prediction tool for metallic components operating at high temperatures, also in support of the recently launched Code of Practice for Small Punch Testing (CEN/WS 21) [2].
The SP technique has been investigated by several authors around the world and, beyond the promising results, there is no doubt that much work remains to be done.

3. THESIS OBJECTIVES

The main objective of this research is to assess the suitability and increase the acceptability and competitiveness of the SP technique as a tool for in-situ residual life assessment of new generation ferritic/ martensitic steels and their weldments, also in support to the recently launched Code of Practice [2] for SP testing. The development of a methodology which serves as a verifiable and reliable practical test method for creep damage evaluation will eventually assure the acceptance by the industry of the SP test methodology as a reliable tool for lifetime assessment and for supporting decisions related to lifetime extension

The achievement of the above objective relies on the research activity of this thesis which can be divided into the following steps:

- State of the art literature survey on the problem;
- Defining the experimental matrix;
- Procuring of material and manufacturing of conventional creep samples and SP discs to be tested;
- Conducting conventional uniaxial creep tests to evaluate the creep strength of P91 BM, WM and SE metal at 600^{o}C;
- Conducting conventional tensile test to determine the tensile properties of P91 BM, WM and SE metal, again at 600^{o}C;
- Performing SP creep test of discs, taken from the BM, WM, SE, CG-HAZ and FG-HAZ to be compared with the uniaxial creep tests, improving the SP creep equipment for precise temperature control at 600^{o}C;
- Interpretation of the SP creep data in terms of stress-rupture results and correlating them with the conventional results;
- Developing a FE model, based on the uniaxial conventional creep results to predict the creep behaviour of a SP disc for BM, WM and SE P91 material and subsequently verifying the model's validity by means of the experimental SP test curves recorded for these materials;
- Carrying out low temperature SP tests to evaluate the fracture properties – ductile-to-brittle transition temperature and fracture toughness of BM, WM and SE P91 material and correlating the results obtained from the SP test with the conventional Charpy and fracture toughness data reported in the literature.

The successful completion of the present work will contribute to increasing the applicability and reliability of the SP testing methodology, making it more effective and the results more reproducible and precise. The better the SP tests are defined and the better a testing routine can be reproduced and performed, the more the results can be considered reliable and the methodology utilised in structural integrity and safety assessment as an indispensable alternative mechanical test technique for direct evaluation of damaged material.

4. EXPERIMENTAL

In this chapter the experimental procedures adopted to assure the repeatability and trustworthiness of the results will be detailed.

4.1 Testing equipment

The main test facilities employed in the current work were two SP creep testing rigs for high temperature tests and a single SP tensile rig for low temperature tests. The SP creep equipment was designed originally by the University in Wales Swansea (UK) and was modified during the work to assure accuracy of the data recorded. The SP tensile test rig was designed according to a technique developed by Dr. Whelan of the JRC in Ispra, Italy.
Additionally, equipment for standard uniaxial testing was employed to obtain the creep and tensile material properties of the test materials to support the evaluation of the results of this work.

4.1.1 SP Creep facilities

General layout

The SP equipment working at constant load has been developed in the University of Swansea under the direction of Prof. Parker and Dr. G. Stratford (ref). Prior to the work conducted for the purposes of this thesis, the rigs were involved in an international round robin exercise, which involved three others laboratories, including Swansea University (ref).
The SP testing machines (Figure 4.1) consist of a hemispherical-ended puncher, specimen holder, loading system, furnace working at relatively high temperatures, inert gas for oxidation prevention, measuring devices – LVDTs and thermocouples, and data acquisition system. The puncher is made of creep resistant Nimonic alloy and machined by CNC (Computer Numerically Controlled) technology to have a perfectly hemispherical tip with diameter of 2mm. It is pushed against the specimen by a constant force. The stainless steel specimen holder is composed of upper and lower dies and one positional ring that clamp the sample around its edges. By screwing together the upper and lower die the sample disc is firmly fixed to prevent upward or sideways displacement during punching. A hydraulic piston working with compressed air was used to allow rapid and constant loading and to guarantee reproducible loading conditions. The load accuracy achieved was within ±0.5% which falls well inside that specified in the Code of Practice [2]. To maintain the sample at the desired temperature, the whole arrangement, holder/ specimen/ puncher/ thermocouple, is

Fig. 4.1 SP testing equipment (JRC-IE lab)

enclosed in a cylindrical furnace, controlled by a Eurotherm controller. To prevent oxidation of the specimens, the tests were carried out in a constant flow of argon gas. The specimen deflection was monitored by 2 LVDTs, one measuring the displacement of a quartz rod, which is in a contact with the lower surface of the sample, and the other the displacement of the puncher rod itself.
The SP testing set-up is illustrated schematically in the figure below (Figure 4.2).

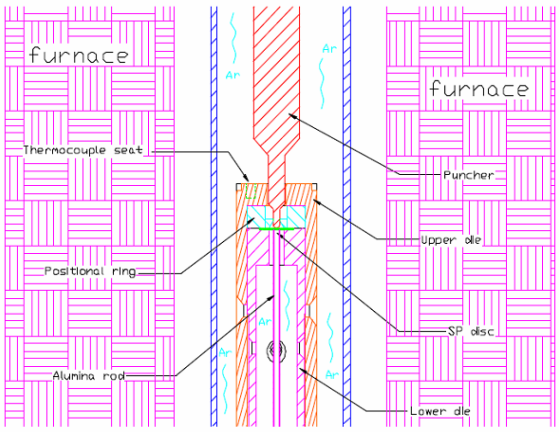

Fig. 4.2 Schematic of the experimental SP set-up

The SP specimen with an initial thickness of h_o=0.5 mm is located in a recess on a stainless steel die and clamped around the edges by a stainless steel upper die, which works also as a guide for the puncher. The puncher is pushed against the specimen by a constant force. The clamping force is presumed to be high enough to avoid any sliding due to the absence of any sign of sliding on the SP disc at the end of the test. A circular hole of D=4mm diameter is located in the die below the specimen, into which the sample bulges under the action of the punch at the specified load. To avoid friction of the disc with the inner wall of the lower die [216], the geometries respect the empirical relation:

$$D \geq 2r + 2 \cdot h_o \qquad (4.1)$$

To maintain the sample at the desired temperature, the whole of the die/specimen/punch arrangement is enclosed in a cylindrical furnace. The furnace is based on a resistance heating system and controlled by the Eurotherm® 2132 temperature controller. Based on the input of a thermocouple mounted next to the wall of the furnace a solid state relay closes or opens the circuit following the need for heating or cooling thereby keeping the temperature of the sample within ±2°C. In the two opposite sides of the furnace a cooling system works by circulating cold water to maintain the temperature of those two cold points at temperature below 50°C in order to prevent damage to the rubber ‘o’ rings, which seal the gas system. Type N thermocouples are used to measure the temperature. The temperature of the sample is taken from a thermocouple placed as close as possible to the specimen top surface due to the impossibility to fix the thermocouple directly on the sample during the test. More regarding the temperature monitoring control is given in the temperature calibration description further.

All tests were performed in a protective atmosphere of argon with an industrial purity (argon 4.6). A valve regulates the flux of argon at 0.3 l/min. Such a flow was verified not to influence at all the temperature field around the sample. The gas should be evacuated only from the valve fixed in the bottom part of the equipment to assure the sample was not in contact with an appreciable quantity of oxygen. A rubber bellow was employed to avoid leaking of argon from the connection between the mobile puncher and the fixed part of the equipment.

The central deflection was measured by two LVDT extensometers type AG 1.0 manufactured by Solartron®. The data was triggered by the transmitter Solartron® OD2. The range of operability was of 2 mm and the deviation from linearity is shown in the paragraph dedicated to the calibration procedure. One of these LVDT (Bottom LVDT) was directly taking measurements from the displacement of a ceramic (quartz: Al_2O_3) rod applied on the lower surface of the disc. The rod was ceramic to assure the absence of any appreciable false reading due to marked thermal expansion. The contact between the rod and the lower surface of the sample was assured by a small spring. Furthermore, the contact had to be as flat as possible in order to assure the reading referred only to the central bulge of the sample. The second LVDT (Top LVDT) was taking measurements by an aluminum rod (far away from the hottest point of the equipment) attached to the puncher and it was reading the distance moved by the puncher at the point where the rod was attached. The heat coming from the furnace can influence the measurement of the Top LVDT. To limit this effect a heat sink was positioned on the puncher below the rod connected to the LVDT. Because of the greater reliability for the measurement coming from the Bottom LVDT all the results were given referring to this LVDT. The Top LVDT was thus employed just as controller and back-up extensometer.
The loading system consisted of hydraulic piston working with compressed air. It was added in order to allow instantaneous loading within 2-3 sec, as recommended in the SP Code of Practice, in order to guarantee the reproducibility. During the loading the puncher had to be slightly raised for some seconds to avoid eventual vibrations and impacts on the sample surface. Small temperature variations (less then ±2ºC) induced in the sample lasted just few minutes, but they cannot be considered crucial.
In order to automate the data acquisition system and make easier the recording, a LabView software was developed in the institute for managing the data by a Field-Point National Instrument hardware (Figure 4.3).

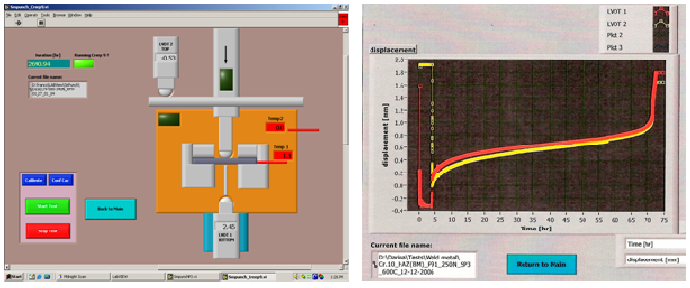

Fig. 4.3 SP control interface (Lab View) & typical examples of SP creep curves registered during SP creep testing

The resulting measurements were continuously recorded in ASCII files on a PC. A friendly interface was created to set up the test parameters such as the rate for recording the data. The system was capable of recording displacements and temperature at any desired interval of time and for any event the user wished to consider. In general any variation of temperature greater than 0.5°C and any displacement greater than 10 mm were recorded. The software was also capable to trigger the recorded data with specific events such as the switching on or off of the furnace.

Calibration

The whole process involves measurement of load, temperature, and displacement. Among these the temperature was the more important because of the sensitive role it plays in the creep phenomena.

- *Temperature*

Creep is a thermally activated process and the precise measurement of the testing temperature is therefore crucial to obtain trustworthy results. Special attention was paid to the experimental control conditions, in particular exact temperature measurement - a known problem in the SP test implementation.
In the SP equipment, thermocouples of type N were used. Under the current conditions they can be considered reliable with a degree of uncertainty of ± 0,5ºC. Each of them was calibrated by a reference furnace ISOTECH® with a certification declaring uncertainty of ± 0,5ºC in the range of temperature from 200º to 650ºC. In the ISOTECH reference furnace narrow deep cavities hold the thermocouples to be calibrated together with the reference thermocouple. As a result of the calibration a correction factor for each thermocouple was obtained for 600ºC. The correction factor was expected to provide a reliable value of temperature within the limit of precision of the type N thermocouple.
Another factor affecting the uncertainty of the temperature value was the stability of the furnace in the SP equipment. From the reading obtained during the tests it appeared that the furnace was stable and the variation of the measured temperature of the sample was kept in the range of ± 2ºC. In the SP CoP a variation of 2.2ºC is envisaged for 600ºC.
Another important aspect to take into consideration was the impossibility to fix a thermocouple directly on the sample during the test. The main difficulty for direct temperature monitoring relates to the thin section of the specimen and lack of space (specimen is tightly enclosed into the holders/dies). This makes it not feasible to weld a thermocouple on the specimen surface for direct temperature measurement as in conventional creep tests. Moreover, the only way for accessing the specimen from below is restricted because of the extensometer, used to measure the vertical displacement. The information found in the literature on temperature monitoring was either too sketchy or simply missing. The most common way of measuring the temperature of the sample, according to the literature, is through a thermocouple affixed to the specimen holder (upper die). As a result, the distance between the specimen surface and temperature measuring point was around 10mm. That led to a temperature gradient of approximately 25–30^{o}C. To minimize the gradient, the design of the holder was slightly modified. Extra co-axial holes were drilled into the upper die and the clamping ring, enabling

access to the sample surface. Additionally the retainer, where the sample lies, was made deeper for a better clamping contact. The positioning of the measurement operational thermocouple is shown schematically in Figure 4.4.

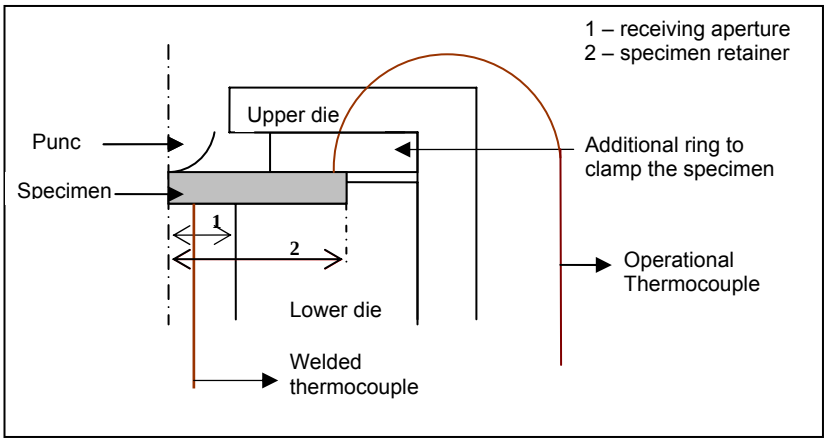

Fig. 4.4 Schematic of the SP temperature calibration

Temperature calibration of the SP test equipment was done by removing the lower LVDT and welding a thermocouple on the sample underside. In all our experiments, another thermocouple, reaching the top surface of the sample through the drilled holes, was employed. Both thermocouples were calibrated beforehand by the reference furnace as usual with an expected precision of ± 0.5ºC. A difference in the temperature of the two thermocouples was assessed. Correction factors of either 5.4^{o}C or 7.4^{o}C for each of the SP creep testing devices were introduced during setting-up the SP tests. Once the correction was known the real temperature of the sample was calculated subtracting this difference from the reading of the thermocouple.

- *Load*

The employed weights were calibrated by a balance with a precision of ± 5gr.(± 0.05N). Other small mechanical factors, such as the small spring employed to keep the ceramic rod in contact with the sample and the effect of the rubber elbow restraining the spring from below were not considered significant. Thus, a final accuracy for the load of ± 0.05 N was assumed.
During the SP test, it had to be assured that the load was applied perpendicularly to the top surface of the sample and that the sample was perfectly parallel. A spirit level was employed in order to guarantee the horizontality of the SP device, and a weight suspended by a thread to check if the frame guiding the puncher was perpendicular to the sample. Eccentricity of loading were not so important because the sample was securely clamped around its border and an eventual eccentricity of the load resulted just in a slightly off centre deformed bulge.

➢ *Displacement*

Two LVDTs were used to measure the deflection of the disc. The linearity of the transducers was assessed by inserting ceramic gauge-blocks under the measurement tip of the LVDT. The signal was from 4 to 20 mA current and the calibration was performed reading the signal twice increasing and decreasing the displacement respectively. The average value (S_a) of the two readings was then linked to the displacement (u) by the relation:

$$u = (S_a - Zero)* Gain \quad (4.2)$$

where (Zero) was an arbitrary value and the (Gain) was fixed in order to minimize the deviation from linearity. The linearity of the transducers was evaluated comparing the result of the Eq. 4.2 with the real thickness of the gauge-block (t) by the percent of deviation (Eq. 4.3):

$$dev\ \% = (t - u)/2 * 100 \quad (4.3)$$

The LVDTs showed in the working range a deviation from linearity less than 0.1 %.

4.1.2 SP fracture test facilities

This equipment was employed to investigate the potential of the SP testing technique for assessing the fracture properties of materials.

General layout

An INSTRON 5586 electromechanical load frame machine equipped with a load cell of 5kN and operated with the control software Bluehill2 was employed for low temperature SP fracture tests. The test configuration allowed the sample to be tightly clamped inside two coupled cylindrical pieces which formed the specimen holder. The holder itself is positioned between 2 blocks fixed firmly together by bolts (Figure 4.5)

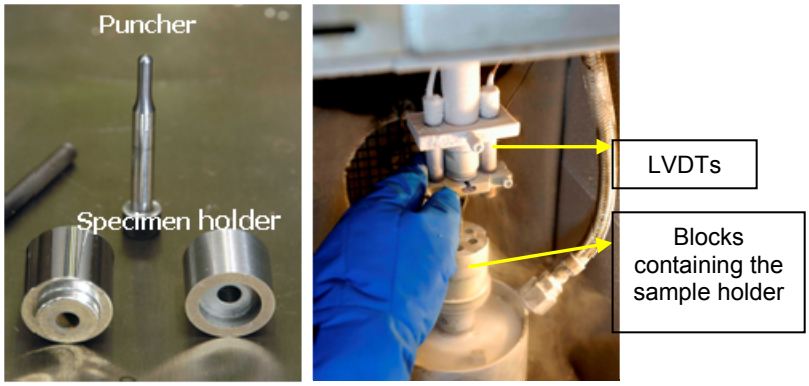

Fig. 4.5 SP fracture test implement

A central through-opening along the axis of the assembly allowed the travel of a puncher with a hemispherical tip with diameter of 2R=2.5mm touching the upper side of the sample disc. Two side grooves are present in the upper block for

positioning the displacement transducers. A thermocouple was placed at a few millimeters from the specimen surface. The blocks were fastened onto a load frame with long bar-shaped pieces which provide the necessary clearance for operation inside the environmental chamber.
The schematic of the SP fracture test implemented is presented in Figure 4.6.
The machine was adapted with a special environmental chamber for working over a range of temperature between -158°C and 300°C (Figure 4.7). Liquid nitrogen was introduced as cooling agent.
For experiments requiring temperatures lower than -158°C, two extra vessels for liquid nitrogen were built and connected to the machine. The first vessel comprised the SP disk together with the sample holders and was connected with the second vessel, fixed outside the chamber where liquid nitrogen was filled. In these tests the environmental chamber was used to reach -158°C temperature, after that the vessels were filled up with nitrogen allowing cooling the sample down to -192°C (Figure 4.8).

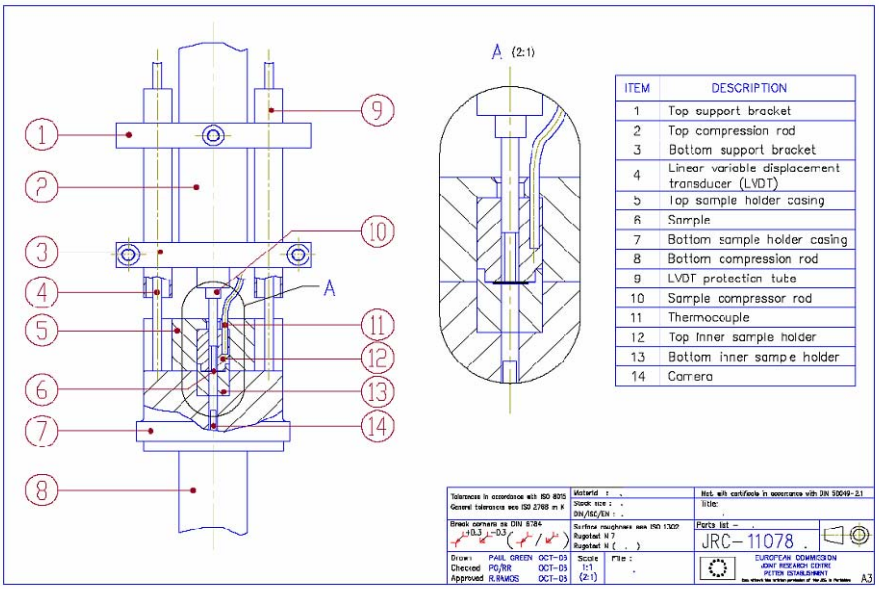

Fig. 4.6 Schematic drawing of the SP low temperature fracture test equipment

Fig. 4.7 SP fracture equipment with environmental chamber mounted

Fig. 4.8 Liquid Nitrogen cooling system used for temperature of -192°C

The lower bar was designed to house the lens of a digital camera, allowing visual monitoring of the specimen and image capture. Images were captured for room temperature SP tests visualising the crack initialization and opening (Figure 4.9). For very low temperatures it was impossible to use the camera inside the chamber.

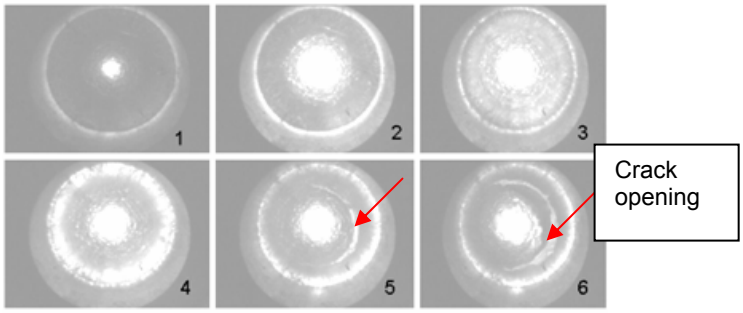

Fig. 4.9 Images registered by the camera during the SP fracture test

The signals from the different transducers were connected to a set of signal conditioners NI Field-Point, from where a customized LabView application obtained the input data. The channels registered were: load, time, temperature, crosshead position and displacement – right and left LVDT (Figure 4.10).

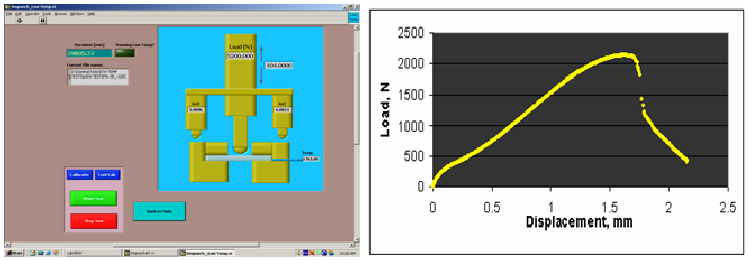

Fig. 4.10 LabView control interface & load-displacement curve registered during the SP fracture test

Calibration

- *Load*

The electromechanical load frame Instron 5586, equipped with 5 kN load cell was used for the SP fracture tests. The maximum relative error of the measured load was 0.3% [(1)].

- *Displacement*

Two linear variable differential transducers (LVDTs) LIN56, operating in ±5 mm range over temperature range from -220 to 600ºC, were employed for vertical displacement measurements of the puncher, which was consistent with the disc deflection. The LVDTs were connected to amplifiers RDT E725 to change the signals into an analogue output 0-10 volts.
Before the initiation of every set of tests a calibration of the LVDTs was carried out (Figure 4.11). Using a set of ceramic gauge blocks [(2)], measurements were taken over a range of 3 mm with intervals of 0.2 mm. The zero point for calibration was set at the initial test position of the LVDTs, and as close as possible to their electrical zero - around 5 volts in the analogue output of the amplifier. Averaging the difference of the readings against the nominal dimensions of the calibration blocks, the gain and the zero offset were determined and entered in the data acquisition software to correct the rough values from the transducers. The corrected readings presented a relative error ≤2.5% for a single measurement while the linearity error was <1% full scale [(3)]. By removing the major fluctuations in the readings, the practical resolution was determined to be 0.01 mm.

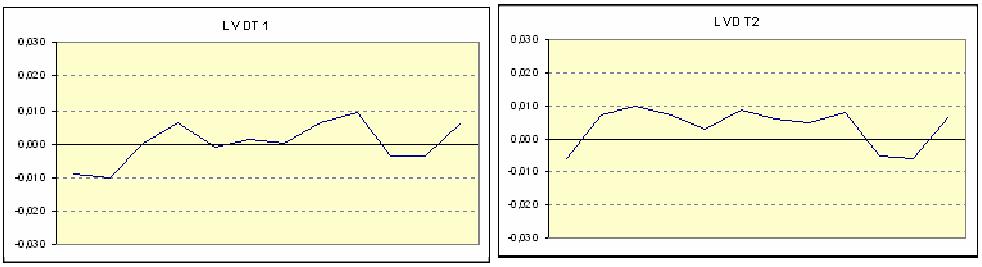

Fig. 4.11 LVDT calibration graphics

- *Temperature*

Thermocouple type T, range -200 to 350ºC, estimated uncertainty ±2ºC [(4)].

---

(1) Equipment yearly verified / calibrated by Instron Benelux.
(2) Mitutoyo 516 Series, accuracy class 1, subject to yearly calibration by ETMS.
(3) From the manufacturer specifications. The transducers were internally calibrated before the tests as described in the test procedure.
(4) Instrument yearly verified / calibrated by ETMS.

4.1.3 Uniaxial creep equipment

The uniaxial creep tests have been performed in the Institute for Energy creep laboratory. The uniaxial creep equipment employed in this project is presented in Figure 4.12.

Fig. 4.12 Uniaxial Creep testing devices (JRC-IE lab)

The whole assembly: sample/ hangers/ LVDTs/ thermocouples, is illustrated in Figure 4.13.

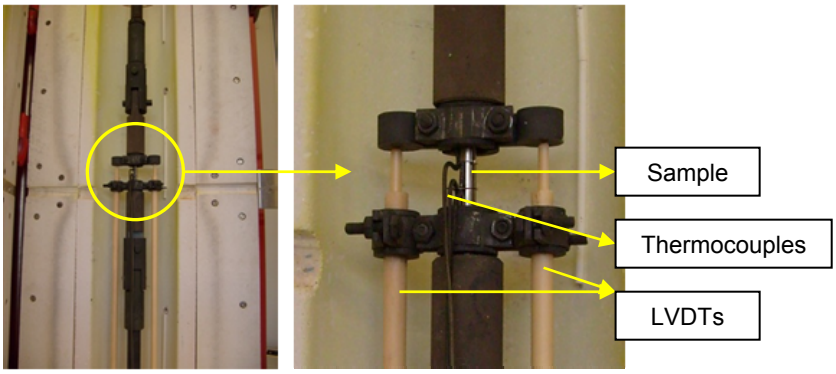

Fig. 4.13 Sample/ hangers/ LVDTs/ thermocouples assembly

The sample is screwed in between upper and lower hangers and the LVDT ceramic tubes are attached in their brackets. The displacement rods are inserted and lightly attached in the tubes. Two thermocouples are attached on the specimen surface. The whole assembly is enclosed into a furnace which ensures the constant testing temperature. The load is applied through a lever arm counter balance at the rear of the machine and it is kept constant during the test. The loading arm and the thermocouples were periodically calibrated and the accuracy for the applied stress evaluated as ±1 MPa, and for temperature of ±1°C. The

displacement transducers were working in a range of 0-10 mm with a deviation from linearity of ±0.5 %.
The measurements of the LVDTs and calculated strain (elongation) values, the readings of the thermocouples, and the duration of the test were constantly recorded using LabView software. A strain – time curve is registered as an output at the end of the test.

4.1.4 Uniaxial Tensile Equipment

All high temperature tensile tests were conducted on a digitally controlled servo-hydraulic test rig (INSTRON 8500) at 600°C in the institute. The heating was achieved by a resistance furnace (SFL MD1060A). Within the gauge length of 8mm, temperature was maintained within ±2°C by controlling the temperature by a Type N thermocouple, which was spot-welded on the shoulder of the specimen (outside the gauge length) with a Type N thermocouple of the resistance furnace. The assembled specimen/ grips/ extensometer is presented in Figure 4.14.
The load-cell used was Sensotec 75/L509-OL. For the purpose of the present test series, the extensometer and the load-cell had been re-calibrated to Class1. To avoid load train misalignment, a self-aligning specimen holder was used (Figure 4.14). The actual specimen diameters and gauge lengths of the Sandner clip-on extensometers were determined individually to 10μm accuracy (3 repeated measurements). Stress-strain curves are registered as output data.

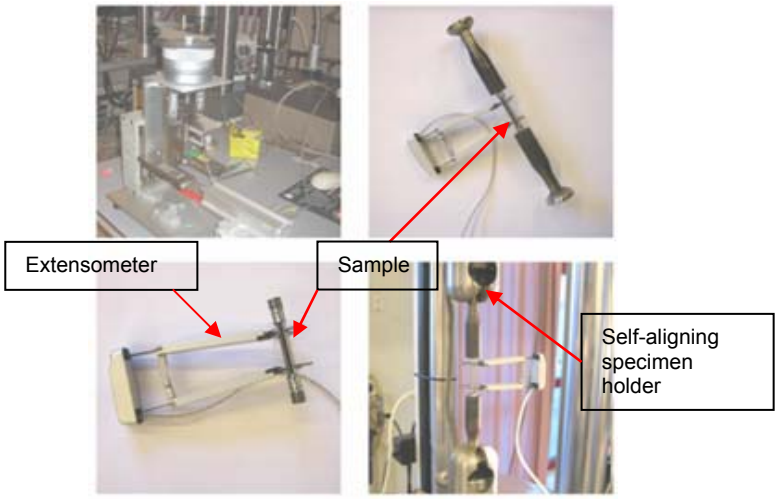

Fig. 4.14 Experimental of the tensile testing set-up (JRC-IE lab)

4.2 Materials & Specimens

For the purposes of this thesis 9% Cr commercial high-alloy steel grade P91 has been used. The testing materials were procured from both BRITE-EURAM LICON Project [217], related to life time conditioning, and from the INTEGRITY of repair welds Project [218], both EC funded. The following specimen abbreviations were used in this study:

- BML - Base Metal LICON (virgin material)
- BMI - Base Metal INTEGRITY (tested material)
- WML - Weld Metal LICON
- WMI - Weld Metal INTEGRITY
- SE - Service Exposed base material INTEGRITY
- FG-HAZ - Fine-Grain Heat-Affected Zone (adjacent to the BM) INTEGRITY
- CG-HAZ - Coarse-Grain Heat-Affected Zone (adjacent to the WM) INTEGRITY

Since the service exposed and HAZ material investigated here were taken only from the INTEGRITY project, the letter "I" is omitted for simplicity.

4.2.1 Small Punch Specimens

4.2.1.1 LICON material sampling

A section of P91 BM pipe, manufactured by Mannesmann Forschungsinstitut GmbH (MFI) for the purposes of the LICON project [217], having a wall thickness of 50mm, was used for sampling. A cylindrical piece 8mm in diameter was extracted in the axial direction from the middle part of wall. A number of small flat disks 0.6mm thick were sliced using a high precision FANUC wire erosion electric discharge machine, numerically controlled with diameter of the wire 0.25mm. The disks were then attached to a disc grinder and both sides ground with 800 and then 1200 grit SiC emery paper and finally diamond polished to reach final thickness of 0.5mm. Each sample's thickness was measured afterwards in 5 positions and only specimens with a tolerance of ± 5μm were allowed for testing. This final metallographic sample preparation was applied for all SP samples tested for the purposes of the present work.
The chemical composition of the LICON P91 BM is summarized in Table 4.1.

	C	Si	Mn	P	S	Cr	Mo	V	Ni	Nb	N
wt, %	0.10	0.27	0.53	.007	0.01	8.76	0.91	0.2	0.35	0.04	.0038

Table 4.1 Chemical composition of LICON P91 base metal

The material was normalized (1060^{o}C x 70min a.c.) and tempered (760^{o}C x 140min a.c.), so that the steel obtained had the following mechanical properties: $\sigma_{0.2}$ = 507-522 MPa, UTS = 673-682 MPa, A = 24-24.5 %.
Microstructural SEM images of non-tested LICON base material are presented in Figure 4.15. The first image displays clearly the laminate martensitic structure of the steel, and the second one shows the grain sizes of approximately 20-40 μm and small carbide particles on the grain boundaries.

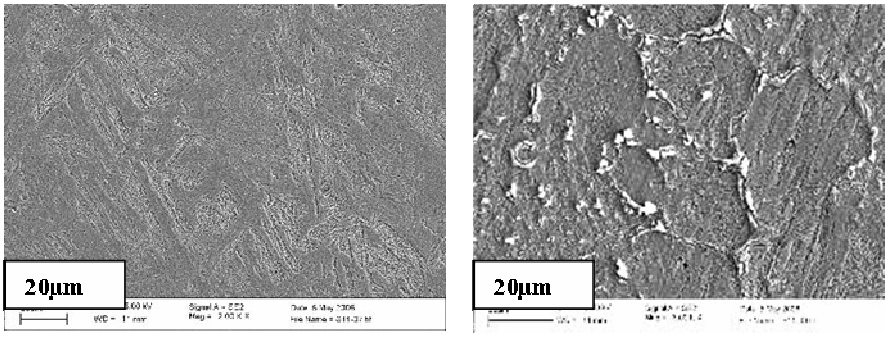

Fig. 4.15 SEM images of P91 LICON material (grain size 20-40µm)

4.2.1.2 INTEGRITY material sampling

The tested BM, SE material, weld and HAZ material for this study has been procured through the EC supported INTEGRITY of repair welds project [218]. The test component, manufactured by Instituto de Soldadura e Qualidade (ISQ) is a full repair welded joint of service exposed P91 steel pipe, procured by ELSAM, Denmark and virgin material P91 pipe supplied by ENEL, Italy (Figure 4.16).

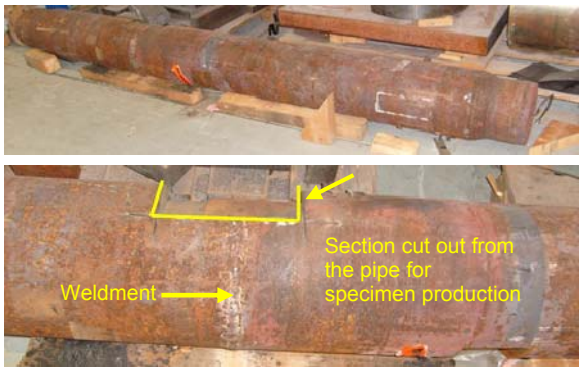

Fig. 4.16 INTEGRITY of repair welds test component

Service conditions of the ELSAM pipe were 60kh of service at 565^{o}C under an internal pressure of 250bar. The welding method used by ISQ for the circumferential weld was GTAW for the root weld and SMAW for the rest. The preheating temperature was 225^{o}C and interpass temperature < 315^{o}C with the PWHT of 760^{o}C for 3h. In the INTEGRITY project, the entire test component was subjected to a 4-point bend (4PB) test under 75.89kN and internal pressure of 160bar at 600^{o}C for 5000h.

The dimensions of the test pipe were length 2000mm, outer diameter 275mm and wall thickness 35mm. A section from the weldment zone, containing all representative pipe materials – base metal, service exposed material, weld metal, and heat affected zone materials, was cut out from an unloaded (neither tension nor compression) part of the pipe at the zone of the welding (Figure 4.18).

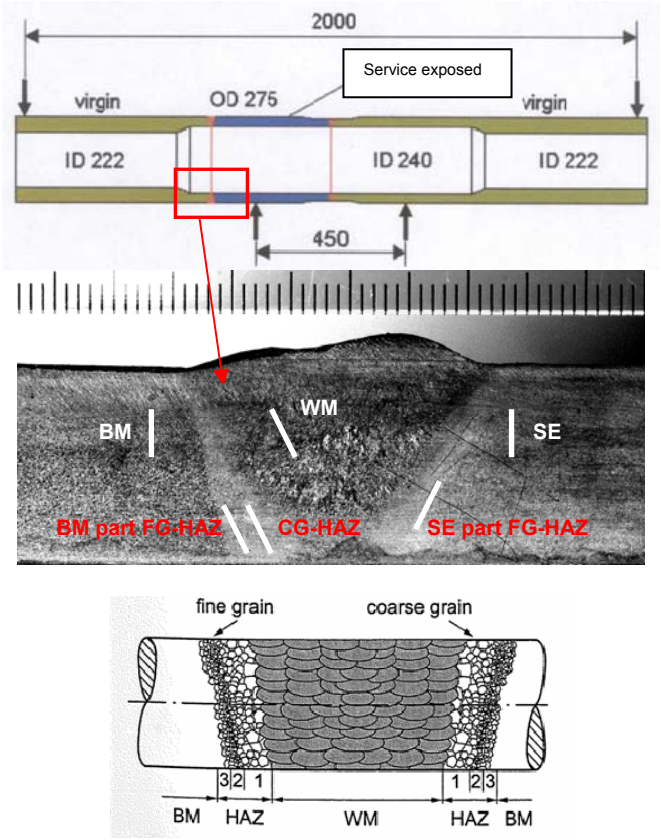

Fig. 4.18 Schematic of the INTEGRITY pipe; Optical image of the welding zone; and schematic of the weldment microstructure

The way of extracting 8mm diameter bars from this section is presented in Figure 4.19.

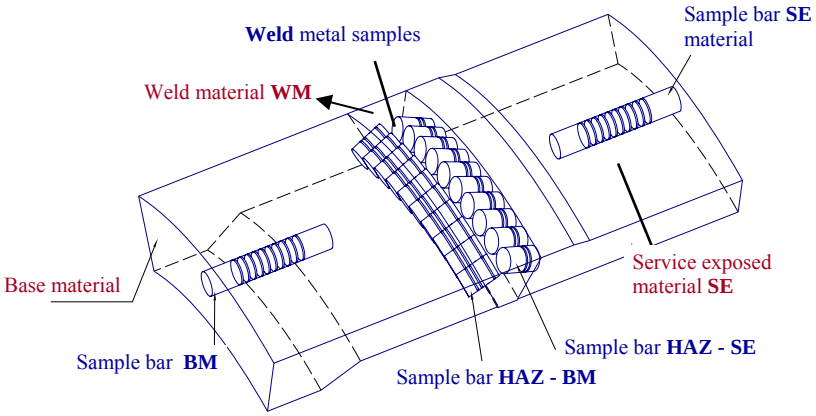

Fig. 4.19 Extracting bars from the INTEGRITY pipe weldment section

Bars 8 mm in diameter were extracted in axial direction at the BM and SE material side. The bars from the weldment were extracted at angle to assure the production of homogeneous WM, fine-grain and coarse-grain HAZ samples. Special attention has been given to the precise manufacturing of HAZ samples. The small width of the HAZ zones (approximately 2-3mm) and vague and uneven limit between base and weld metal present particular difficulties to produce homogeneous samples, which is very important in order to avoid ambiguity in the test results. Practically it was impossible to distinguish between the fine grain and intercritical HAZ zone.
Finally, a number of flat disks 0.6mm thick, representative for the base metal, service exposed material, weld metal, fine-grained heat-affected zone adjacent to the BM side (FG-HAZ), and finally, coarse-grained heat-affected zone adjacent to the WM side (CG-HAZ) were extracted from the bars as shown in Figure 4.20. The final thickness of 0.5mm and final surface polishing was achieved as described above. SEM micrographs showing the microstructure of the HAZ, WM and SE materials are shown as well. The microstructure of the BM is similar to that of the SE metal and for that reason is not shown.

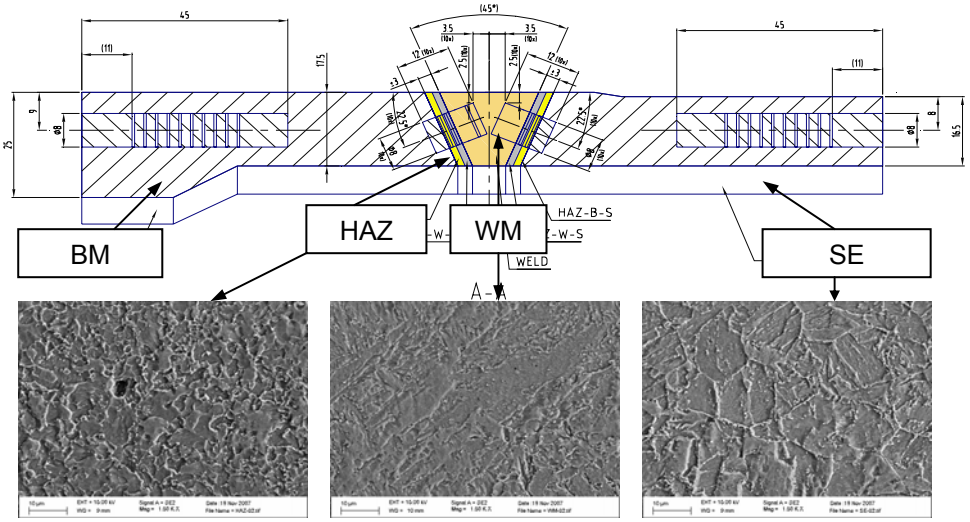

Fig. 4.20 Lateral view of the weldment section & SEM images of untested HAZ material, WM and SE material respectively

4.2.2 Uniaxial Specimens

4.2.2.1 Uniaxial Creep Specimens

In total 9 cylindrical pieces were extracted from both LICON and INTEGRITY pipes. Again a section from the unloaded part of the INTEGRITY pipe was used. Afterwards they were machined in order to obtain conventional uniaxial creep specimens as illustrated in the Figure 4.21.

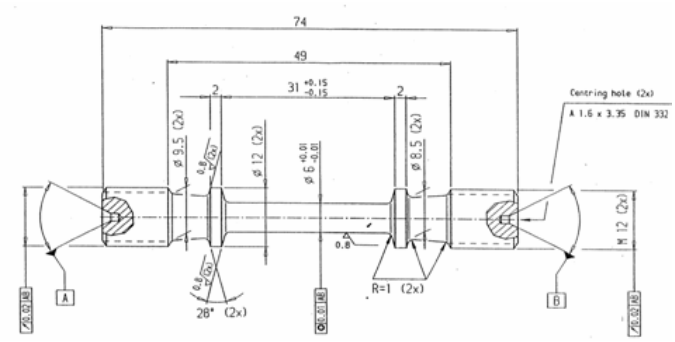

Fig. 4.21 Uniaxial creep sample

Fig. 4.22 Uniaxial creep sample – before and after the testing

Samples representative for BML, BMI, and SE material were produced in axial pipe direction, thus, assuring that the cross section of the uniaxial sample would be in the plane of the small punch disks. The weld metal uniaxial samples were extracted along the welding in circumferential direction because of the impossibility to be produced in axial direction due to size limitations.
A uniaxial creep sample before and after testing is presented in Fig. 4.22.

4.2.2.2 Uniaxial Tensile Specimens

Due to material shortage, in particular in the weldment zone, it was impossible to produce the same size uniaxial tensile samples as the ones used for obtaining the uniaxial creep properties. The design chosen for the tensile specimens is presented in Figure 4.23. Again the BM and SE material samples were extracted in the axial direction, and the weld samples – in circumferential direction.

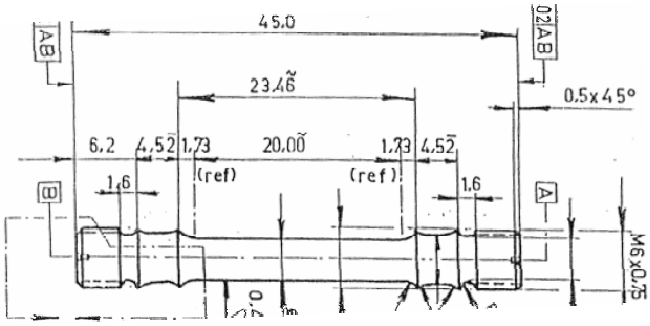

Fig. 4.23 Uniaxial tensile sample

4.3 Small Punch Test Set-up

4.3.1 Small Punch Creep Test Set-up

To set-up a SP creep test the CEN/ WS 21 Code of Practice (CoP) Part A [2] for the application and use of the SP test for creep rupture properties determination of metallic materials was strictly implemented. The CEN CoP was primarily developed as a result of research coordinated by the European Pressure Equipment Research Council (EPERC). Following a questionnaire distributed to several EPERC members, interested in this test method, a number of laboratories volunteered to participate in a SP Round Robin test programme [219] consisting of high temperature creep tests on disc specimens. The participating laboratories were CESI in Italy, Krakow Technical University in Poland, JRC-Institute for Energy of the EC in the Netherlands, and The University of Wales Swansea (UWS) in the UK. It was decided that, even though the SP technique could also be applied for fracture mechanics tests as well, the EPERC Round Robin would be limited to creep tests only.

The Round Robin exercise was organised primarily in order to contribute to the harmonisation of the test procedure for this new emerging method. Particular attention was to be paid to geometrical features of the test technique as well as test procedures. Main findings with a full discussion on partner inter-comparability of SP results were reported by Bicego [219]. A standardisation initiative for the SP test method, following on from the Round Robin, covering creep testing but including low temperature testing for the determination of tensile and toughness properties of metallic materials, has been made using of the CEN Workshop route, culminating in a Code of Practice (CoP) or CEN Workshop Agreement, CWA 15627 [2] published in December 2006. The proposals proscribed in the CoP such as test-piece and punch design and manufacture, application of load, temperature and strain measurement along with provision of a protective inert environment have been applied in their entirety to the 600^{o}C SP creep testing of P91 weldment material.

Although conceptually the SP creep test is quite simple – to apply a force to a test specimen and measure its dimensional change over time with exposure to a relatively high temperature – in practice it is more complicated. The experimental schematic SP creep set-up is illustrated in Figure 4.24.
Temperature control is critical (fluctuations must be kept within ±2.2^{o}C for 600^{o}C tests according to the Code of Practice), and the resolution and stability of the extensometers are an important concern as well. In addition environmental effects can complicate creep tests possibly leading to premature failures.

Another key aspect when applying the SP CoP is determining the load which has to be applied on the disk. In a conventional uniaxial creep test the key mechanical parameter is “stress” i.e. load/area whilst in the SP creep test it is only “load”. To set-up the SP experiments and to interpret the results of the test it is necessary to establish a correlation between the load F and the stress σ. The basic idea for determination of test load F is to answer the question: “What is the load value to use in the small punch test to obtain the same time to rupture as in a uniaxial conventional creep test?”

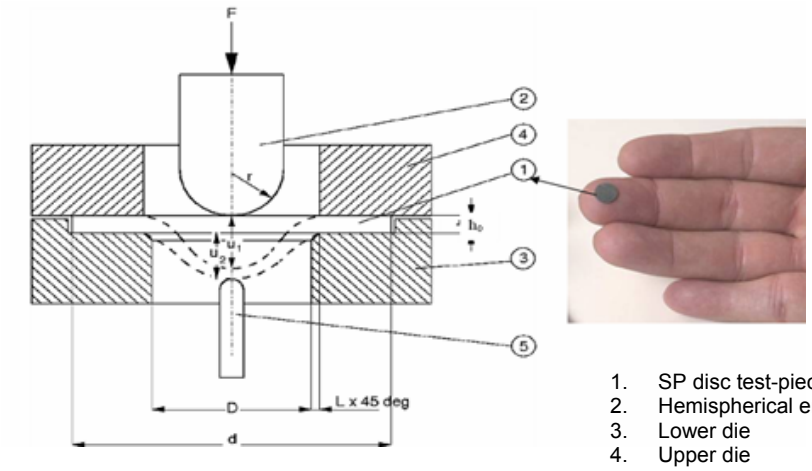

1. SP disc test-piece
2. Hemispherical ended punch
3. Lower die
4. Upper die
5. Dilatometer push rod

Fig. 4.24 Schematic of experimental SP set-up [2]

The load levels were calculated using equation (4.4), derived from the stretching membrane theory [182], giving the ratio of SP test load (F_{SP}) to the uniaxial creep stress (σ), as proposed in the CoP for SP Creep Testing, namely:

$$F_{SP}/\sigma = 3.33\, k_{SP}\, R^{-0.2}\, r^{1.2}\, h_o \qquad (4.4)$$

where r is the radius of the punch indenter, h is the thickness, R is the radius of the receiving hole and h_o is the initial disc thickness. The k_{SP} is a constant for the material under test (see Figure 4.25). The first tests were set up assuming that k_{SP} =1. According to the Code, after a series of SP tests, through comparison with the conventional uniaxial creep data, the calculated real value of k_{SP} should be determined and applied in the subsequent experiments. In this study, taking k_{SP} = 1.0, the ratio was calculated to be:

$$F_{SP}/\sigma = 1.4\ [mm^2] \qquad (4.5)$$

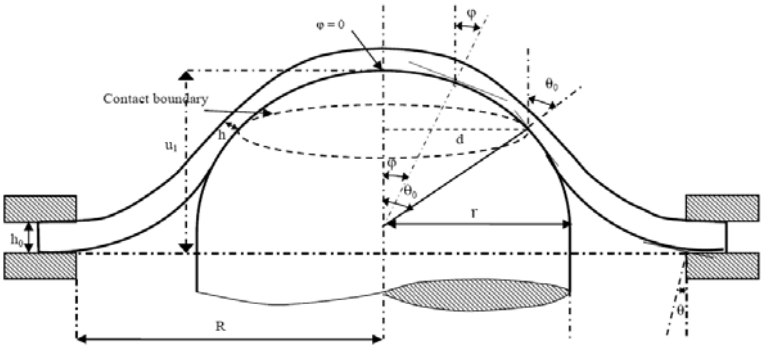

Fig.4.25 Geometry of deformation (CoP [2])

Test procedure

To set up a SP creep test the following procedure was applied:

- *Assembling the test*

- The bottom extensometer (LVDT1) was fixed at the completely horizontal main platform and was adjusted to correspond to ~ 15mA in the LabView SP control interface. The correction factors from LVDT1 and LVDT2 calibration procedure were inserted into "zero LVDT" and "Gain LVDT" fields beforehand.

- The SP sample was positioned in the recess of the lower die and clamped firmly around its edges by the upper die with the help of a stainless O- ring.

- The ceramic rod, used to obtain readings from the LVDT1, was inserted and fixed into the lower die in a way that the spring at the lower part of the rod allowed relatively free movement of the rod. The upper part of the rod was touching the underside of the sample.

- The test thermocouple (Temp.1) was fixed at the appropriate location in the upper die.

- The whole system - bottom LVDT/ lower die/ upper die/ sample/ thermocouple – was enclosed in a cylinder fixed on the main platform by 4 bolts.

- The furnace was inserted around the upper die. Thermal insulation was placed around it. The lower O-ring from the cooling system was fixed under the furnace itself.

- Stainless tube was inserted around the dies into the furnace and fixed firmly over the lower cooling O-ring. Consecutively the upper cooling O-ring and stainless heat sink were assembled on the top of the tube.

- The puncher rod was inserted carefully inside the system. It is important to avoid any impact which could deform the sample. Once the puncher was placed in contact with the sample the sealing assured the argon flux was provided by an open circuit. The puncher weight of approximately 17N, defined as so called pre-load, was consequently subtracted from the final load applied on the sample.

- A control thermocouple was placed into a small hole made in the furnace wall and another thermocouple was fixed for coolant temperature readings (Temp.2).

- *Heating phase*

- The furnace was switched on and the sample was heated up gradually- the time needed to reach and stabilise the test temperature was about 2h.

- While heating up the equipment, the bottom extensometer was also subjected to heating to a certain degree and was continuously changing its readings for that

reason; therefore, once the test temperature was reached the extensometer was set to zero before starting the test.

- *Loading phase and starting the test*

When the temperature of the sample was stable and full loading was applied, the test was started in the LabView interface: the output of the SP creep test was a graph where the vertical displacement was plotted versus time. Vertical displacement measurements were digitally recorded by the Field-Point and LabView interface at not regular time intervals: 1 measurement per each displacement of 10 microns or for each variation of temperature greater than 0.5°C. The temperature of the sample was controlled and maintained within ± 2^{o}C during the entire test.

4.3.2 Small Punch Fracture Test Set-up

To set-up low temperature SP fracture tests the CEN/ WSA 21 Code of Practice Part B [2] for the application and use of the SP test for tensile and fracture toughness properties determination of metallic materials was applied.

The aspects related to the precise temperature monitoring control and the stability of the extensometers is vital also here. Additionally, difficulties were imposed due to the very low temperatures applied: down to -192^{o}C. The extreme shrinkage of the specimen holder's material caused very strong friction between the puncher and the supports. As a result of this the registered curves were not reliable. Therefore, for these tests special cryogenic material Kel-F (PCTFE) was used for machining the specimen holders. Calibration of the LVDTs was done before every test.

Test procedure

- *Assembling the test*

- Mounting the SP sample: firstly the sample was clamped inside the holders. The clamping force had to be enough to avoid any sliding of the sample during the test.

- Positioning the holders: the holders were then positioned in the SP testing equipment and fixed. For room temperature tests the endoscopes of the camera were also fixed in order to allow images to be taken of the underside of the sample.

- Fixing the thermocouple: the thermocouple is located in a hole in the specimen holder, a few mm from the sample surface.

- The puncher was inserted and positioned in contact with the top surface of the sample; the loading head was fixed above the puncher and a preloading of about 60 kN was applied below the material elastic limit.

- Once all the equipment had been set up and before the initiation of every set of tests, the verification of the LVDTs was carried out as described in section 4.1.2 to assure their work in the calibrated range. Since movements due to mechanical

tightening amongst the different parts of the assembly were observed over the early stage of the test, several blank runs were performed in order to asses the possible influence in the displacement records. A solid block was placed in the position of the specimen, and loaded up to 150N. The outcome of the displacement readings showed a substantial deviation in the lowest range of load, up to approximately 65kN. From that point, the displacement values became almost constant. Taking this into account and from the analysis of the data series in the force range above 65kN (typically the start force of the tests), a maximum error on the average displacement due to this effect of ±0.005 mm was estimated.

- *Cooling and preload phase*

If the test had to run at a different temperature than room temperature the cooling chamber was activated. The electronic control of the chamber regulated the nitrogen flow to reach the target value, while the temperature of the specimen was monitored with the reading of the thermocouple. This equipment was designed to work down to cryogenic temperatures. During the cooling process, the force was kept by means of a cyclic method in the control software of the load frame, but the operational limitations of the machine and the fast shrinkage of the hardware due to very low temperatures imposed a practical margin in the preload of 65 to 80 kN. When the thermocouple indicated that the temperature in the proximity of the sample had reached the test temperature, a stabilization interval of 15 minutes was taken before starting the load stage.

- *Loading phase*

- The deflection rate was defined and introduced by the controller of the INSTRON machine. For all the tests the load was applied by fixing a constant displacement rate in compression - 0.003 mm/s.

- The LVDTs were set to zero and test started as the load increased with the displacement following the hardening law of the material. Since the SP sample was clamped strongly at its edge, under the action of the load it was forced to deflect in the receiving aperture of 4 mm diameter.

- The load, displacements from the two LVDTs and from the head of the INSTRON machine, and the temperature was recorded through a PC on to ASCII files. The load versus extension curve was recorded and monitored during the test on a chart displayed by the control program, revealing possible anomalies in the punch pin travel. When the fracture was detected by the sharp decline in the load value, the load was interrupted and the specimen retrieved.

- The output of the SP tensile test was a chart where the load was plotted versus the displacements recorded from the both LVDTs.

NB: Test procedures for uniaxial creep and tensile tests are not described in detail here, considering that these are standard tests and that they were only auxiliary tests in the present work.

5. RESULTS & DISCUSSION

The experimental results obtained in this thesis are grouped according to the type of testing technique and material investigated with a detail explanation of the trends in behaviour reported. The results can be categorized in two main groups:

- High temperature **creep**, and
- Low temperature **fracture** results

The **creep** results themselves are divided in two categories: conventional uniaxial tensile and small punch (SP) equi-biaxial *constant load* test results.
The **fracture** results obtained were SP equi-biaxial *constant rate* test results. They were compared with conventional fracture results (ductile to brittle transition temperature and fracture toughness data) obtained by other authors.
Additionally, high temperature tensile test were performed and results were used as an input for the FE model developed to predict the creep deformation of SP disc sample.

5.1 Creep Results

The creep results themselves are divided in two categories: conventional uniaxial tensile and small punch (SP) equi-biaxial const load test results.

5.1.1 Conventional Uniaxial Creep Results

The uniaxial creep testing consists in the following: a cylindrical specimen is loaded by a const tensile force parallel to its longitudinal axis (Figure 5.1). The sample is heated up to the desired temperature before the loading and is kept at that temperature during the whole test. The temperature is measured through a thermocouple attached to the sample. An extensometer, also attached to the sample, is used to measure the strain. The data recorded during the test are: test duration, temperature of the sample, stress applied, and the strain.
The outcome is registering of creep curve: strain versus time to rupture. A typical uniaxial creep curve is given in Figure 5.1. Four stages are distinguishable on the curve:

- Instantaneous initial elastic-plastic deformation;
- Primary creep (Stage I): during this stage deformation takes place and the resistance to creep increases as a results of which, the creep strain rate decreases;
- Secondary steady state creep (Stage II): the strain rate is minimum and it is considered to be a constant during this stage;
- Tertiary creep (Stage III): because of reduction in the cross-sectional area due to necking or due to internal void formation the strain rate increases exponentially ultimately leading to rupture.

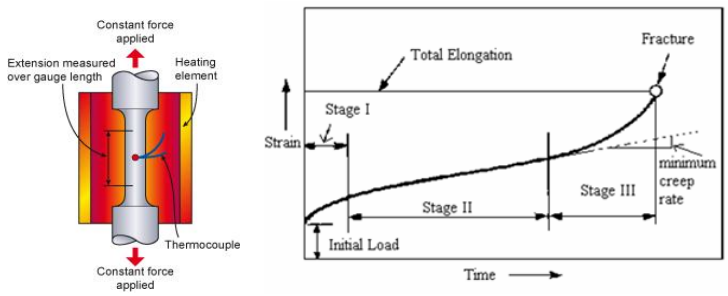

Fig.5.1 Scheme of uniaxial creep arrangement and typical uniaxial creep curve – strain versus time to rupture

Several important creep parameters, used in the remaining life-time evaluation can be estimated from the creep curves: minimum creep strain rate, time to rupture, onset of tertiary creep, creep rupture strength, etc. for specified testing conditions – temperature and stress. They are all key parameters in designing structural components for service at elevated temperatures. The rupture time, the onset of tertiary creep, and the creep rupture strength can be directly estimated from the creep curve. The time derivate of the secondary creep strain, i.e. the slope of the secondary creep stage, will give the minimum strain rate $\dot{\varepsilon} = \dot{\varepsilon}_{min} = \dot{\varepsilon}_s$ (Eq. 5.1), a function of the material properties, time t, temperature T and the stress σ:

$$d\varepsilon/dt = \dot{\varepsilon} = f(\text{mat.prop.}, t, T, \sigma) \qquad (5.1)$$

In total nine conventional uniaxial creep tests at 600°C on massive specimens (Figure 4.21) were carried out during the experimental programme. Together with six uniaxial tests performed for LICON project, they form the complete uniaxial testing data base used in the present work. The existing uniaxial creep data from LICON project for P91 base and weld metal were used as bases for determining the loading conditions for INTEGRITY material. In this way prognoses for the expected rupture times could be done. Once those uniaxial tests were concluded, the loads adopted in the equivalent (same temperature) small punch tests were chosen to give approximately the same lives.

5.1.1.1 LICON Uniaxial Creep Results

Four conventional uniaxial creep tests for fresh BM (BML) and two tests for weld material (WML) at 600°C were available from LICON data base. The stresses applied were: 120MPa, 135MPa, 145MPa and 150MPa for the base material, and 135MPa and 145MPa for the weld metal. For completeness and clarifying the tendency of the creep results, one more test on base LICON material at higher stress level – 160MPa was performed during the thesis experimental programme. Conventional creep curves obtained for BML and WML are shown in Figure 5.2 a&b.

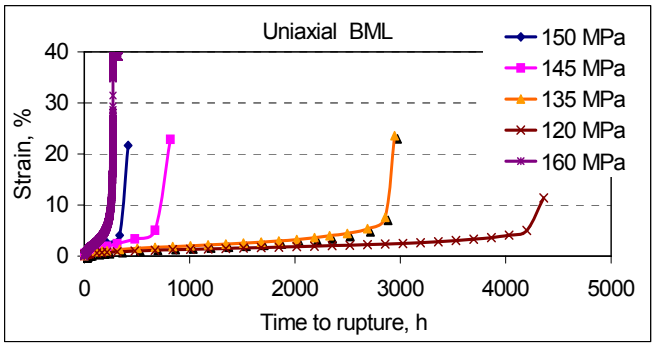

a)

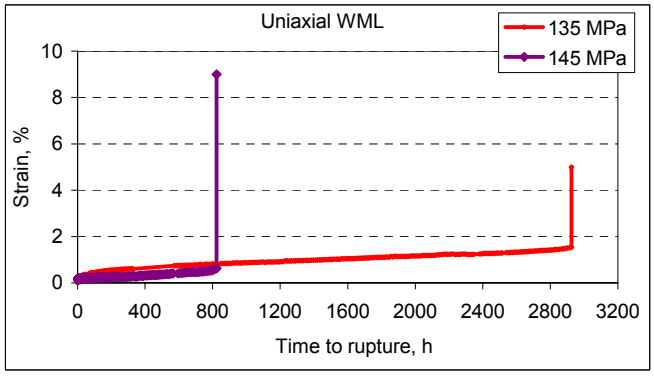

b)

Fig.5.2 Creep strain versus time for: a) LICON base metal (BML) & b) Weld metal (WML) under different stress conditions

5.1.1.2 INTEGRITY Uniaxial Creep Results

Eight uniaxial creep tests were concluded for the INTEGRITY material: three for the BM, three for the SE material, and only two for the WM, due to the limited quantity of weldment material available for testing. As indicated in the experimental chapter, only the non-stressed zones (neither tension nor compression) of the pipe were utilised for specimen production. All the tests were conducted again at 600^{o}C. Several stress conditions were employed to investigate the creep response and obtain stress rupture results. The stress levels adopted for the INTEGRITY testing material were comparable with the LICON stresses.

The uniaxial creep curves, representative for the BMI, SE metal, and WMI, under different stress conditions are shown in Figure 5.3 a, b and c respectively.

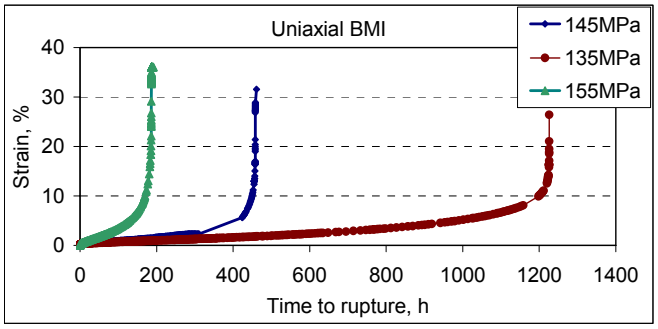

a)

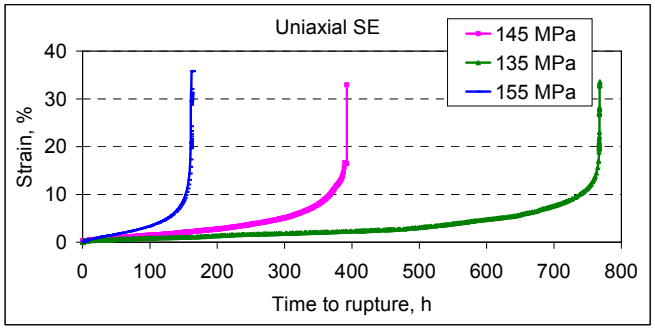

b)

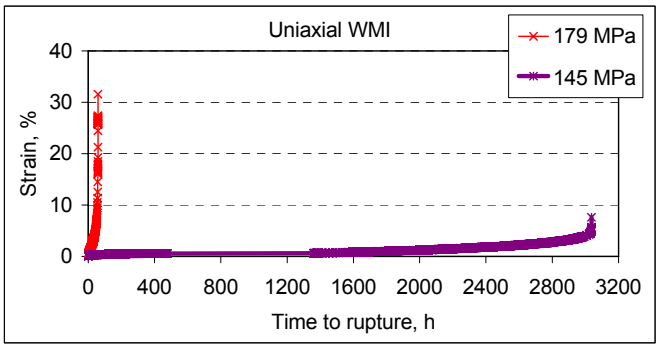

c)

Fig.5.3 Creep strain versus time for: a) INTEGRITY BMI; b) SE material; and c) WMI under different stresses

The effect of the stress on the creep parameters – strain, time to rupture, creep strain rate, is clearly visible from the above plots. The higher stresses cause reduction in the primary and secondary creep stages. The shorter secondary creep stage results in a higher creep strain rate and earlier failure. Specimens with higher strain rate exhibit also higher final strain. The influence of the stress on the primary creep and on the creep strain rate is more distinguishable if only the very first part

of the creep curve is plotted. Examples are given in Figure 5.4 for both base metals investigated.

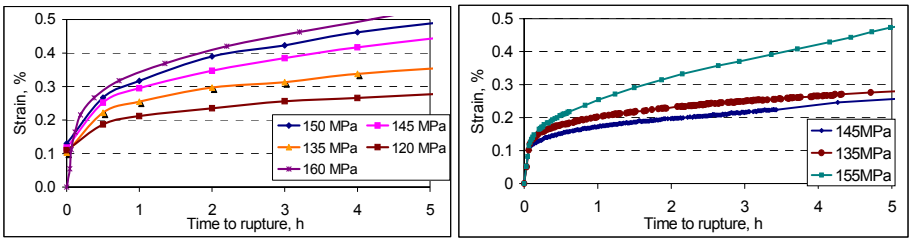

Fig.5.4 Creep strain versus time for BML & BMI (very first part)

To illustrate the creep response of the different materials investigated under single testing conditions, the creep curves are grouped according to the stresses applied. Thus, a comparison of uniaxial creep curves for BML, BMI, SE, WML & WMI samples under single testing conditions – 145MPa and 600°C is presented in Figure 5.5a. Again for better displaying of the creep strain rate tendency, only the initial part of the curves is plotted in Figure 5.5b (WML is missing in Fig.5.5b due to its coincidence with the WMI when using such scale).

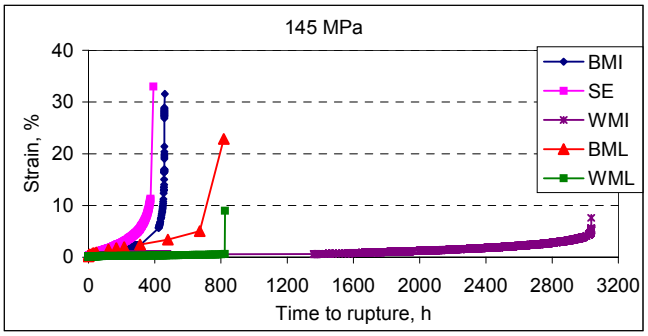

a)

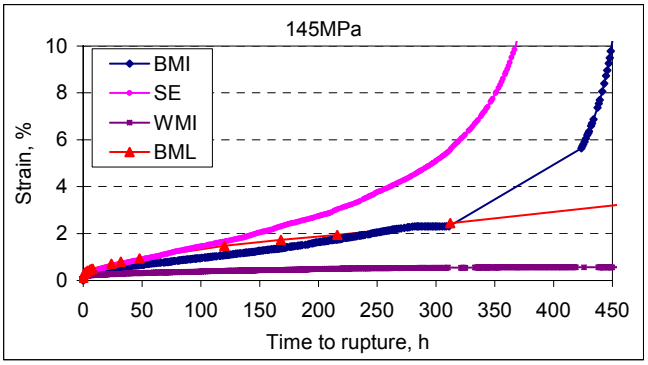

b)

Fig.5.5 Creep strain versus time for different materials under single testing conditions – 600°C and 145MPa: a) Complete curves & b) The very first parts

As can be seen from the graph above, SE material exhibits the highest creep strain rate, which makes it the weakest material. It is followed by the BM – LICON and INTEGRITY, and the strongest material with the minimum creep strain rate is the weld metal. The difference in the creep behaviour of the base metals might be due to the fact that the LICON BM is fresh material, and the Integrity BM was exposed for 5000h under internal pressure of 160bar at 600°C and subjected to a 4-point bending under 75.89kN loading.

Once the creep curve is registered the creep strain rate can be calculated for every time increment and the minimum strain rate can be determined, as well as, the onset of the tertiary creep stage. Examples of the time dependences of the creep strain rates for the INTEGRITY base metal under different stresses are presented in Figure 5.6 a, b & c.

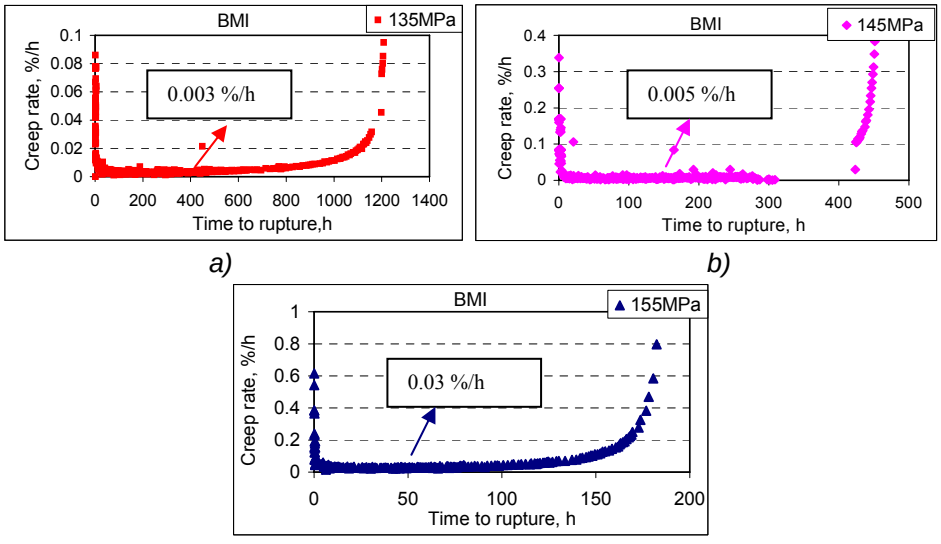

Fig.5.6 Creep strain rate versus time to rupture for BMI under: a) 135MPa; b) 145MPa and c) 155MPa

The test conditions and results for all uniaxial creep tests are given in Table 5.1.

Material	Stress MPa	Time hr	Strain %	Onset %	dε/dt %/h
BML	120	4361	11.4	4.1	5.62E-4
BML	135	2945	23.6	4.4	9.77E-4
BML	145	817	22.9	4.9	6.63E-3
BML	150	417	21.7	5.0	1.06E-3
BML	160	313	39.0	5.6	1.70E-2
BMI	135	1226	26.4	4.5	3.07E-3
BMI	145	461	31.6	2.4	5.09E-3
BMI	155	187	36.1	4.8	2.95E-2
SE	135	768	33.6	3.1	1.94E-3
SE	145	392	33.0	5.2	1.11E-2
SE	155	163	35.8	5.5	2.50E-2
WML	135	2925	5.0	1.5	2.50E-4
WML	145	824	9.0	0.6	3.33E-4
WMI	145	3036	7.6	4.7	1.42E-3
WMI	179	59	31.6	1.5	1.16E-1

Table 5.1 Conventional uniaxial creep tests results at 600^{o}C.

5.1.1.3 Stress-rupture results for uniaxial creep tests

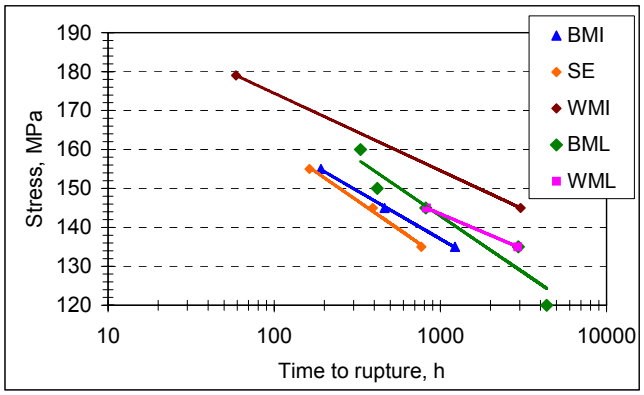

Fig.5.7 Uniaxial stress-rupture results

Stress-rupture tests are used to determine the time necessary to produce failure. Data are plotted in log-log scale. A straight line or best fit curve is usually obtained at each temperature of interest. This information can then be used to extrapolate time to failure for longer times.

The stress-rupture curves obtained for the investigated materials are put together in a one plot presented in Figure 5.7. A log/linear presentation is used for more clarity over this narrow stress range and there is no intention to indicate the kind of relationship which ensues.

In other words, the creep behaviour trend for all investigated materials could be approximated by a straight line at least for test durations up to ≈ 3000 hours. The above trends have to be confirmed for longer test durations, 10 000 hours and more, by completing more experiments.
According to the graph in Figure 5.7 the higher creep strength is exhibited by the weld metals, followed by the base metals from the two projects. Both weld and base metals follow the same trend in the stress-rupture curves – weld metals rupture dependences are parallel to each other and the same is valid for the two base metals stress-rupture curves. The weakest is the creep strength exhibited by the service exposed material from INTEGRITY project. Predictions on the duration of creep test performed under different stresses for the investigated materials can be done simply by extrapolating the trends shown above. Later these trends will be used to draw correlations for the SP tests.

5.1.2 Small Punch Creep (SPC) Results

To gain experience and calibrate the SP creep devices, located in the Mechanical Testing Lab of the Institute for Energy (IE), Joint Research Centre (JRC) preliminary experimental work during the first stages of the current project was completed. Calibration of the equipment has been performed several times during the experimental program. Some test results were disregarded and test repeated due to doubts in the experimental set-up, lack of readings, temperature uncertainty or equipment breaks-down. The results given below are only results that can be considered repeatable and trustworthy.

In total 29 SPC tests have been completed. The test itself consists in the following: a non-deformable puncher is pushed under a const force F against a disc, heated up in advance to a desired test temperature and maintained at that temperature during the whole test (Figure 4.24). As a result, the disc bulges into a hole. The data registered during the test are: time, temperature and displacements of two LVDTs. One of the LVDTs (bottom one) measures the central deflection of disc and the second (back-up) one measures the displacement of the puncher rod. The difference between the two measurements, which is minimal, determines the central disc thinning. The main SP test result is a SPC curve representing central vertical deflection (mm) versus time to rupture (h).

The test specimens were discs 8mm in diameter and 0.5mm thick, made of P91 high-alloy martensitic steel and its weldment. All SP creep tests were carried out at 600^{o}C and loadings ranging from 189N up to 280N, following exactly the procedures prescribed in the Code of Practice part A [2].
The SP creep curves presented below are grouped accordingly to the type of material investigated and testing conditions applied. Two test components were used as sources to produce SP samples: LICON fresh material pipe [217] and welded INTEGRITY pipe [218].

5.1.2.1 LICON SPC Results

The LICON base material was the first to be available for SPC testing. The aim was several preliminary tests to be conducted to calibrate the equipment and compare subsequently the results with the BM taken from the INTEGRITY project, which was the main material source considered for the scope of the thesis.
A circular rod of 8mm in diameter was extracted from a section, taken from the LICON fresh BM pipe in axial direction and sliced into discs with 0.5mm thickness. Four SPC tests under different loadings – 189N, 217N, 240N and 250N, have been completed. The registered SPC curves are presented in Figure 5.8.

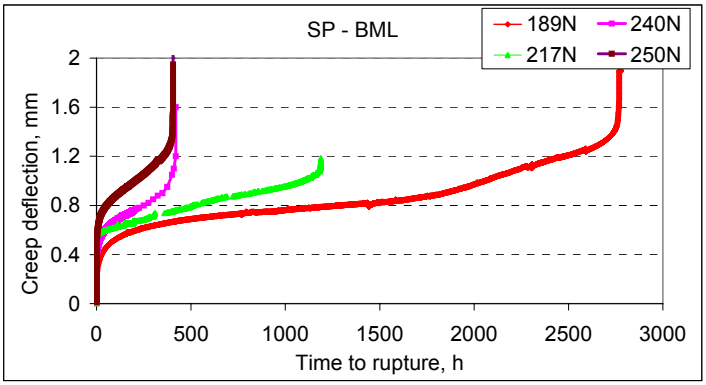

Fig.5.8 SPC curves under different loadings for LICON material

5.1.2.2 INTEGRITY SPC Results

Small disc were produced from different zones of the weldment of the INTEGRITY pipe, as described in Chapter 4. Totally 25 SPC tests for the base material, service-exposed metal, weld metal and heat-affected zone (respectively FG-HAZ, CG-HAZ on both BM and SE pipe sides) were completed. The registered SPC curves are presented in the figures below: Figures 5.9 to 5.14.

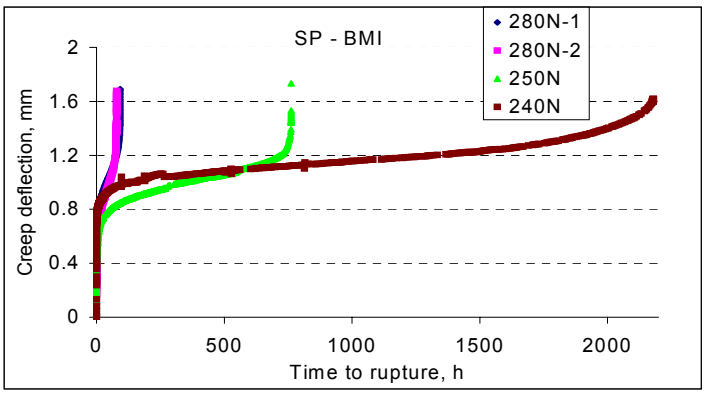

Fig.5.9 SPC curves for BMI under different loadings

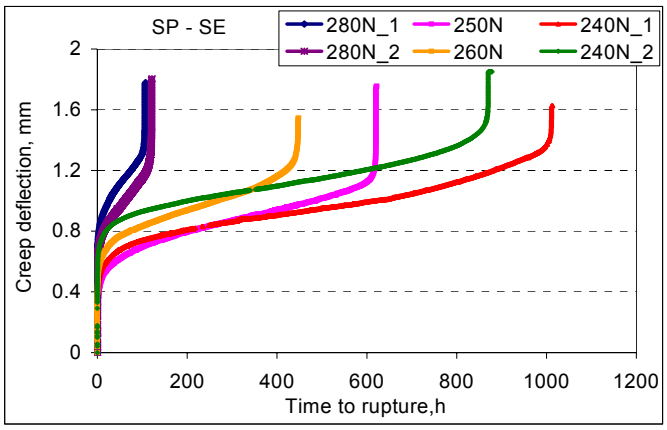

Fig.5.10 SPC curves for SE metal under different loadings

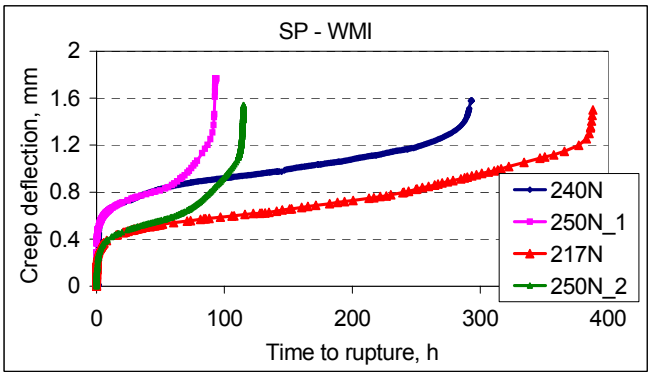

Fig.5.11 SPC curves for WMI under different loadings

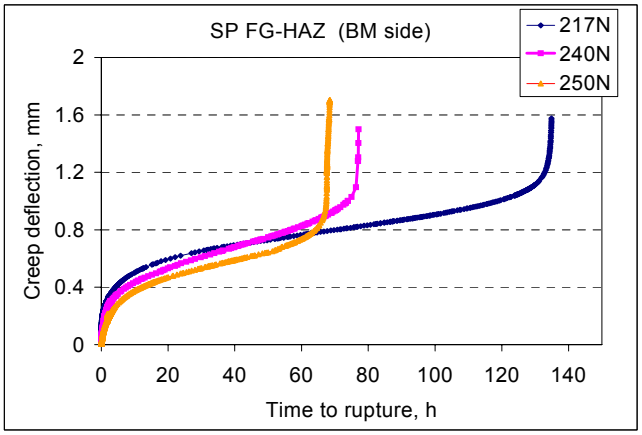

a)

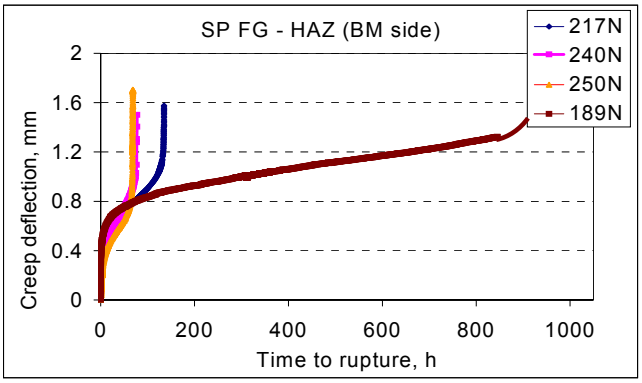

b)

Fig.5.12 SPC curves for FG-HAZ (BM side) under different loadings; a) Only 3 loadings included; b) All 4 loadings included

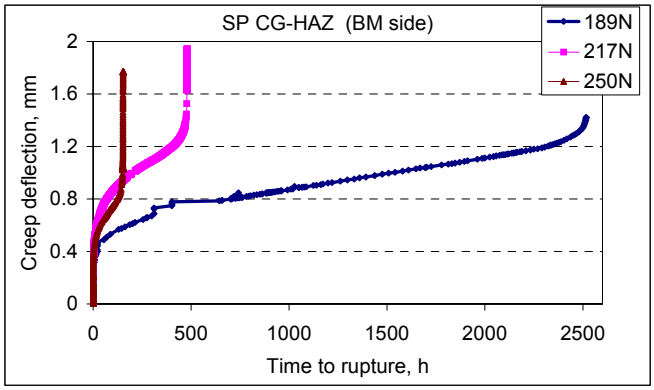

Fig.5.13 SPC curves for CG-HAZ (BM side) under different loadings

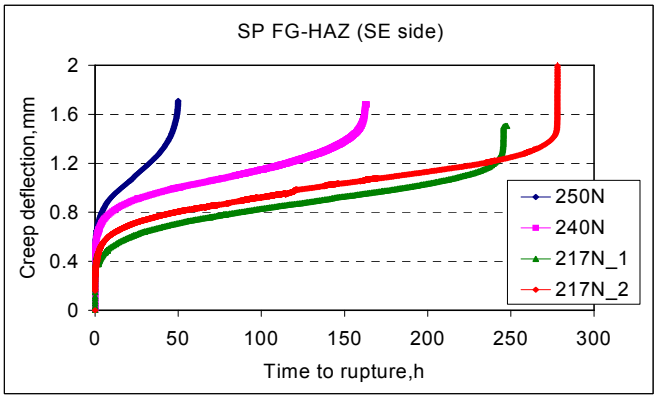

Fig.5.14 SPC curves for FG-HAZ (SE side) under different loadings

A comparison of the SPC curves under a single loading condition is shown in Figure 5.15, which particularly emphasizes the limited secondary regime for all components of the weldment (weld and HAZ) when compared to the P91 alloy. The FG-HAZ exhibits much shorter rupture times than the BM and SE samples, under the same testing conditions. The weld material has a similar rupture time to the CG-HAZ sample.

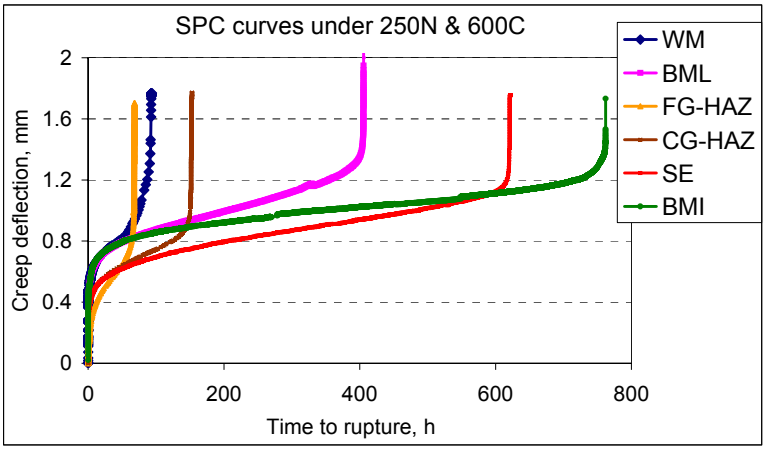

Fig.5.15 SPC curves for the investigated materials under single testing conditions

From the SPC curves presented above it is clear that the initial instantaneous deflection does not play a crucial role in terms of both creep deflection rate and time to rupture. The initial deflection depends to a considerable degree on the loading mode. Fast (within 2-3 sec) but smooth loading needs to be applied initially on the sample surface. Any vibrations and impacts that could influence the initial deformation of the sample must be avoided as much as possible. In our case pistons working with compressed air were employed to load the samples.

The complete list of the creep SP test results obtained for the purposes of thesis is presented in Table 5.2.

Material	Load, N	Calculated stress, MPa	Creep deflection, mm	Time to rupture, h
BML	189	135	1.58	2766
BML	217	155	1.19	1188
BML	240	171.5	1.6	420
BML	250	178.6	2	405
BMI	240	171.5	1.62	2180
BMI	250	178.6	1.5	762
BMI	280	200	1.68	79
BMI	280	200	1.69	92
WMI	217	155	1.5	388
WMI	240	171.5	1.58	293
WMI	250	178.6	1.54	115
WMI	250	178.6	1.77	94
SE	240	171.5	1.63	1013
SE	240	171.5	1.85	878
SE	250	178.6	1.76	621
SE	260	185.7	1.55	448
SE	280	200	1.8	122
SE	280	200	1.78	108
CG-HAZ (BM side)	189	135	1.42	2517
CG-HAZ (BM side)	217	155	1.94	480
CG-HAZ (BM side)	250	178.6	1.77	153
FG-HAZ (BM side)	189	135	1.81	999
FG-HAZ (BM side)	217	155	1.58	134
FG-HAZ (BM side)	240	171.5	1.5	77
FG-HAZ (BM side)	250	178.6	1.7	68
FG-HAZ (SE side)	217	155	1.6	278
FG-HAZ (SE side)	217	155	1.5	248
FG-HAZ (SE side)	240	171.5	1.7	163
FG-HAZ (SE side)	250	178.6	1.7	50

Table 5.2 Small punch creep test results at 600^{o}C

5.1.3 Comparison between uniaxial and SP curves

The overall shape of the SPC curves as a function of applied load is qualitatively similar to that recorded during conventional uniaxial creep tests for the same material and test temperature (Figure 5.16).

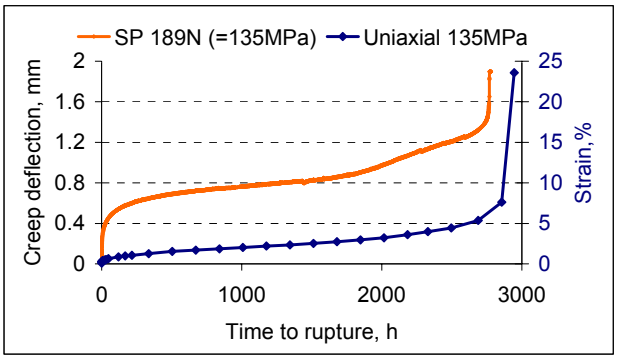

Fig.5.16 Comparison between equivalent LICON BM uniaxial and SPC curve

Four stages are clearly detected in both types of creep curves: in the initial stage, strain occurs at a relatively rapid rate – elastic/plastic bending deflection stage; it is followed by primary creep stage when deflection rate gradually decelerates until it becomes approximately constant during the third stage. This constant creep rate is called the minimum creep rate or steady-state creep rate since it is the slowest creep rate during the test. In the fourth stage – tertiary creep, the strain rate starts to increase indicating the onset of final fracture of the specimen and it accelerates until failure occurs.

Thus, similar shapes of both plots allow evaluation of analogical parameters of both types of creep tests:

- Primary stages with decreasing rates of strain or deflection;
- Stages with minimum rates of strain $\dot{\varepsilon}_s$ or the deflection rate $\dot{\delta}_s$;
- Time to rupture or bursting of the disc t_r; and
- Creep ductility or total deflection.

In principle, the only directly comparable parameter appearing in time dependences is the time to rupture t_r; the other corresponding parameters have different physical dimensions, e.g., minimum strain rate $\dot{\varepsilon}_s$[1/h] and relevant minimum deflection rate $\dot{\delta}_s$ [mm/h]. Therefore, only time to rupture can be used as the reference quantity in an evaluation of relationships between the results of conventional creep and SP creep test. The time to rupture is used as a reference also to establish F_{SP}/σ ratio when setting-up the SPC test.

The shape of the SPC curves is changing as a function of applied load in a manner similar to that in the conventional creep tests (Figure 5.17 a & b).

Just as for the conventional tests, the rupture lives are found to increase with decreasing load. Higher loads reduce the extent of the primary creep stage and

practically eliminate the secondary creep stage, with the results that the creep rate accelerates almost from the beginning. With decreasing loads, these two stages become clearly defined, usually at the expense of the tertiary creep stage. A major difference in the curves can be noticed in the first two regions: the initial deformation (elastic + some plastic deformation) and primary creep stage. During these two stages bending is the main process that controls the deformation in the SP test which is missing in the uniaxial test.

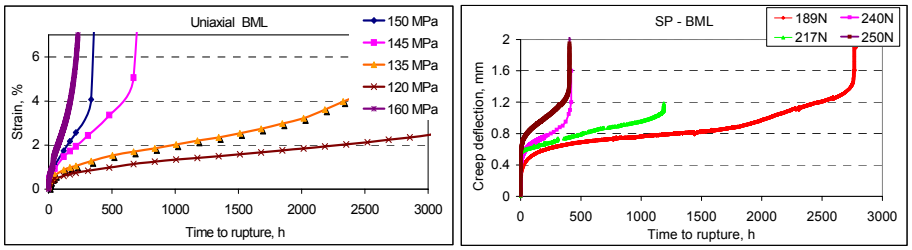

a) *b)*

Fig.5.17 a) LICON uniaxial creep curves under different stresses and b) LICON SPC curves under different loads

5.1.4 Stress/load dependence of the minimum strain/deflection rate

There is a straight relationship between the applied stress and the minimum strain rate, which characterizes the secondary steady state creep: the higher stresses accelerate the creep strain rate with the result that specimens fail in a shorter time (see Figure 5.18). However, the creep rate varies non-linearly, but as a power function with the stress, according to the Norton creep law (Eq.5.2). Therefore, the stress dependence of the secondary creep strain rate in case of uniaxial creep testing is generally expressed as:

$$\dot{\varepsilon}_s = A\,\sigma^n \qquad (5.2)$$

where "A" and "n" are stress independent constants, that characterize creep behaviour. Similarly, in case of SP creep test, the force dependence of the small punch creep behaviour is approximated by using the central deflection rate $\dot{\delta}_s$ at the secondary stage for $\dot{\varepsilon}_s$ and the force F for σ. Thus, the power (Norton) creep law in case of the SPC test can be re-written as:

$$\dot{\delta}_s = A^* F^{n^*} \qquad (5.3)$$

The stress dependence of the minimum strain rate $\dot{\varepsilon}_{min} = \dot{\varepsilon}_s$ and the force dependence of the minimum deflection rate $\dot{\delta}_{min} = \dot{\delta}_s$ both in log/log scale are illustrated in Figure 5.18 a&b. The creep parameters "n & A" for uniaxial testing and respectively "n* & A*" for SPC testing for BMI, SE, and WMI can be determine from these plots. The values of the force exponent "n*" are only to show the similarity of the SP tests with the uniaxial tests. They have no meaning and are not supposed to be used when calculating the creep parameters used later in the modeling

stage. However, the same variation in the stress exponents "n" for the three materials is observed also for the force exponents "n^*". A factor of $\Psi = n/n^* \approx 1.2$ is needed to correlate directly the uniaxial with the SPC results.

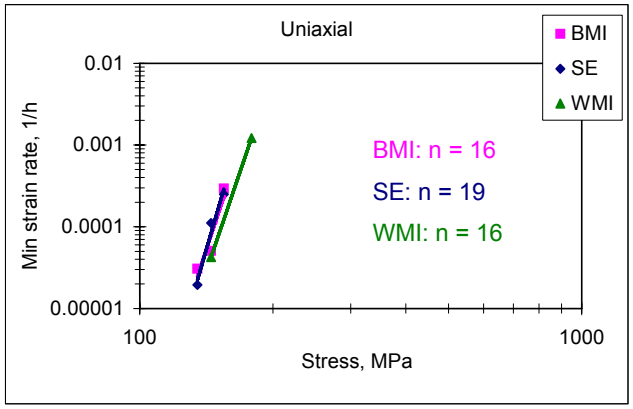

a)

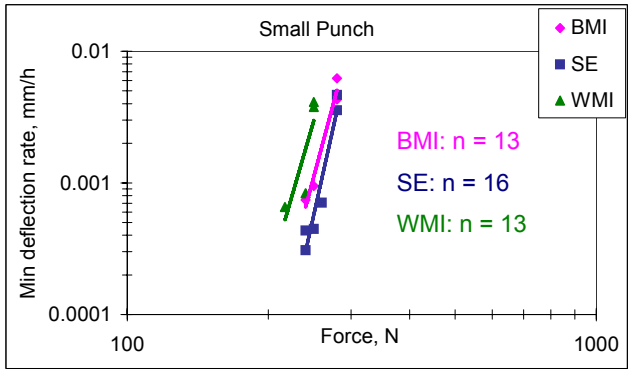

b)

Fig.5.18 a) Stress (MPa) dependences of the min creep strain rate (1/h) and b) SP force (N) dependence of the min deflection rate (mm/h)

Milička and Dobeš [201] correlating P91 BM uniaxial creep and SPC results for three different temperatures – 823K, 848K and 873K, and using $F/\sigma = 1.6$ mm^2 obtain stress exponent "n" and force exponent "n^*" both equal to 12, thus giving a correlation factor of $\Psi = 1$. For comparison the number of tests in their experimental programme is considerably greater and for a more precise calculation of Ψ more numerous tests must be accomplished for the INTEGRITY material. Another factor that could influence the discrepancy in the Ψ is the duration of the tests. While the maximum test duration in this thesis is 3036h, tests up to 1000h only are accomplished in [201]. Extrapolation to longer test times could be the subject of dispute as the longer the test time, the greater is the corrosion damage of the thin disc surfaces, even under a relatively good protective atmosphere. The influence of the surface corrosion on the results of the SPC tests has not yet been studied. However, from the thesis results for BM, SE and WM and from the results obtained

by Milička and Dobeš [201] for P91 BM at different temperatures, it could be concluded that the same Ψ factor could be used for P91 steel, independently whether the BM or weldment material is under consideration and no matter what testing temperature is chosen.

5.1.5 Time dependence of the minimum (strain/deflection) rate

The dependence of rupture life on secondary creep strain rate in a conventional uniaxial test is well documented and it is usually described by the Monkman-Grant relation [192].

$$M = \dot{\varepsilon}_s . t_r \quad \text{or} \quad \dot{\varepsilon}_s \propto t_r^{-p} \tag{5.4}$$

Power law relations for the secondary deflection rate could be drawn also for the SPC tests (Figure 5.19). Thus, it can be written:

$$M_{(SP)} = \dot{\delta}_s . t_r \quad \text{or} \quad \dot{\delta}_s \propto t_r^{-p^*} \tag{5.5}$$

where "p" and "p^*" are time exponents for uniaxial and SP test.

To check the validity of this relationship the time to rupture t_r which is the common quantity in the both type of experiments is plotted as a function of the minimum strain rate, corresponding to Eq. (5.4) and minimum deflection rate, corresponding to Eq. (5.5). For direct comparison the minimum strain and deflection rate are plotted on one graph using double y-axis for each material - BMI (Figure 5.19 a), SE metal (Figure 5.19 b) and WMI (Figure 5.19 c).

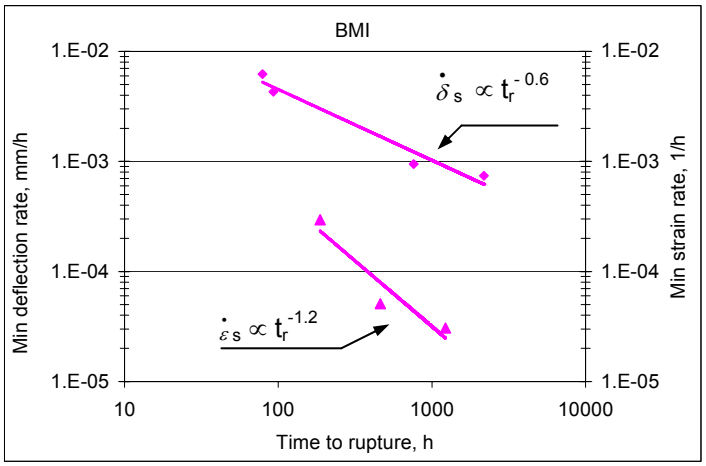

a)

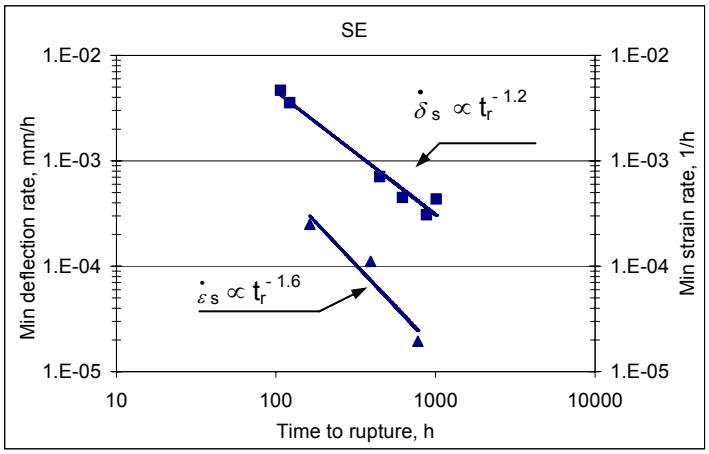

b)

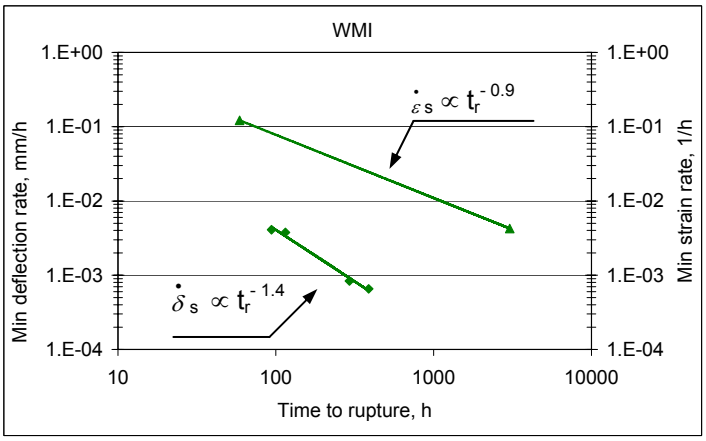

c)

Fig.5.19 Time dependence of the uniaxial minimum strain rate (1/h) and the SP minimum deflection rate (mm/h) for a) BMI, b) SE and c) WMI

From the present results it is difficult to draw a conclusion on the time exponent that should be used to correlate uniaxial with the SPC results. No unique time exponent can be determined from the available results. Again the reason for that might be the large difference in terms of test duration.

From Eqs. (5.4) and (5.5) the relationship between $\dot{\delta}_s$ and $\dot{\varepsilon}_s$ can be derived by a comparison of their values corresponding to identical times to rupture t_r:

$$\dot{\delta}_s \propto (\dot{\varepsilon}_s)^{p/p^*} \propto (\dot{\varepsilon}_s)^{\Phi} \tag{5.6}$$

$\Phi = 2$ for BMI, $\Phi = 1.3$ for SE and $\Phi = 0.6$ for WMI.

Milička and Dobeš [201] obtain analogous time exponents: p=1.1 and p^*=1 for P91 BM conventional and SPC data respectively for a test duration up to 1000h, which confirms the close similarity of the two types of test. Thus, the Φ ratio determined from their experiments is ≈1.1.

Finally it can be concluded, that the Monkman-Grant relation for SPC testing follows the same pattern as that for the uniaxial creep test. The above reported relation could be used in two different ways, the first being purely practical. Since the minimum creep strain/deflection rates are attained at times smaller than the time to fracture, the Eq. (5.4) and Eq. (5.5) can lead to an improved assessment of expected time to fracture in an unfinished test. The second way is connected with the possibility of correlating the results of conventional and small punch tests. It is hoped that relationships can be established which correlate minimum creep strain rate from a conventional uniaxial creep test and the minimum deflection rate from a punch test and vice versa.

5.1.6 Stress-Rupture results: comparison between uniaxial and SPC test results

5.1.6.1 P91 Base Metal & Service Exposed material

The stress rupture results from conventional creep tests for LICON base metal and those obtained from SP tests based on the SP load/stress ratio, taken from the Code of Practice (Eq.4.4) are shown in Figure 5.20a. A divergence, between the two stress-rupture curves, is evident and it gets more pronounced for the shorter tests, i.e. when the higher loads are applied. However, a good correlation is apparent for the longest test time ~3000h.

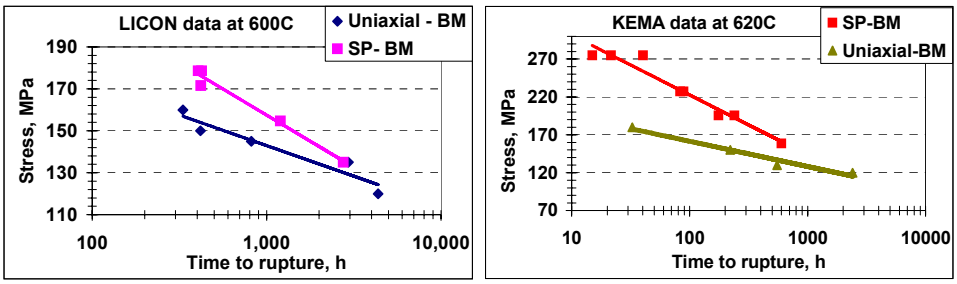

a) *b)*

Fig.5.20 Uniaxial and SP stress-rupture data comparison for: a) LICON and b) KEMA [220]

Similar disparity between SPC and uniaxial creep results was reported for P91 also by Li and Sturm [220] shown in Figure 5.20b. The presented SPC test results for P91 base metal were obtained at a temperature of 620°C and loadings ranging from 300N to 520N. They were plotted together with uniaxial creep test data obtained at the same temperature and stresses ranging from 120MPa to 180MPa. As for the LICON base material, the SP tests were less conservative for the higher loads, i.e. shorter tests. If the SP stress-rupture curve is extrapolated for longer test times (approximately 3000 hours) it will coincide with the uniaxial results. The load-

stress ratio used from the authors was $F_{SP}/\sigma = 1.89*k_{SP}$, while the one used in the thesis was $F_{SP}/\sigma = 1.4*k_{SP}$. The difference arises from the difference in the puncher radius: 1.25mm used in [220] against 1mm used in the present load-stress ratio calculations.
The parameter k_{SP} is proposed as an indicator of material creep ductility and is introduced in the Code of Practice for SP testing to enable correlations between SP and conventional tests to be made for different materials exhibiting different creep ductilities. The above SPC stress-rupture results for both LICON and KEMA were obtained using ductility factor $k_{SP}=1$ for all applied loading conditions.
It is evident, that the SPC tests conducted under higher loadings, being also higher ductility tests would need a ductility factor $k_{SP}>1$ to compare directly the rupture times obtained by the SPC and the uniaxial tests. In fact, a ductility factor ranging from $k_{SP}=1$ to $k_{SP}=1.15$ for the LICON material (Figure 5.20a) and $k_{SP}=1$ to $k_{SP}=1.52$ for the KEMA material (Figure 5.20b) should be used to get down the SPC results to the stress levels used in the uniaxial tests. In this case the stress-rupture results obtained by SPC and uniaxial creep tests would be directly comparable – comparable creep strengths for the same rupture times.
A load dependence of the ductility factor can be drawn taking into account both LICON and KEMA data (Figure 5.21). Nevertheless, the results were obtained from different material batches, different testing temperatures and different equipment employed, in particular different puncher radius, the points lie on a single straight line with a negligible discrepancy. This could be a reliable way to calculate the k_{SP} when setting-up the SPC test in order to obtain comparable rupture times with the uniaxial test corresponding to the same creep strength. To verify this curve of course, more tests under lower (<189N) and higher (>520N) loadings for P91 BM should be included.

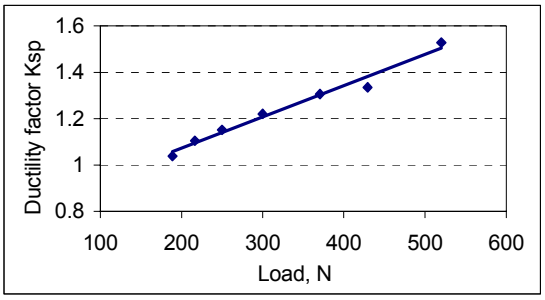

Fig.5.21 Load dependence of the ductility factor k_{SP} determined from LICON and KEMA creep results

Milicka and Dobes [38] determined a ductility factor $k_{SP} = 2.85$ again for P91 steel over the temperature interval from 823K to 873K. Practically identical values of $k_{SP} \cong 2.6$ were obtained in not very extended experiments on other heat-resistant steels [224]. On the other hand, values substantially lower ($k_{SP}<1$) were obtained in other metallic materials and metal matrix composites, e.g. [225].
However, a single material with significantly different creep ductilities at different stress levels is, in fact, also behaving like another material and the simplistic concept of a constant k_{SP} for a single material should be re-assessed.

The INTEGRITY base and SE metals show similar creep behaviour (Figure 5.22 a&b). Microstructural examination of the SE material shows no evidence of creep damage prior to the SP test. The longest test was only 2180 hours. Longer term tests (3000 hours and more) should be completed to confirm the tendency observed above and the "k_{SP} theory". Due to limited time it was not possible, but it should be re-considered as future work.
Plotting together the stress-rupture results from the uniaxial and SP creep test a nearly parallel trend-line tendency is observed, i.e. unique but larger correction value of the ductility factor k_{SP} (~1.28) must be employed for the applied load/stress interval to bring the governing creep stresses closer together. Possible concurrence of the longer term SP and uniaxial results should be expected also for BMI and SE material, thus passing from $k_{SP} \approx 1.28$ to $k_{SP} = 1$.

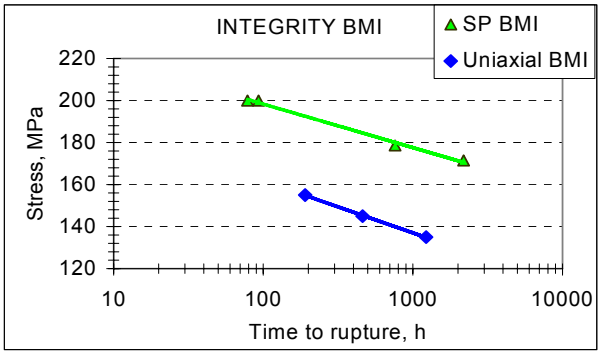

a)

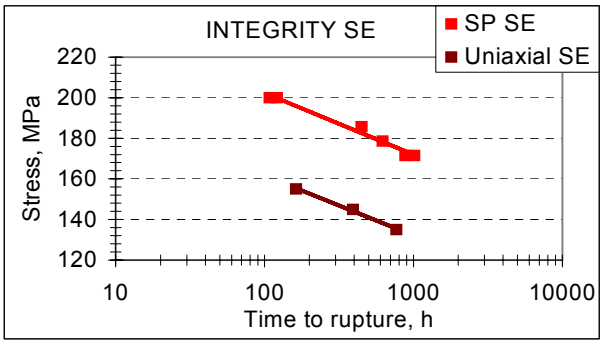

b)

Fig.5.22 Uniaxial and SP stress-rupture results for a) BMI & b) SE material

The curve giving the load dependence of the ductility factor k_{SP} can be re-plotted including also the INTEGRITY results (Figure 5.23). Some discrepancy is observed for loads about 250N and the reason for that could be the lack of longer term test data from the INTEGRITY material. For test durations of 3000h and more, k_{SP} factor close to 1 could be expected, thus, most likely reducing also slightly the k_{SP} values for higher loads. Still the accuracy is acceptable and the curve could be used for a prior k_{SP} evaluation.

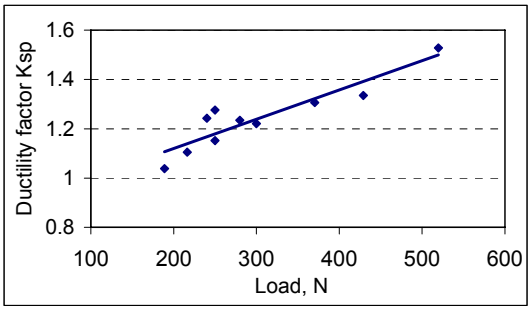

Fig.5.23 Load dependence of the ductility factor k_{SP} determined from LICON, KEMA and INTEGRITY creep results

5.1.6.2 Welded P91 material

The stress-rupture results for WM uniaxial and SP specimens are presented in Fig.5.24. The uniaxial weld stress rupture LICON and INTEGRITY results were found to be very similar to that reported by Seitisleam et al [96] for conventional tests on P91 weld material at the same temperature. As can be seen from the graph the discrepancy is almost negligible and ductility factor k_{SP} =1 could be simply applied to pass from load (N) in SP test to stress (MPa) in uniaxial test.

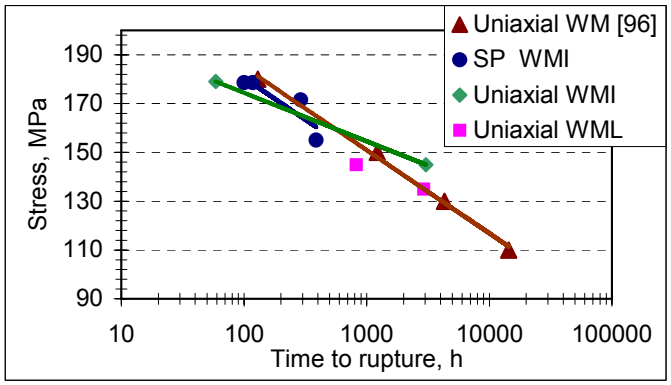

Fig.5.24 Uniaxial and SP stress-rupture results for P91 weld metal

Obviously, since weld metal tests are low ductility tests, applying k_{SP}=1 will be appropriate for correlating the SPC results with those from the uniaxial tests.

The stress-rupture results obtained from all investigated INTEGRITY materials – BMI, SE, WMI, FG-HAZ and CG-HAZ are presented in Figure 5.25. The weld material compared to the other investigated materials has exhibited creep lives longer than for the FG-HAZ, which exhibits the most inferior stress rupture behaviour, but still much shorter than those for the base & SE metal. The SPC results for the CG-HAZ are quite similar to those for the weld metal.

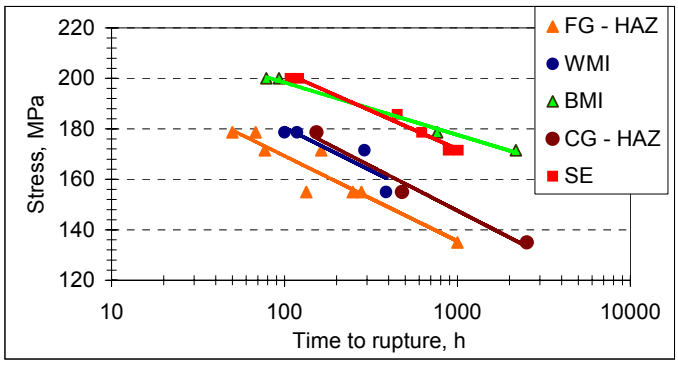

Fig.5.25 Comparison between SP stress-rupture results obtained from different zones of the INTEGRITY pipe

The results for the FG-HAZ have been determined from both sides of the weld, as mentioned above and they exhibited similar stress-rupture values. For a better presentation they are given just in one colour - orange. Still the discrepancy in the results looks bigger than it is in real life due to the linear type "stress" axis instead of logarithmic type.

It is impossible to consider the contribution of k_{SP} values for the HAZ as no uniaxial data could be possibly procured from the actual INTEGRITY HAZ. This could only be done from a simulated HAZ material [96, 217]. However, considering that the HAZ ductility is even lower than the weld metal ductility, k_{SP} = 1 should be suitable also for HAZ SPC results. Indeed the very purpose of developing the SP test is to be able to understand the creep behaviour of areas too small for extracting conventional or even miniaturized creep specimens.
To check the k_{SP} theory for the HAZ material the SP HAZ data obtained from INTEGRITY material was compared with the uniaxial data obtained from a simulated (Sim) HAZ of P91 material by Sandstrom et al. [96] and simulated HAZ of LICON material, all tested at 600^{o}C.

Sandstrom et al. [96] conducted a series of furnace thermal simulations to reproduce microstructures appearing in the actual HAZ of a P91 welded pipe. To do this, the as received parent material was furnace heat treated at given austenitizing temperatures varying from 760^{o}C to 1300°C. After a holding time of 20 minutes, the material was cooled in air. The material was then tempered at 760°C for 2 hours followed by air cooling. Those treatments at temperatures of 1100°C and above, i.e., above AC_3, resulted in a complete martensite-to-austenite phase formation, austenite grain growth and carbide dissolution. These microstructures have the same type of grain structure as in the coarser part of the HAZ of a P91 weldment. However, the simulated prior austenite grain size is larger than in the actual weld, see Figure 5.26 a&b. This is the reason why the authors calls this zone "extra" CG-HAZ. Treatments at temperatures of 850^{o}C and 900°C, i.e., between AC_1 and AC_3, gave rise to a partial martensite-to-austenite phase formation and carbide dissolution. These microstructures match that in the intercritical FG-HAZ of the weldment; see Figure 5.26 c&d.

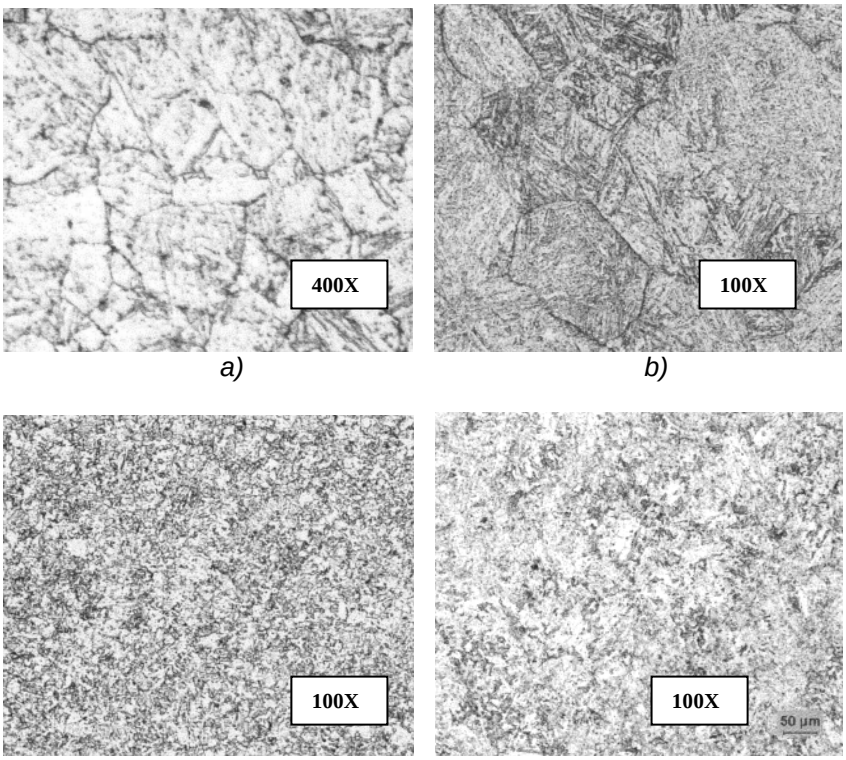

a) *b)*

c) *d)*

Fig.5.26 Optical micrographs showing microstructures of: a) CG-HAZ at 400X magnification; b) Simulated CG-HAZ at 1300^{o}C at 100X; c) FG-HAZ at 100X; and d) Simulated FG-HAZ at 850^{o}C at 100X [96]

SEM images of the INTEGRITY FG-HAZ and CG-HAZ are presented in the next Figure 5.27a&b. The microstructure can not be directly comparable with the micrographs above due to the bigger magnification used. However, the difference between the microstructure of the FG-HAZ and CG-HAZ is clearly visible.

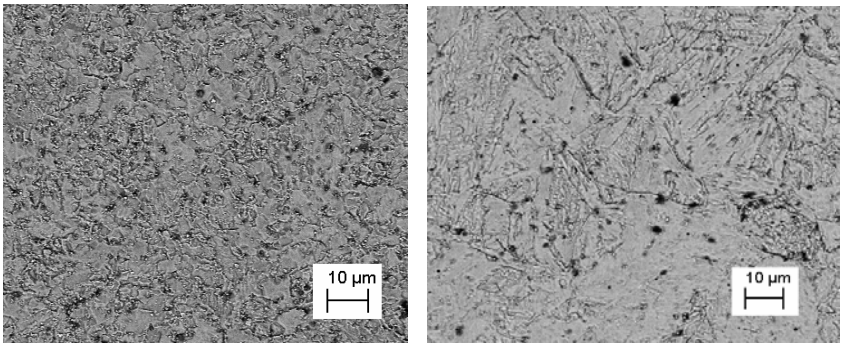

a) *b)*

Fig.5.27 SEM microstructural images of: a) INTEGRITY FG-HAZ and b) CG-HAZ

As for the LICON FG-HAZ simulation treatment, it consisted in a heating/cooling cycle in a salt bath with a peak temperature of 870^{o}C followed by tempering.

Stress-rupture uniaxial results for simulated FG-HAZ taken from LICON and Sandstrom et al. [96] are plotted together with the INTEGRITY small punch FG-HAZ stress-rupture results in Figure 5.28. The INTEGRITY SP data are very much consistent with the uniaxial simulated FG-HAZ data [96] and k_{SP}=1 is needed to correlate the SP data with the uniaxial data.
The LICON simulated FG-HAZ exhibited lower creep strengths, not directly comparable with the INTEGRITY small punch data. This is not so surprising taking into account the difference between the LICON and INTEGRITY base metal stress-rupture results. Moreover, there are inherent difficulties in relying on simulated structures due to the complicated production route.

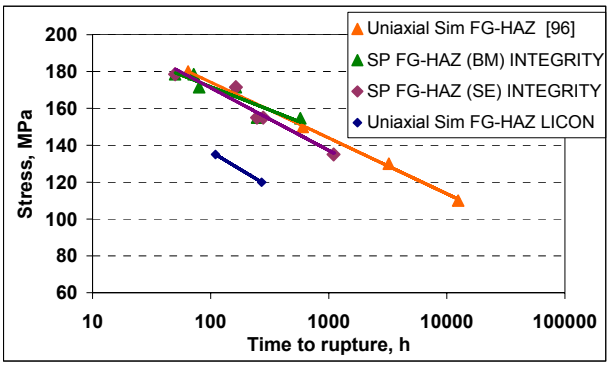

Fig.5.28 Uniaxial and SP stress-rupture results comparison for FG-HAZ

Apparently, only the weld metal data for these two batches are consistent, although only two tests for each batch were conducted.
With regard to the CG-HAZ, stress-rupture results for the uniaxial simulated extra CG-HAZ [96] and the INTEGRITY small punch CG-HAZ are shown in Figure 5.29. Unlike for the FG-HAZ material no correlation can be found between the simulated uniaxial and SP tests. This is not surprising as the simulated CG-HAZ exhibits much higher creep strengths than the simulated FG-HAZ and even the BM materials, as shown in Figure 5.30.

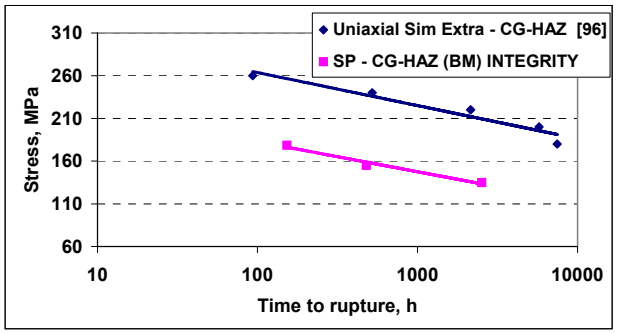

Fig.5.29 Uniaxial and SP stress-rupture results comparison for CG-HAZ

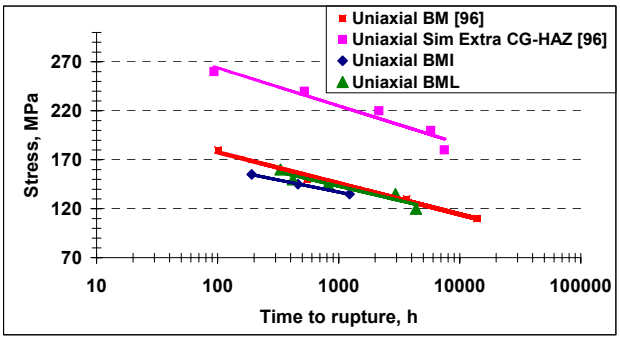

Fig.5.30 Uniaxial stress-rupture results comparison between BM (INTEGRITY, LICON & [96]) and Simulated Extra CG-HAZ [96]

5.2 FE Modeling of SPC test

Numerical simulations by implementing the Norton law into the ABAQUS finite element code were used to predict the deformation of the SP disc during a creep test. Taking advantage of the rotational symmetry of the experimental set-up, a 2D-axisymmetric finite element model was developed (Figure 5.31).

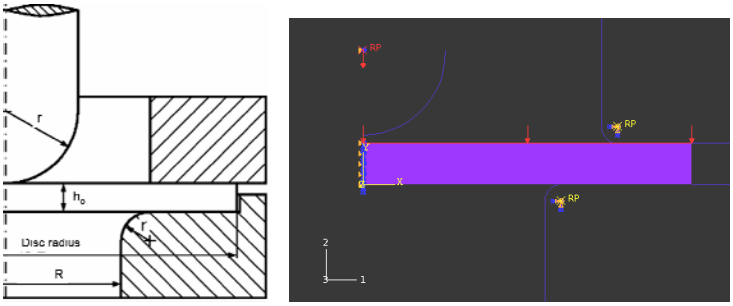

Fig.5.31 Test schematic used for the FE model geometry

The puncher and the dies were implemented as rigid bodies. The disc was modeled with 6000 axisymmetric linear reduced integration elements (CAX4R). This element type was selected since it is the most suitable in analysis that involves large strains and strain gradients as well as in contact interaction problems. The number of elements was enough for the convergence and reconstructed properly the experimental curves. A small force was applied between the upper and lower dies during the deformation, which prevented the specimen to slip away. A friction coefficient of 0.25 applied between the puncher and the disc was found to be the most appropriate to reproduce a deformed shape of the SP disc similar to the real one. The calculations were run by imposing a vertical concentrated force on the puncher.

Finally, a constitutive behaviour had to be assigned to the disc. BMI, SE and WMI materials were considered for the modeling. For the three materials, the elastic properties, which are the Young's modulus E, the Poisson's ratio ν and the yield stress $\sigma_{0.2,}$ defined at 0.2% plastic strain for 600^{o}C, are summarized in the Table 5.3. For the plastic behaviour, the ABAQUS code also requires the plastic behaviour represented by the flow stress,σ, as a function of the plastic strain ε_{pl}, which can be written as:

$$\sigma = \sigma_{0.2} + \sigma_{pl}(\varepsilon_{pl}) \qquad (5.7)$$

The $\sigma_{pl}(\varepsilon_{pl})$ values were derived from the uniaxial tensile behaviour.

Material	E, GPa	ν	$\sigma_{0.2}$, MPa	UTS, MPa
BMI	149.8	0.3	229.0	250.0
SE	149.5	0.3	262.6	281.7
WMI	146.6	0.3	309.5	333.5

Table 5.3 Tensile results for BMI, SE and WMI at 600^{o}C

The INTEGRITY uniaxial creep results (Table 5.1) were used to assign creep properties to the materials: the creep parameters “A & n” for the three modeled materials are determined by power fitting of the data points (Figure 5.18a).
To check whether the model is adequate and working properly, a single constant loading rate test was carried out at 600^{o}C using the available SP testing equipment. The loading was implemented within approximately 65-70 seconds at regular intervals: 50N every 4-5 seconds. The max load was 650N and the load-displacement curve was registered. The same testing conditions were applied in the FE calculations. The FE load-displacement curve is consistent and fits well with the experimental one (Figure 5.32).

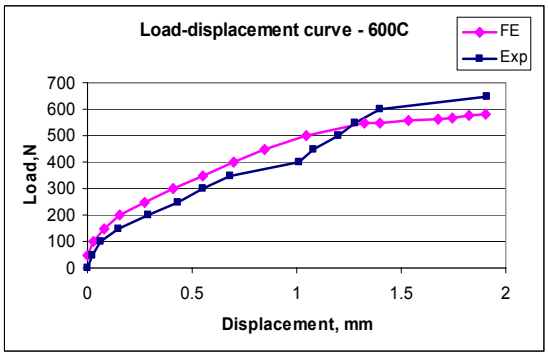

Fig.5.32 Comparison between constant rate test load-displacement (deflection) curves at 600^{o}C – calculated and experimental one

A metallographic cross-section of the tested sample was prepared (Figure 5.33b) and the profile was compared to that predicted by the model (Figure 5.33a).

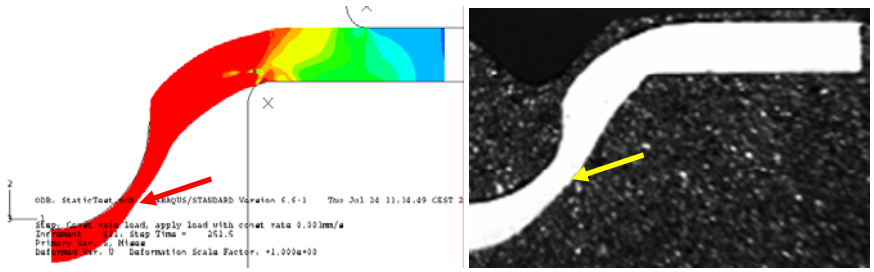

a) *b)*

Fig.5.33 a) Deformed SP disc shape obtained from the FE model after const rate test; b) Optical image of metallographic cross-section of the tested sample

When comparing the FE model with the metallographic cross section it is observed that:

- The deformed shape obtained from the FE model is consistent with the experimental one. The central vertical deflection of the model is identical to that measured in the real creep test;

- Localized necking occurs near the side of the puncher hemisphere, and a circumferential crack initiates at the necking locations (contact boundary), which leads to final fracture.

The evolution of the creep deformation process is presented in the images below (Figure 5.34).

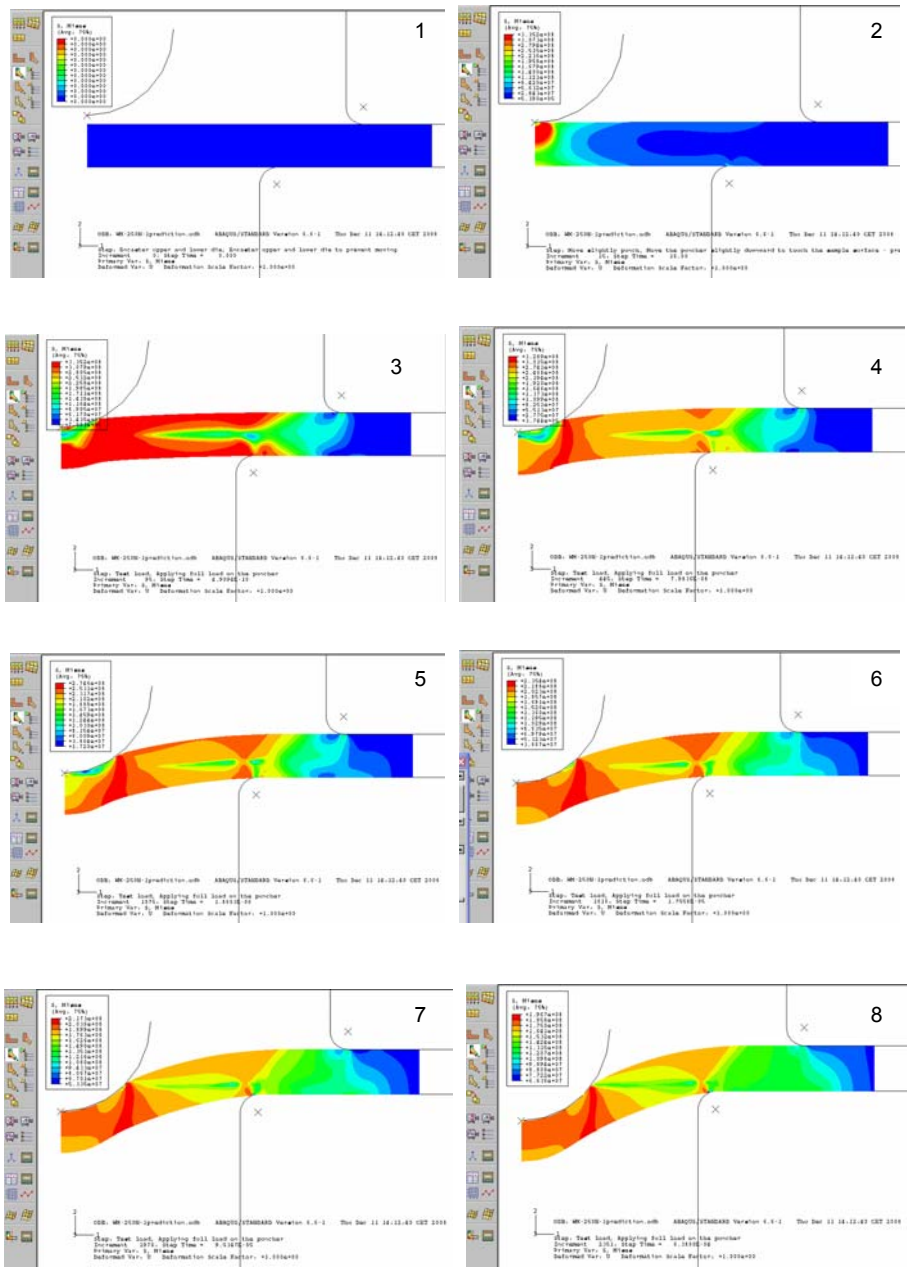

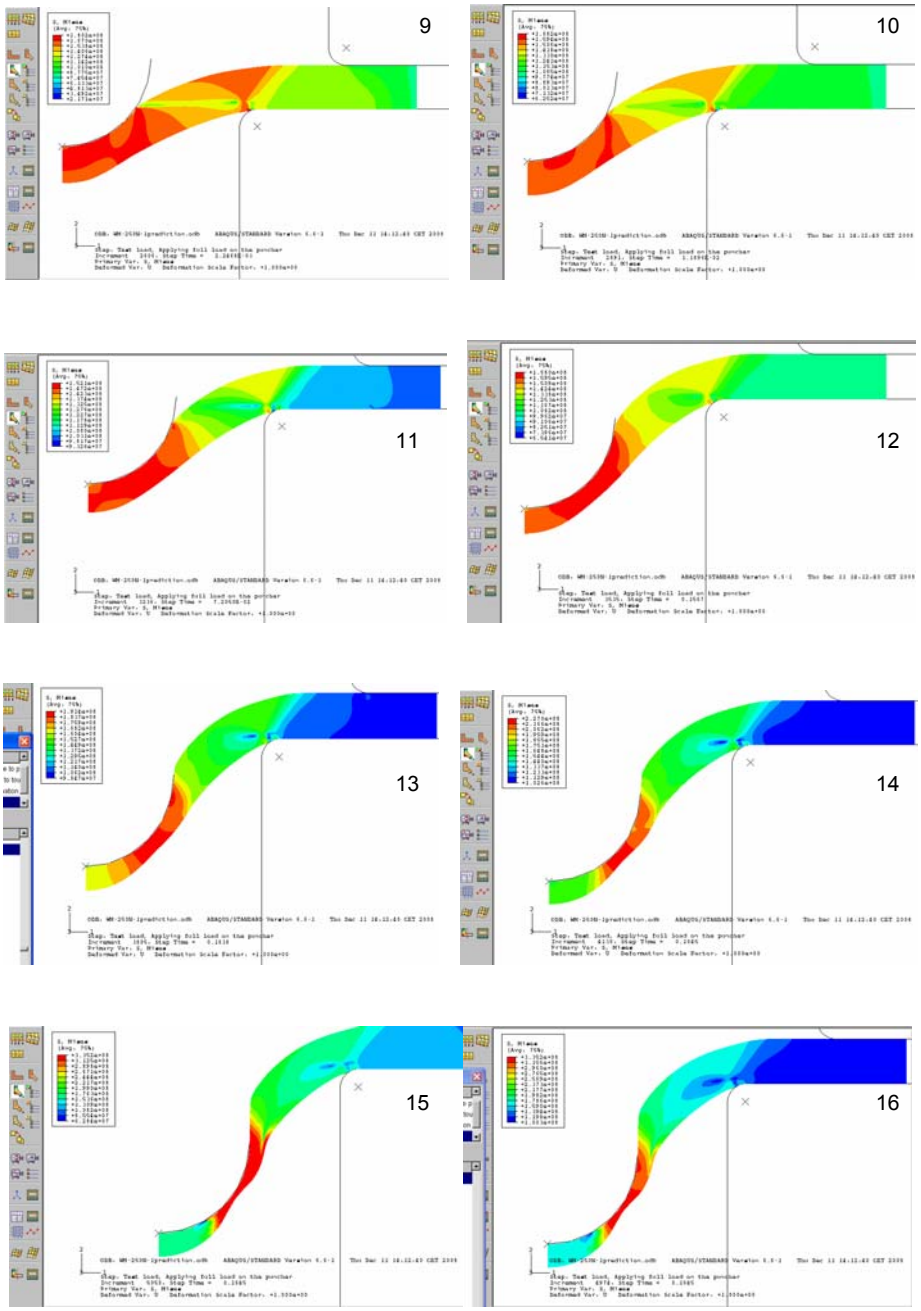

Fig.5.34 Evolution of the creep deformation process during SPC test

There is a difference between the bending and membrane stretching in the contact configuration, when describing the creep deformation process in the SP sample. Bending is a dominant mode of deformation governing the initial plastic deformation and the primary creep region, while the membrane stretching becomes a dominant mode in the secondary and tertiary creep regions. During bending the unsupported area of the sample is stressed and initial localized necking occurs at the contact boundary of the puncher and the disc, but still the thickness is not reduced.

During the membrane stretching mode the contact area is already controlled by reduction in thickness. The rapid increase of the central deflection during the tertiary creep might be due to initial localization of deformation (nucleation and growth of creep cavities) in a small annular region, followed by the initiation of the creep crack (linkup of the creep cavities) and its propagation until the final failure of the sample.

The area beneath the puncher probably contributed little to the results. The annular area where the deformation is localized is what should be compared with uniaxial testing, where deformation is localized within a gauge length of controlled dimensions. However, it should be mentioned here that the stress state of the SP specimens may vary with the deformation process in contrast with uniaxial creep specimens. Thus, detailed stress and strain analyses for SP test are required to demonstrate more quantitative correspondence between the two test methods.

Comparison between calculated and experimental curves for BMI under 250N, SE metal under 260N and WMI under 240N is shown respectively in Figure 5.35 a, b and c. The FE model demonstrates very good prediction in terms of initial deformation (instantaneous elastic deflection + plastic strain + primary creep), as well as, secondary creep deflection rate for BMI (Figure 5.35a). Because of the huge computational memory the model could not be run until the very end.

The precision in predicting secondary creep deflection rate for the service exposed material is acceptable, although not as good as for the BMI. Unfortunately, only two WM uniaxial creep tests results were available for calculating the stress parameters used in the model, and they were, obviously, not enough to obtain a good precision. The predicted secondary deflection rate for the WMI under 240N load (3.49E-03 mm/h) was quite lower than the experimental one (6.54E-03 mm/h), which resulted in much longer predicted lifetimes.

From the comparison between the calculated and experimental results above it could be said that the model needs to be tuned further particularly for the WM when more test data are available as two tests are not sufficient to represent the creep behaviour of a material. Improvements for simulating the tertiary creep stage should be made in order that the model can be used completely independently for creep lifetime predictions. At this stage, the model can be used together with the Monkman-Grant relationship to make approximate predictions for the creep rupture times.

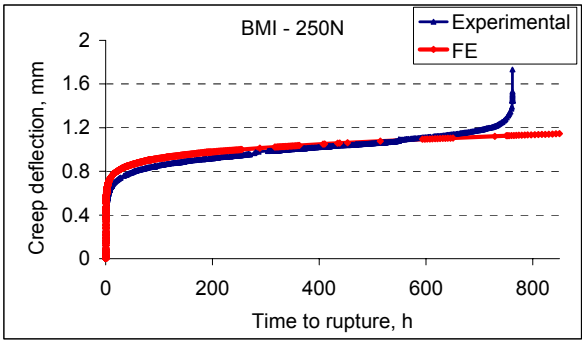

a)

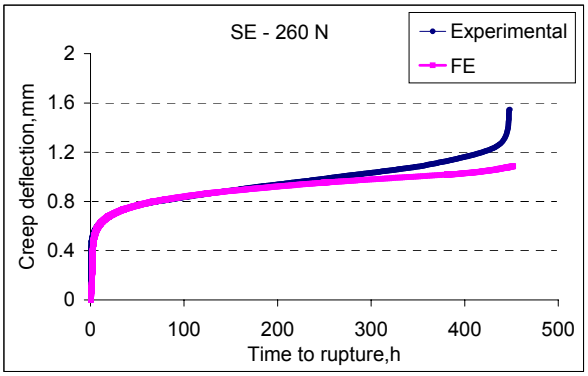

b)

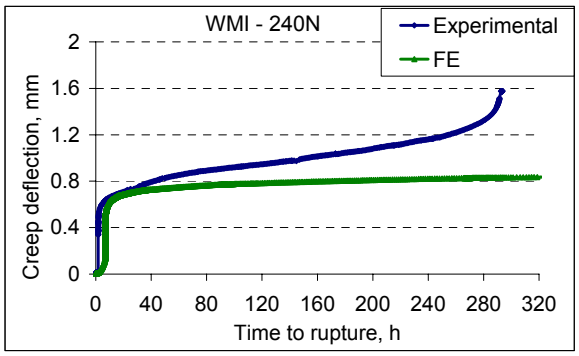

c)

Fig.5.35 Comparison between calculated FE & experimental SPC curves for a) INTEGRITY base; b) Service exposed and c)Weld material

5.3 Small Punch Fracture (SPF) Results

An INSTRON 5586 electromechanical universal testing machine equipped with an environmental chamber to achieve low temperatures was used to produce SP fracture results. In the SPF test the puncher penetrates through the disc at a given constant rate of motion and the force F is measured. During this test, a relationship between the force, F, and the central disc deflection (or puncher displacement) δ is examined. To a certain degree, this test is similar to the conventional stress versus strain test under a constant strain rate. This similarity is apparent from the SP force/load – deflection curve and conventional stress-strain curve, both recorded for P91 BMI at room temperature, illustrated in Figure 5.36.

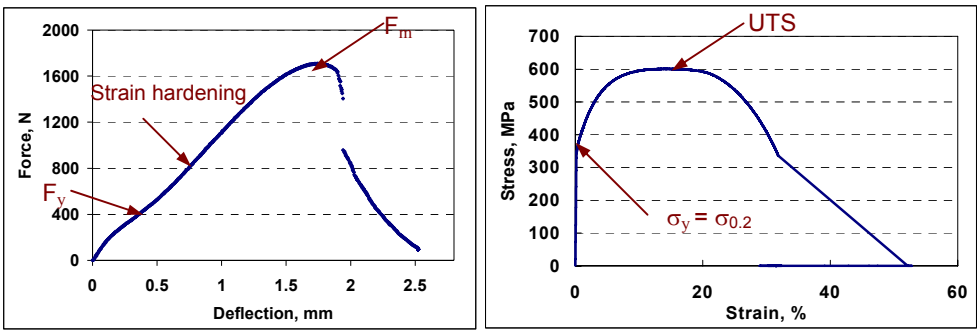

a) *b)*

Fig.5.36 a) SP force-deflection curve and b) Conventional stress-strain curve

From the SP curve several parameters similar to those obtained from conventional stress-strain curves can be evaluated. The early part of the plot is linear and corresponds to the elastic bending of the disc. After a "yield point" F_y corresponding to $\sigma_y = \sigma_{0.2}$, the specific shape of the "strain hardening" appears and, finally, a maximum force F_m corresponding to the "ultimate" tensile strength UTS is reached. Then the force F decreases probably due to accelerated strain of the most highly stressed parts of the disc, unstable crack growth and disc rupture occurs. This is associated, more apparently at room temperature, with a strong decrease ("jump") of the force F.

The SPF test can be divided in different phases, which are marked by the evolution of the load during the test (Figure 5.37):

- Phase 1: Elastic bending in the whole specimen (up to A).

In this phase, the stress-strain state is governed by the Young's modulus with the only exception of the area beneath the puncher where the indentation forces the material to yield. The point A defines the departure from linearity and marks the beginning of the Phase 2, where the deformation is still in bending mode, but in a plastic regime. Unfortunately, at such low loads, the definition offered by the instrumentation was not adequate for determining the exact position of such a point.

- Phase 2: Plastic bending in the whole specimen (from A to B).

In this second phase, the yielding surface is expanding very fast, affecting large portions of the disc, with the stress-strain state governed mainly by the yielding stress of the material and the hardening rate. Later, the deformation mode switches into the membrane mode, which actually increases the capacity of the sample for bearing load.

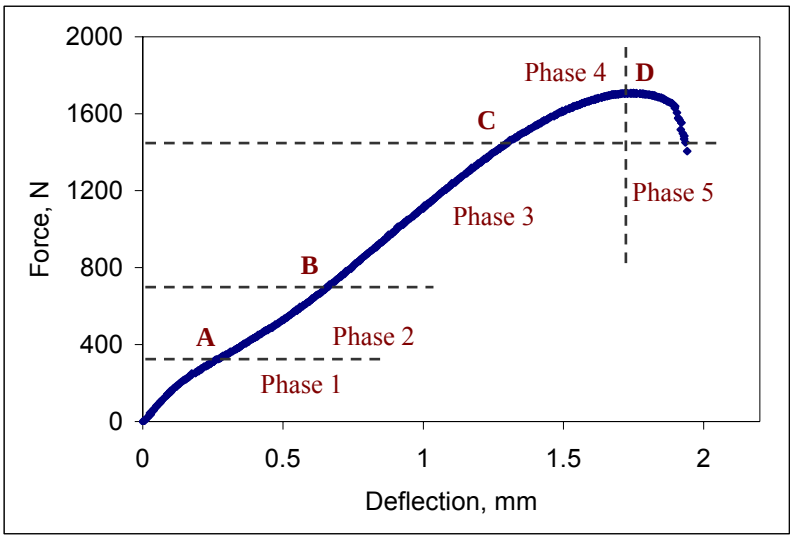

Fig. 5.37 Stress regimes at different stages of the SPF test

- Phase 3: The membrane stress regime occurs in the contact region. All along this region the membrane stress regime is expending together with the contact region (from B to C).

The beginning of the Phase 3 - the starting point B can be easily found at the inflection point of the load curve. The hardening rate is definitely governing this phase although the membrane stress regime is present only in the SP specimen contact region, while the unsupported region is still controlled by the bending stress regime.

- Phase 4: The membrane stress regime start to expand very fast in most part of the sample interesting also the unsupported region (from C to D).

At the point C the membrane stress regime is starting to expand very fast in most parts of the SP specimen, affecting also the unsupported region. This marks the beginning of the Phase 4, where the strain in the material is so high that the capacity for bearing load is decreasing fast, up to the point D which represents the maximum load and the point where the material reaches its plastic instability.

- Phase 5: An annular necking appears and further deformations are concentrated in such area, leading at fractures and at the final failure (from D to fail).

Then necking is appearing and further deformation will be mainly concentrated in the annular area where finally the cracks will start and grow leading to failure.
All SPF experiments were carried out at a deflection rate of 0.003mm/s. Only INTEGRITY material was used for this type of experiment. In total 33 SPF tests were completed for BMI, SE and WMI materials at temperatures ranging from -192^{o}C up to 20^{o}C, following the Code of Practice Part B [2]. Some tests were repeated for a better precision. Unfortunately the HAZ material was insufficient to produce enough samples for the fracture tests. The data registered during the test were: load, time, temperature and displacements. Two LVDTs were employed (left and right – see Figure 4.10), as well as measurements of the crosshead displacement, and these were registered during each test. Force-deflection curves were recorded as an output data of the SPF tests.

Examples of SP force-deflection curves obtained for the BMI together with SEM images, representative for different fracture modes: fully ductile (from -120^{o}C to 20^{o}C), mixed fracture mode with different percentage of the ductile and brittle components and fully brittle (-192^{o}C), are given in Figure 5.38.

Four deformation regimes can be associated with the shape of the force-deflection curves. First, the curve shows an approximately linear initial loading up to about 400N, considered as an elastic bending. Second, a plastic bending regime occurs after an extensive yield zone has developed. Third, after the inflection point located around a deflection of 0.5-0.6 mm (Figure 5.38a), the deformation mode becomes predominantly membrane stretching and finally, near the max load, cracks are expected to develop in the specimen, followed by ductile propagation (in the ductile case) and local strain may also occur as well. The combination of these phenomena results in a decrease in load. In the brittle case the four deformation regimes cannot be so clearly identified from the shape of the test curve. In particular, the inflection point associated with the beginning of the membrane stretching regime has particularly disappeared. Clearly, the difference in the constitutive behaviour plays an important role in the shape of the force-deflection curve.

Scanning Electron Microscope (SEM) images of fractured samples are used to illustrate the microstructural features of the different fracture modes. The metals tend to fail by one of two mechanisms, microvoid coalescence or cleavage. Microvoid coalescence is the more common fracture mechanism where voids form as strain increases, and these voids eventually join together and failure occurs. This is the fracture mechanism characteristic for a ductile material (Figure 5.38 (+20^{o}C)).
Of the two fracture mechanisms, intergranular fracture by cleavage involved far less plastic deformation and hence absorbs far less fracture energy. The cleavage fracture with its characteristic facets is the predominant fracture mechanism observed in brittle materials (Figure 5.38 (-192^{o}C)).

For -150°C the fracture mode is mixed: the fracture surface comprises brittle facets and microvoids on the facets' borders (Figure 5.38 (-150°C)).

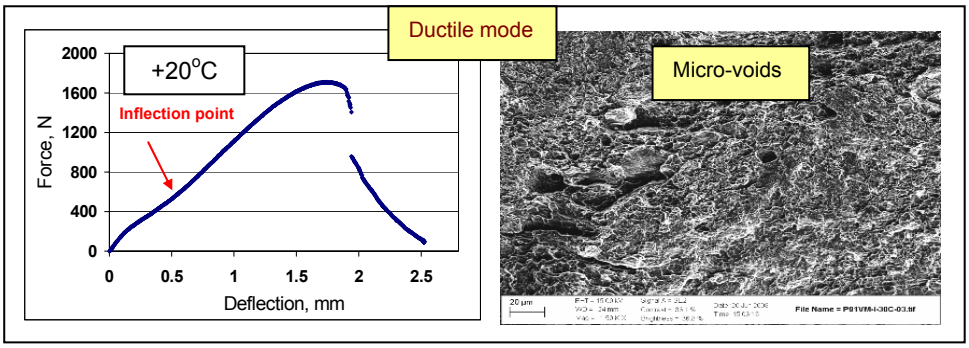

a)

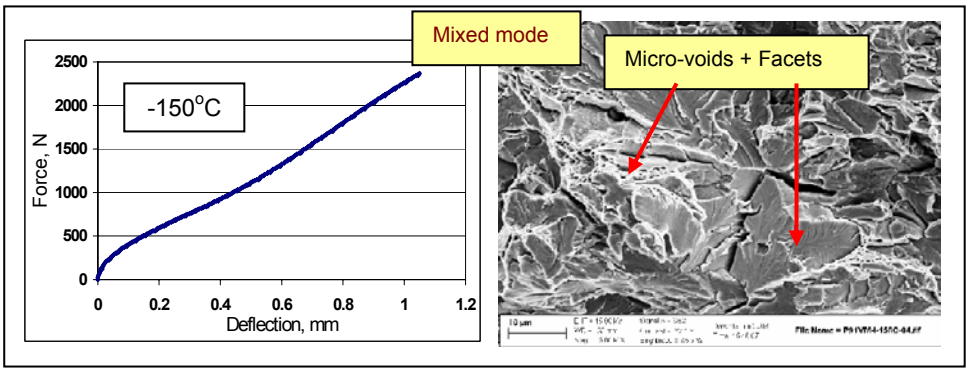

b)

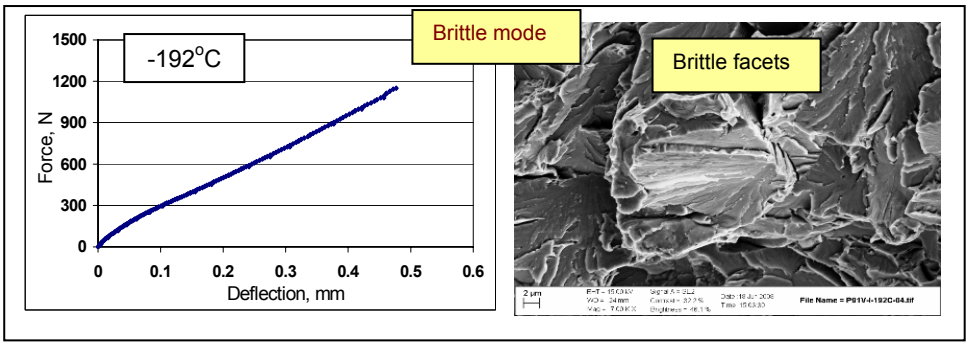

c)

Fig.5.38 SP force-deflection curves characteristic for: a) Ductile; b) Mixed and c) Brittle fracture mode & SEM images of the fracture surfaces

The as-received SP curves were used for fracture properties evaluation: ductile to brittle transition temperature (DBTT) and fracture toughness (J_{IC} and K_{IC}) evaluation following the CoP part B.

5.3.1 Ductile-to-Brittle Transition Temperature (DBTT) evaluation

The evaluation of transition behaviour of ferritic steels is based on the temperature dependence of the fracture energy. The testing method required for DBTT evaluation (measured by FATT – fracture appearance transition temperature, and/or 41J absorbed energy) is the standard Charpy V-notched (CVN) impact testing.

The impact tests are designed to measure the resistance to failure of a material to a sudden applied force. The test measures the impact energy, or the energy absorbed prior to fracture. Impact energy is a measure of the work done to fracture a test specimen. When the striker impacts the specimen, the specimen will absorb energy until it yields. At this point, the specimen will begin to undergo plastic deformation at the notch. The test specimen continues to absorb energy and work hardens at the plastic zone at the notch. When the specimen can absorb no more energy, fracture occurs.

The standard Charpy equipment and specimen design is shown in Figure 5.39a. Charpy test specimens normally measure 55x10x10mm and have a 2mm deep V-shaped notch, with 45° angle and 0.25mm radius along the base.

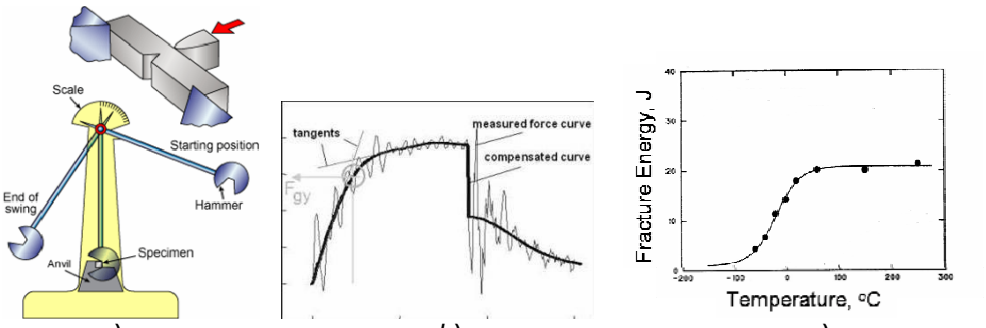

a) b) c)

Fig.5.39 a) Conventional Charpy equipment and CVN specimen; b) Load-displacement curve recorded during Charpy test at a given temperature; c) CVN curve

Load-displacement curves are registered during Charpy test at a given temperature and used for fracture energy calculations, by integrating the area under the curves. Example of such curve characteristic for a ductile fracture is given in Figure 5.39b.

This absorbed energy is a measure of a given material's toughness and acts as a tool to study temperature dependent brittle-ductile transition. Tough materials absorb a lot of energy, whilst brittle materials tend to absorb very little energy prior to fracture.

When the impact (fracture) energy is plotted as a function of temperature the resultant curve will show a rapid dropping off of impact energy as the temperature decreases. If the impact energy drops off very sharply, a transition temperature can

be determined (Figure 5.39c). This is often a good indicator of the minimum recommended service temperature for a material.
Similar transition behaviour with decreasing the test temperature is observed also in the SPF test of disc samples. A series of SPF tests over a wide temperature range is needed to determine the ductile-to-brittle energy transition behaviour (from relatively high upper-shelf energy (USE) to low lower-shelf energy (LSE)) for the material in question.

The SP fracture energy E^{SP} (the energy required for the complete break-down of the disc) is defined by the area under the load punch displacement curve, up to deflection at onset of fracture/failure, which is defined as the punch displacement at 20% load/force drop after max load (Figure 5.40). A series of tests ranging typically from -196°C to 25°C needs to be done to determine T_{SP}. The SP specimen orientation is such that the normal to the punch disc plane is parallel to the Charpy specimen crack propagation direction. T_{SP} is determined as the temperature where E^{SP} has its mean value of the highest and the lowest values in the transition region (Figure 5.41).

The E^{SP} values for all 33 specimens are presented in Table 5.4.

Temp °C	E^{SP} J	h_f mm	ε_f (CoP)	ε_{qf} (Mao)	u_m mm	F_m kN	σ_f^{SP} MPa	J_{Ic} kJ/m^2 (CoP)	J_{Ic} kJ/m^2 (Mao)	K_{IC} MPa m$^{1/2}$
BMI										
21	1.94	0.18	1.02	0.85	1.75	1.71	566	**236**	**189**	-
0	1.93	0.21	0.88	0.85	1.57	1.68	604	**196**	**188**	-
-10	2.15	0.14	1.29	0.88	1.62	1.87	650	**313**	**195**	-
-30	1.97	0.18	1.03	0.85	1.60	1.61	577	**238**	**189**	-
-60	2.25	0.19	0.97	0.89	1.64	2.02	789	**222**	**199**	-
-70	2.03	0.18	1.04	0.85	1.59	2.00	729	**241**	**187**	-
-100	2.26	0.14	1.28	0.76	1.48	2.40	928	**308**	**163**	-
-120	2.34	0.20	0.93	0.84	1.58	2.41	931	**211**	**185**	-
-130	2.13	0.29	0.55	0.79	1.48	2.51	1009	**104**	**170**	-
-130	2.10	0.29	0.56	0.77	1.50	2.56	1000	**106**	**165**	-
-150	1.29	0.32	0.43	0.46	1.09	2.37	911	**72**	**78**	**-**
-158	1.30	0.35	0.37	0.49	1.10	2.37	914	**55**	**87**	**-**
-192	0.63	0.42	0.16	0.45	1.04	1.48	336	-	-	**3.4**
-192	0.74	0.42	0.19	0.45	0.60	1.48	448	-	-	**4.1**
SE										
23	2.02	0.21	0.87	0.86	1.60	1.83	633	**193**	**191**	-
0	2.06	0.18	1.02	0.80	1.53	1.95	693	**235**	**175**	-
-10	2.08	0.18	1.02	0.83	1.56	1.94	691	**236**	**182**	-
-30	2.35	0.20	0.91	0.94	1.70	2.16	803	**204**	**213**	-
-60	2.28	0.20	0.92	0.88	1.63	2.21	827	**208**	**197**	-
-100	1.99	0.21	0.86	0.80	1.52	2.28	868	**192**	**173**	-
-120	1.99	0.32	0.44	0.77	1.49	2.41	935	**74**	**166**	-
-135	1.33	0.32	0.45	0.48	1.09	2.31	879	**76**	**85**	**-**
-158	1.42	0.36	0.33	0.51	1.13	2.44	951	**44**	**92**	**-**
-192	0.88	0.43	0.14	0.46	1.06	1.59	508	-	-	**4.5**
-192	0.82	0.42	0.18	0.35	0.88	1.84	639	-	-	**5.2**
WMI										
23	1.88	0.23	0.78	0.92	1.67	1.83	634	**167**	**207**	-
-100	2.03	0.24	0.76	1.00	1.77	2.20	824	**161**	**230**	-
-158	0.95	0.36	0.34	0.65	1.33	1.51	466	**44**	**132**	**-**
-158	0.64	0.37	0.30	0.31	0.81	1.56	489	**35**	**36**	**-**
-192	0.68	0.48	0.04	0.45	1.03	1.46	439	-	-	**4.0**
-192	0.44	0.43	0.15	0.19	0.59	1.46	439	-	-	**4.0**
-192	0.58	0.43	0.16	0.40	0.96	1.27	338	-	-	**3.4**
-192	0.78	0.48	0.04	0.49	1.10	1.49	455	-	-	**4.1**

Table 5.4 SP fracture test results

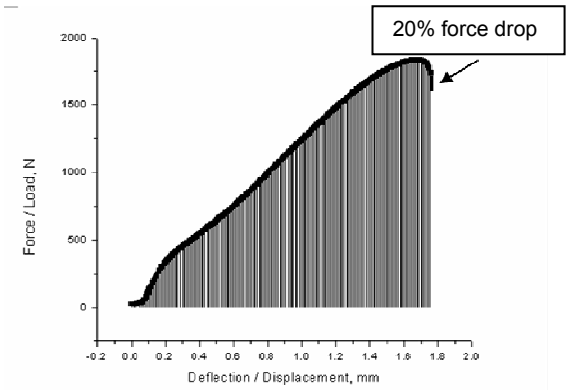

Fig.5.40 Integrating SPF force-deflection curve

The temperature dependence of the fracture energy for INTEGRITY BM from standard Charpy CVN tests has been compared with fracture energy data obtained from the SPF tests for BMI, SE and WMI materials, plotted together on a single graph (Figure 5.41). For a certain temperature the SP fracture energy values shown sudden decrease which is assumed to correspond to ductile-to-brittle behaviour transition. Usually FATT is determined as ½ of this transition region (Figure 5.41).

T_{SP} is correlated with the DBTT obtained by Charpy testing (FATT), where T_{SP} and FATT are expressed in K, using the following equation (CoP Part B):

$$T_{SP}\,(K) = \alpha * FATT_{Charpy}(K) \qquad (5.8)$$

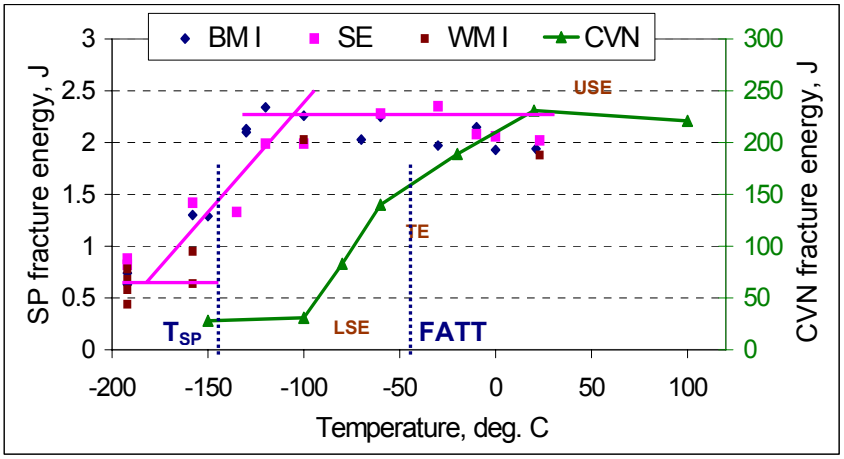

Fig.5.41 Temperature dependence of SP & CVN fracture energy

T_{SP} is found to be around 100°C shifted downward from the DBTT obtained by the Charpy test method. On the one hand, the shift of the DBTT to the lower temperature range is attributed to the lower strain rate involved in the deformation

and rupture of the specimen during the small punch test. Baik et al. [157] studied the strain rate effect in small punch tests on Ni-Cr steels and showed that a hundredfold increase of the displacement rate leads to 20% increase of the DBTT. On the other hand, the size effect is also significant for the transition temperature. Reducing the specimen size from a full-size standard 10x10x55mm to sub-size 3x4x27mm results in a shift of the DBTT towards the lower temperatures with around 50-60^{o}C [235].

A correlating factor α was calculated from the SPF test conducted for the purposes of the thesis and standard Charpy results made available from the Mannesmann Institute, as follows:

$$T_{SP} = 0.6 * FATT_{Charpy} \quad (5.9)$$

For a comparison, confronting T_{SP} with the Charpy FATT on different structural steels, the ratio of $\alpha \approx 0.35$ has been obtained in refs. [180, 232-234].
Because of the significant data scatter due to the miniature specimen scale, it was not possible to distinguish different correlating factors for BMI, WMI and SE materials. Possibly more numerous SPF tests in the transition region need to be completed, emphasizing also the need for test rig calibration after every test, in order to be able to determine more precisely the T_{SP} values for different materials. Modified SP specimen design with 1 mm of thickness and O-ring notch is considered in future to improve the reliability of the SPF results by reproducing more closely the stress concentration and crack propagation observed in a standard Charpy test. Nevertheless, the application of this empirical correlation is very promising for the determination of the FATT of in-service aging components, especially when the material properties in the as-received condition are unknown.

SEM images of base metal SP fractured samples at temperatures -30^{o}C, -158^{o}C and -192^{o}C, corresponding to a ductile fracture mode (upper shelf energy region - USE), mixed fracture mode (transition energy region - TE) and brittle fracture mode (lower shelf energy region - LSE) respectively, are presented in Figure 5.42. The difference in the final specimen shape is obvious – lateral and frontal views of the discs are shown for better visualization. At -30^{o}C the material is very ductile and large plastic deformation occurs before initiation of the circular crack and final breaks of the sample. At -158^{o}C the material has a different percentage of ductile and brittle fracture. A limited plastic deformation occurs before formation of the crack. At -192^{o}C the material becomes completely brittle. The crack starts immediately with applying the loading without any plastic deformation. The main crack is not circular but several radial cracks starts at the contact boundary when the disc is punched.

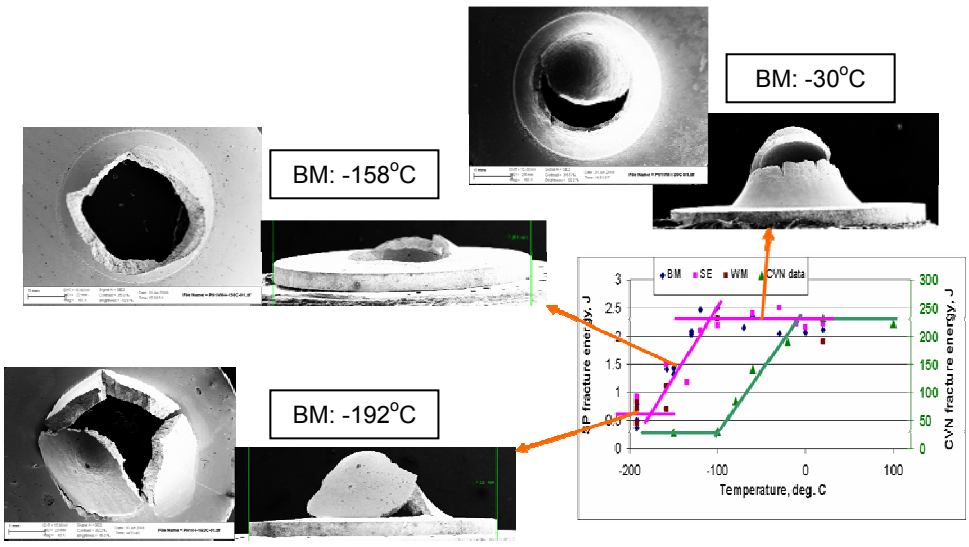

Fig.5.42 SEM images of lateral and frontal views of discs failed at temperatures corresponding to different fracture modes

5.3.2 Fracture toughness J_{IC} and K_{IC} evaluation

The risk of catastrophic rupture of operating components is a function of the tolerable size of flaws or defects, which, in turn, are directly and quantitatively related to the component material fracture toughness K_{IC} (or J_{IC}).
As for the FATT estimations, the significant volume of sample material required for conventional measurements of K_{IC} makes application of the direct testing approach impractical in the case of many in-service components. The SP test in conjunction with the miniature sample removal proposes a good alternative for accurate component- and component location-specific assessments of in-service material degradation.
The early research on the use of a SP mechanical test configuration was initially driven by the demand to assess material mechanical properties from a volume of material small enough to fit into the irradiation test assemblies designed for evaluating the effects of irradiation on material properties [228]. The various aspects of miniature specimen testing, including small punch testing, have been recently reviewed by Lucas [184], to which the reader is referred.

There are three approaches, described in the CoP Part B [2] for material fracture toughness estimations by the SP test. Two of them are material dependent and based on empirical correlations [227, 229, 230]. The third one is based on purely analytical interpretation of the test results. It is material independent and requires no prior knowledge of mechanical material properties.

1) Two-step method of determination of K_{IC}

The first step is to determine the correlation between T_{SP} and FATT as it has already been shown above. Determining the T_{SP} value and knowing the correcting factor for the material in question, the FATT estimation can easily be done using only SP specimens. The second step is using a direct empirical correlation between FATT and K_{IC}.

This method has been well-explored and continues to be applied. However, the following aspects of the approach partially limit its field of applicability:

- The procedure relies on an empirical correlation that is material-dependent; therefore its application is limited to the alloys or class of alloys for which the correlation has been developed.
- The scatter in the correlation can be large enough to make choice of a lower-bound FATT estimate to be potentially excessively conservative. The scatter bound using this method was reported to be about 50% [171, 231]. An example of K_{IC} – FATT empirical correlation for CrMoV steel is presented in Figure 5.43 [233]. Since the empirical K_{IC} – FATT correlation for P91 steel was not found during the literature survey, its implementation for calculating fracture toughness from SP results was not possible.
- Additional conservatism can be introduced into a flaw tolerance-based integrity assessment when estimating fracture toughness, K_{IC}, from a lower bound K_{IC} – FATT correlation. This limitation applies to any and all FATT measurement procedures, including traditional full-size Charpy test methods.

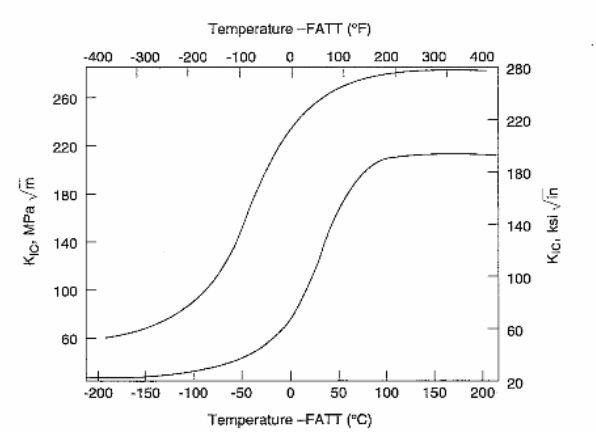

Fig.5.43 K_{IC} – FATT empirical correlation for CrMoV steel [233]

2) EPRI-FAA Innovative approach

In this approach [171, 227] the criterion used for fracture is the strain energy density (strain energy absorbed per unit volume) required to produce crack initiation in a solid un-cracked specimen. This criterion is then applied, as a crack initiation criterion, to the crack tip of a standard specimen loaded via computer simulations.

The procedure used to determine material fracture toughness from a single SP test is as follows:

- Conducting a SP test and recording the load-displacement curve; the sample is monitored for identification of crack initiation;
- Determination of the uniaxial tensile stress-strain constitutive behaviour from the recorded load punch displacement curve by optimal fitting to the punch test data;
- Determination of local strain energy density, corresponding to crack initiation in the small punch test using FE analysis, i.e. fracture criterion;
- FE analysis of cracked compact tension (CT) specimen;
- Estimation of the CT specimen load at the point where crack tip strain energy density reaches critical level (fracture criterion);
- Computation of fracture toughness J_{IC} for compact tension (CT) specimen by handbook.

This approach differs greatly from previous attempts to interpret small punch test data for fracture toughness estimations. It offers the following advantages:

- Unifies the strain- and stress-based fracture criteria by using an energy-based criterion;
- Uses a predominantly analytical-based interpretation of the SP load-displacement curve;
- Uses the critical experimental aspect of identifying the point (temporal and spatial) of fracture initiation during the test.

Applying this approach for the purposes of this thesis was not considered because of time restrictions; developing additional FE models would require more time, whereas the highest priority of this thesis was placed on the analysis of the creep behaviour during SP testing. It is however well worth considering as a continuation of the present work. Another difficulty to apply this method for lower temperature tests comes from the technical impossibility to use the camera lenses at such low temperatures for identification of crack initiation.

3) Empirical, direct correlations from SP to K_{IC}

The empirical direct approach is used in this thesis to estimate the material fracture toughness (K_{IC} and J_{IC}) by SP tests, suggested also in the Code of Practice.
This approach is based either on the measurement or estimation of equivalent fracture strain ε_{qf}, and its correlation with fracture toughness J_{IC} for the ductile case; or the estimation of the small punch fracture stress σ_f^{SP} and its potential correlation with fracture toughness K_{IC} for the brittle case.
The method has been principally proposed by Mao [169, 203, 206] and is based on Bayomi & Bassim's [205] work for ductile behaviour and Takahashi's [203, 226] work for brittle behaviour.

5.3.2.1 Ductile behaviour

- *Mao's criterion*

In the ductile case, which most often applies to Grade P91 steel, the semi-empirical method is based on a linear correlation between J_{IC} and the equivalent (Von Mises) fracture strain ε_{qf}, in a predominantly biaxial stress loading condition:

$$J_{IC} = k\,\varepsilon_{qf} - J_o \qquad (5.10)$$

where k and J_o are empirically determined constants. Mao and Takahashi suggest that k and J_o are invariant, material-independent constants; k =280 and J_o = 50 [206].

J_{IC} is in kJ/m^2 and ε_{qf} is dimensionless and can be approximated by:

$$\varepsilon_{qf} = 0.15\,(u^* / h_o)^{3/2} \qquad (5.11)$$

where u^* is the displacement at fracture. The equivalent fracture strain is averaged throughout the initial specimen thickness h_o.

The critical issue is defining when fracture occurs. A discussion exists as to the use of the maximum peak load or maximum force F_m to determine u^*, or whether fracture starts much earlier. Examples of force-deflection curves for specimens exhibiting macroscopically brittle and ductile behaviour are shown in Figure 5.44. Weld material failed at -192°C was chosen to illustrate the fully brittle case and WM failed at room temperature to show the fully ductile case (see Figure 5.44).

While in the brittle case the crack initiation and the unstable crack growth undoubtedly coincide with the maximum force, in the ductile case, the point of apparent crack initiation is believed to be well before the peak force (Figure 5.44), hence it must be considered as a limiting case. This idea was introduced by Foulds and Viswanathan [227].

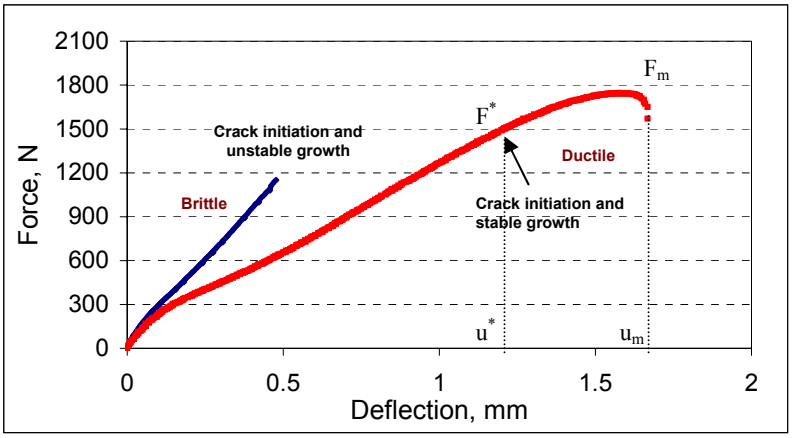

Fig.5.44 SP force-deflection curves for specimens failing in brittle and ductile manner [227]

The constants k and J_o have been determined from test results wherein fracture has been defined to occur at the peak load F_m in the force-deflection curve.

In the thesis calculations, u^* is approximated by the maximum deflection u_m in accordance with the Mao's formula for calculating ε_{qf}. Thus, the biggest deviation in the fracture toughness values will be found for the fully brittle fracture mode. For example, if instead of using u_m in the ductile case shown in Figure 5.44, u^* values are considered, this would give around 45% lower value for J_{IC} according to Mao's criterion, which makes the method non-conservative.

If the fracture strain is greater than 0.25 the material is considered to be ductile, according to Mao et al. [203]. Thus the formula for J_{IC} could be used in the fully ductile and in the mixed fracture case.

- *CoP criterion*

This limitation in the way of fracture strain evaluation is avoided in the Code of Practice Part B [2] by not using the force deflection curves, but the fractured discs geometry. This makes it more precise and reliable when compared with Mao's criterion described above. The effective fracture strain, ε_f, in this case is defined as:

$$\varepsilon_f = \ln (h_o / h_f) \qquad (5.12)$$

where h_o is the original thickness of the test specimen and h_f is the final thickness adjacent to the area of failure. In order to measure this, the specimen has to be sectioned through the position of fracture after the test as can be seen in Figure 5.45.

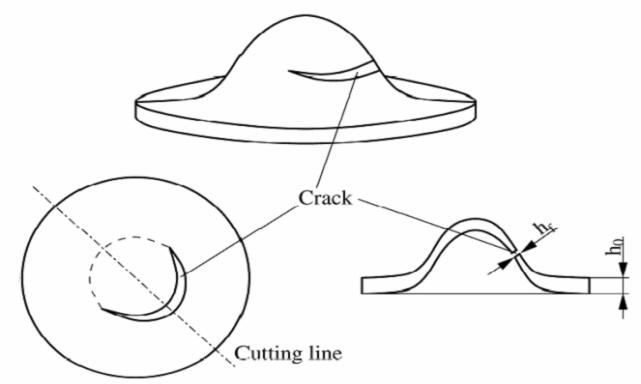

Fig.5.45 (top) schematic drawing of a cracked small punch specimen; (left) top view to the cracked small punch specimen with the line indicated where to cut the Specimen; (right) cross sectional view to the cracked small punch specimen with the positions indicated where to measure h_o and h_f [2]

The fracture toughness values in the ductile case, J_{IC}, calculated using the Code of Practice and Mao's formulas for ε_f and ε_{qf} are given in Table 5.4 above. The J_{IC} values, calculated using the CoP criterion, are generally higher than those received by using Mao's criterion.

5.3.2.2 Brittle behaviour

In the low temperature range, a very limited deformation of the SP sample occurs, and to calculate the fracture stress it is assumed that, the applied stress is entirely transmitted for crack propagation.
In the brittle or predominantly elastic case, the fracture toughness K_{IC} is proposed to be related to the SP fracture stress, σ_f^{SP}, by Mao et al. [203] as follows:

$$K_{IC} = C [\sigma_f^{SP}]^{2/3} \qquad (5.13)$$

σ_f^{SP} is empirically estimated from the maximum load in the SP force-deflection curve (Figure 5.44):

$$\sigma_f^{SP} = 130\,(F_m / h_o^2) - 320 \qquad (5.14)$$

C is an empirically determined constant; C = 0.07 [203].
K_{IC} is in MPa $m^{1/2}$;
F_m is the maximum force/load in kN; and
h_o is the initial specimen thickness in mm.
The same formula for K_{IC} is adopted also in the Code of Practice.
This estimate has meaning when fracture initiation occurs at the maximum load otherwise the maximum force/load based estimation of fracture stress could be approximate. In the more general case, when also some plastic deformation occurs when loading the disc, the maximum load would not coincide with the crack initiation. The crack, i.e. fracture, would start somewhat earlier before the maximum force occurs. Thus, the obtained K_{IC} values would be slightly lower which would represent an error of approximately 10-20%.
However, in the present thesis, this formula was used only to calculate fracture toughness in the fully brittle case at -192°C. Since the force-deflection curves for all materials have the shape shown in Figure 5.44, in this case the maximum force used in the formula for σ_f calculation coincides with the point where the unstable crack starts and propagates immediately causing a sudden burst of the disc.

The calculated K_{IC} (J_{IC}) values using the formulas given above for INTEGRITY BM, WM & SE materials are given above in Table 5.4.

5.3.2.3 Comparing the K_{IC} (J_{IC}) values with literature data

- ***P91 BM***

Only limited reports are available in the literature on J_{IC} characterization of P91 steel. Reported J_{IC} values for P91 base steel are found to be between 180 and 344 kJ/m^2 at ambient temperature for un-irradiated material [203, 221-223], which is consistent with the thesis results.

Results of standard fracture toughness tests of P91 base material (in red) with evaluation according to the Master Curve conception (in blue) are summarized in Figure 5.46 [236].

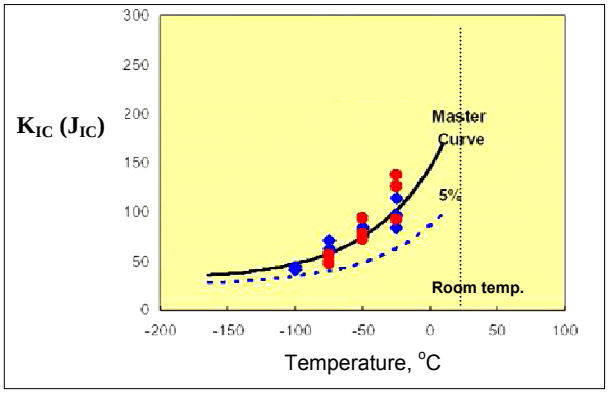

Fig.5.46 Master Curve conception and conventional fracture toughness data of P91 base material [236]

These fracture toughness data, together with CISE conventional results [223] are compared with the J_{IC} and K_{IC} results obtained from the SPF test, using both the Code of practice and Mao's criterion, see Figure 5.47.

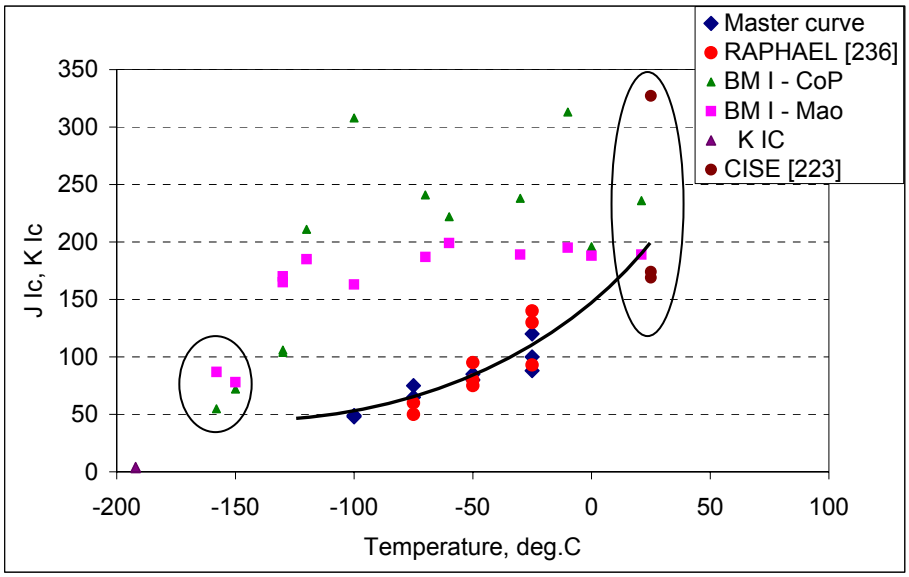

Fig.5.47 Comparison between the P91 fracture toughness Master curve, conventional CT tests [236] and thesis SPF data

Different pattern is noticed in the J_{IC} temperature dependence obtained by SPF tests. A direct correlation might be found for room temperature and temperatures below -150°C. However, for the temperatures in the range from -150°C to +20°C, the obtained values lie quite above the master curve. The CoP criterion gives some higher values for J_{IC}, which makes the method less conservative than the Mao's method. However, the two criteria give comparable values with exception for 2 points, received using CoP criterion. Possible explanation is the subjectivity of the method related to the determination and measurement of h_f.

The possible explanation could be that: because of the low strain rates involved in the SPF tests, the different crack initiation and propagation conditions – no presence of a notch as in the CT conventional specimen, and the particularity of the SP testing – very small discs, presence of a bending stage, biaxial stresses etc, the material behaves in a ductile manner even at very low temperatures, -150°C, as was also apparent when defining the DBTT by SP testing. As was demonstrated from the Charpy data used in the thesis, the same material becomes completely brittle when conventional large samples with a notch are subjected to impact testing. It has been also observed by Foulds et al. [171], that even when the material behaves in a classically brittle fashion, as loaded in a standard Charpy or CT specimen configuration, it often does not behave in a macroscopically brittle manner when loaded in the small punch mode. Indeed, prediction of large-

specimen brittle behaviour can not be made by mere macroscopic indications in the small punch test.
Therefore, in the temperature range where materials behave in a ductile manner, higher fracture toughness values should be also expected than those obtained by testing of large CT samples. Since at room temperature the material behaves as ductile as loaded in Charpy, CT test or SPF, there is also agreement between the fracture values obtained by SP testing and CT testing configuration. An agreement is found also for temperatures lower than -150^{o}C, where even in the SP testing the material is predominantly brittle.

Very limited data are reported in the literature for K_{IC} at very low temperatures, due to also the practical difficulties of reaching cryogenic temperatures. Moreover, the whole assembly (specimen supports, puncher, LVDTs, etc) should sustain these temperatures without deforming. Unfortunately with the modification made in the testing equipment used in this thesis, it was not possible to achieve intermediate temperature levels between -192^{o}C and -158^{o}C.

Toughness values of K_{IC} =32.5 MPa $m^{1/2}$ for 12Cr-1Mo steel and K_{IC} =14.5MPa $m^{1/2}$ for 2.25Cr-1Mo steel, both in as-received condition, obtained by SP testing at very low temperature (-196^{o}C) are reported in [180]. No data for P91 were found for such low temperatures. In this thesis the calculated fracture toughness values, K_{IC}, for BMI at -192^{o}C are 3.4 and 4.1 MPa $m^{1/2}$ even lower than the values reported for 2.25Cr-1Mo steel.

Conventional CT samples should be produced from the SE material and tested in order to compare the results with the SP fracture toughness data. However, the same tendency as for the BMI is expected.

- ***P91 WM***

Fracture toughness values, J_{IC}, of 192, 195 and 208 kJ/m^2 for P91 weld metal at ambient temperature, obtained by CT specimens are reported in [223]. Both SP fracture toughness results using CoP and Mao's criteria are presented. Again as for the BM, the calculated SP fracture toughness values for INTEGRITY weld metal at room temperature agree with the literature findings (Figure 5.48). Applying CoP criterion resulted in lower J_{IC} values. The CT data [223] are closer to the SP facture toughness obtained using Mao's criterion.
No conventional WM fracture toughness data were found at lower temperatures to be compared with the SP results. As for the BMI, the weld metal K_{IC} data obtained by SP testing at -192^{o}C are very low: from 3.4 to 4.1MPa$m^{1/2}$ (Figure 5.48).

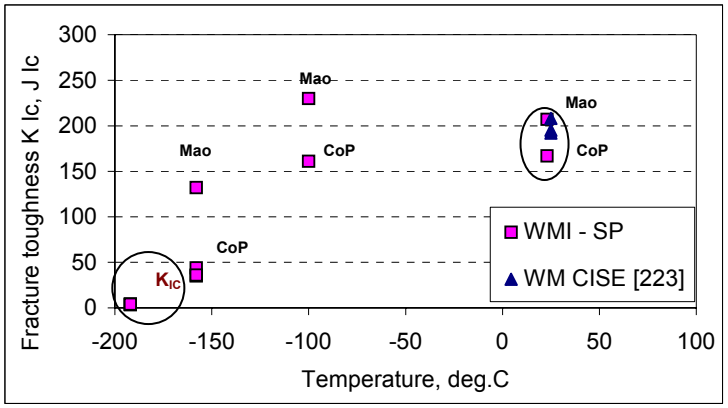

Fig.5.48 Comparison between the P91 WM fracture toughness obtained by SP and conventional CT tests [223]

5.3.2.4 Comparing the SP J_{IC} values for BMI, SE and WMI

- ***CoP criterion***

A comparison between the fracture toughness values of BMI, SE and WMI using the CoP criterion is shown in Figure 5.49. It is difficult to distinguish between BMI and SE results, without curve fitting. This is expected due to the similar properties of these two materials. From the exponential curve fitting it does appear that the SE metal exhibits slightly lower J_{IC} values. From the limited SPF data available for the weld metal it shows the lowest toughness.

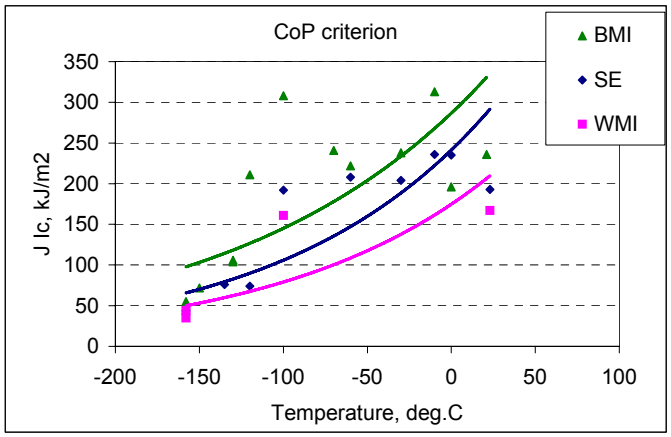

Fig.5.49 Comparison of SP- J_{IC} data of BMI, SE and WMI using CoP criterion

- ***Mao's criterion***

When using the Mao's criterion, the difference between the BMI and SE metal is less obvious. On the other hand, the weld metal, exhibits slightly higher values (Figure 5.50) which is contrary to the results of the previous graph.

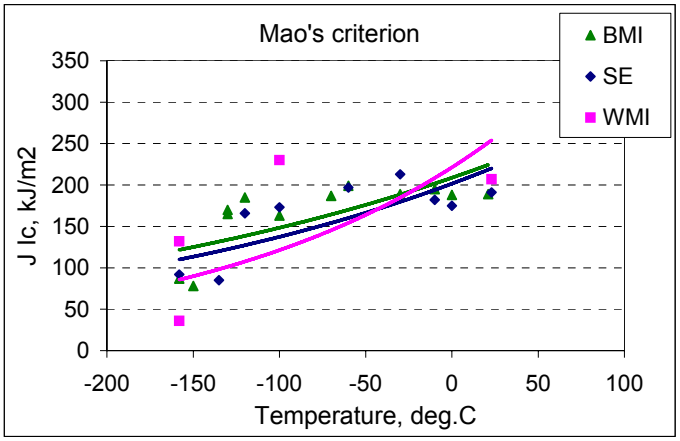

Fig.5.50 Comparison of SP- J_{IC} data of BMI, SE and WMI using Mao's criterion

In conclusion it could be said that the discrepancy in the fracture toughness results in either the ductile or brittle case could be due to difficulties to measure and estimate the fracture strains and stresses and the inherent empiricism in the correlation between these parameters and fracture toughness. Further, the approach excludes consideration of crack initiation, relying on global estimation of strain or stress at the maximum force generally well after initiation in the ductile case (Figure 5.44).

From the results obtained so far, this direct empirical method for fracture toughness evaluation by SPF test indicates some doubts about its applicability over a wide temperature range. However, the estimation of fracture toughness properties from thin discs is an innovative and promising approach. The work of this thesis forms a solid base for further investigations in particular related to the empirical relationships given in the Code of Practice and by Mao. From an experimental point of view it would seem that the technique could be improved by being able to physically detect the crack initiation for precise strain and stress estimation. A further desirable continuation of research on SP fracture testing should consider reproducing similar crack initiation conditions to the conventional test by machining a circular notch on thicker disc specimen configuration. Indeed this approach involving notched specimens would also be interesting in extending the main body of this thesis towards creep crack growth assessment.

6. CONCLUSIONS

From the work performed in this thesis the following conclusions could be drawn:

- The SP test is shown to be a reliable method to depict creep behaviour of alloys. The overall shape of the SP creep curves as a function of applied load is qualitatively similar to that recorded during conventional uniaxial creep tests for the same material and test temperature.

- The shape of the SP creep curves changes as a function of applied load in a manner similar to that in the conventional creep tests with increased creep rates associated with increasing load. Just as for the conventional tests, the rupture lives are found to increase with decreasing load.

- The SP creep results on the base metal (BM) and service exposed (SE) material confirm exactly the trends of the uniaxial creep tests showing the negligible effect of the service exposure and underlining the usefulness of the SP test for non-intrusively investigating creep properties to determine residual life of components.

- The SP test leads to differentiation of creep curves and stress rupture properties for BM, weld and HAZ's. The SP results clearly indicate that the weld metal is weaker than both the BM and SE and the CG HAZ zone behaves similarly to the WM. The FG HAZ is shown to be the weakest component of the weldment.

- A simple linear relationship between the SP load and the equivalent creep stress has been demonstrated, applying the CoP for SP testing. In terms of stress-rupture behaviour there appears to be a good correlation between uniaxial and SP WM tests with the ductility factor k_{SP} from the Code of Practice equal to 1. A similar dependence is found also for the FG-HAZ. Comparing the stress-rupture data of the SP FG-HAZ and simulated uniaxial FG-HAZ obtained by other authors, resulted in a ductility factor k_{SP}=1. Unlike for the FG-HAZ material no correlation can be found between the simulated uniaxial CG-HAZ and the SP tests. The reason for this is thought to be the high creep strength of the simulated CG-HAZ, higher than even the BM strength.

- With regard to the BM and SE metal, from the comparison made between the SP creep (SPC) and uniaxial stress-rupture results acquired for the purposes of the thesis and by other authors over a wide stress interval – from 120MPa to 275MPa, it is obvious that no unique ductility factor should be used to bring the governing creep stresses in the uniaxial and SP test closer together. For the low stress (up to 120MPa) low ductility tests, a k_{SP} =1 works well. Higher is the stress, higher is the ductility factor to be applied to compare directly the results. A linear relationship, based on results received from different material batches, testing temperatures and SP equipment, between the load to be applied in the SP test and the k_{SP} factor is proposed in the thesis.

- The stress dependence of the minimum creep strain rate for uniaxial test has analogical load dependence when compared to the minimum deflection rates found in the SPC tests. As regards the time dependencies of the strain and deflection rates, a discrepancy is observed and no analogical dependence was found.

- A FE model has been developed, based on the Norton creep law, to predict the deformation of the disc during the punch test. It would benefit from being tuned further particularly for the WM when more test data becomes available. Improvements for simulating a tertiary creep stage should be made in order to be used completely independently for creep time predictions. However, the model shows a good prediction in terms of secondary creep strain rate for BM and SE material creep behaviour.

- SP samples have been used to determine the fracture properties: DBTT and K_{IC} (J_{IC}). A similarity between the SP force–deflection curve and the conventional stress-strain curve was demonstrated. A similar temperature dependence of the fracture energy is obtained from SP fracture tests as from the Charpy impact tests. As in the traditional Charpy test for DBTT estimation, the small punch test exhibits a ductile-to-brittle energy transition behaviour associated with an intergranular fracture by cleavage at low temperature and ductile fracture void formations at higher temperatures.
The transition temperature measured by the SP discs, T_{SP}, is found to be around 100^{o}C lower than the FATT due to the very small specimen size and the nature of the SP test. The correlation factor between the DBTT measured by SP test T_{SP} and DBTT measured by Charpy test, expressed in K was found to be:

$$T_{SP} / FATT_{Charpy} = 0.6$$

- An empirical approach was used to calculate the material fracture toughness in the upper-, transition- and lower-shelf regimes taking into account both, CoP and Mao's criteria for the fracture strain determination. From the comparison made with the fracture toughness Master Curve and conventional data reported in the literature is observed that:

In the ductile & mixed fracture case: the SP J_{IC} toughness values received for room temperature and temperatures below -150^{o}C are comparable with those reported in the literature. In these cases the prediction could be judged acceptable, and could be applied for further life assessment calculation. Discrepancy exists for the temperatures in the range from -150^{o}C to +20^{o}C. The SPF values obtained lie quite above the master curve. The CoP criterion gives some higher values for J_{IC}, which makes the method less conservative than when the Mao's criterion is used.

In the brittle case: no conventional data for P91 fracture toughness, K_{IC}, were found for very low temperatures. From the K_{IC} data reported for a similar steel -12Cr, the P91 fracture toughness should be expected to be around 15-20 MPa $m^{1/2}$. The calculated K_{IC} by SPF testing, however, are very low for all the three materials –

BM, WM and SE metal, approximately 3 to 5 MPa $m^{1/2}$, thus indicating some doubt about the applicability of the SP testing for fully brittle materials.
As far as the WM is concerned, the J_{IC} values obtained by SP testing are absolutely comparable with conventional WM fracture toughness results reported in the literature. Unfortunately no lower temperature data were found for comparison.

In summary:

The main objective of the present thesis has been achieved in that the potential of the SP testing for creep properties evaluation for welded P91 materials has been clearly demonstrated, underpinning the case for acceptance in plant component lifetime extension methodologies

As far as fracture properties are concerned, the method works well for DBTT determination. For fracture toughness evaluation in the ductile case, it should be used with some caution and further improved, especially when the material under investigation behaves differently when loaded in the SP test and in the conventional test configuration. The applicability of the SP method at room temperatures was demonstrated for both BM and WM. For fully brittle materials, so far, the SP method is not conclusively demonstrating its potential and requires substantial further development.

REFERENCES

1. Manahan M., Argon A., Harling O, “The development of a miniaturised disk bend test for the determination of post-irradiation mechanical properties”, *Journal of Nuclear Materials*, 103-104, 1981, pp.1545-1550.
2. CEN Workshop Agreement, CWA 15627:2006 E, “Small Punch Test Method for Metallic Materials,” CEN, Brussels Belgium, December 2006.
3. Wyatt D.H. Proc. Phys. Soc. Vol. 66B, 1953, p.459.
4. Herring C., *J. of Appl. Physics*, Vol. 21, 1950, p.437.
5. Wilcox B.A. and Clauer A.H., *Trans. Met. Soc*. AME, Vol. 236, 1966, p.570.
6. Lasalmonie A. and Strudel J.L., *Philosophical Magazine*, Vol. 31, 1975, p.115.
7. Tien J.K., Kier B.H. and Leverant G.R., *Scripta Metalurgica* et Materialia, Vol. 6, 1972, p.135.
8. Lund R.W. and Nix W.D., *Met. Trans. A*, Vol. 6, 1975, p.1329.
9. Rosenhain W. and Ewen D., *J. Inst. Metals*, Vol. 10, 1913, p.119.
10. Jefferies Z., *Science of Metals*, McGraw-Hill, New York, 1924, p.167.
11. Taplin M.F., Ghandi C.and Taplin D.M.R., *Acta Met.*, Vol. 27, 1979, p.699.
12. Hull D. and Rimmer D.E., *Philosophical Magazine*, Vol. 4, 1959, p.673.
13. Speight M.V. and Harris J.E., *Met Sci.,* Vol. 1, 1967, p.83.
14. Raj R. and Ashby M.F., *Acta Met*, Vol. 23, 1975, p.653.
15. Ishida Y. and McLean D., *Met. Sci*, Vol. 1, 1967, p17.
16. Dyson B.F., Met Sci., Vol. 10, 1976, p.10.
17. Beere W. and Speight M.V., *Met Sci*, Vol. 12, 1978, p.172.
18. Wantanabe T., Yamada M., Shinya S. and Karoshima S., *Philosophical Magazine*, Vol. 40A, 1979, p.669.
19. Wantanabe T., Res Mechanica, Vol. 11, 1984, p.47.
20. Dyson B.F., *Met. Sci*., Vol. 10, 1976, p.349.
21. Rice J.R., *Acta Met*., Vol. 29, 1981, p.675.
22. Raj R. and Ghosh A.K., *Met. Trans*., Vol. 12A, 1981, p.1291.
23. Monkman F.C. and Grant N.J., *Proc. ASTM*, Vol. 56, 1956, p.593.
24. Williams K.R. and Wilshire B., *Mat Sci. & Eng*, Vol. 47, 1981, p.151.
25. Cane B.J., *Met. Sci*., Vol. 10, 1976, p.26.
26. Cane B.J., *Met. Sci*., Vol. 13, 1979, p.287.
27. Shin-Ya N. and Keown S.R., *Met. Sci.,* Vol. 15, 1981, p.295.
28. Cane B.J. and Middleton C.J., *Met. Sci*., Vol. 15, 1981, p.295.
29. Tipler H.R and Hopkins B.E., *Met. Sci*., Vol. 10, 1976, p.47.
30. Williams K.R. and Wilshire B., Mat. Sci. & Eng., Vol. 26, 1977, p.289.
31. Williams K.R., Proc. Int. Conf. on 'Creep and Fracture of Engineering Materials and Structures'.
32. Ashby M.F., *Acta. Met*., Vol. 20, 1972, p.887.
33. McLean D., *J. Inst. Met*., Vol. 85, p.486, 1956.
34. Perrin I.J., Fishburn J.D., "A perspective on the design of high temperature boiler components", Creep and fracture in high temperature components – design and life assessment issues, *DEStech Publications Inc*., Lancaster, PA, USA, 2005, pp.46-30.

35. Fujita T..: In: Proceedings of the 3rd Conference on Advances in Material Technology for Fossil Power Plant. Eds.: Wiswanathan, R., Bakker, W. T., Parker, J. D. Swansea, The Institute of Materials 2001, p. 33.
36. Kern T.U. et al. in: Proceedings of the Int. Conference on Materials for Advanced Power Engineering. Eds.: Lecomte-Becker, *J. et al. Forschungszentrum J¨ulich*, 2002, p. 1049.
37. Sturm R., Jenko M., Ule B., "A creep properties evaluation of P91 steel weldments using short term testing", *Materiali in tehnologije*, 36, 2002, p.6.
38. Milicka K. and Dobes F., "Relation between uniaxial and equi-biaxial creep and creep fracture behaviour in P91 steel", *Materials Science Forum*, Vol. 482, 2005, pp.407-410.
39. Sklenicka V., Kucharova K., Svoboda M., Kloc L., Bursik J., Kroupa A.: *Materials Characterization*, 51, 2003, p. 35.
40. Brinkman C.R., Gieseke B.J., Alexander D.J. and Maziasz P.J.,"The Influence of Long-term Thermal Aging on the Microstructure and Mechanical Properties of Modified 9Cr-1Mo Steels", Proc. First International Symposium on Microstructure and Mechanical Properties of Aging Materials, The Minerals, Metals and Material Society, 1993, p. 107.
41. Alexander D.J., Maziasz P.J.and Brinkman C.R., "The Effect of Long-term Aging on the Impact Properties of Modified 9Cr-1Mo steels", ibid, p. 343.
42. KOUKAL J.: "Welding of New Steel P91 for Power Engineering", Zvaranie-Svarovani, 1998, 2.
43. Koukal J. and Schwarz D., "Welding of Steels for Power Engineering", Zvaranie-Svarovani, 1998, 6.
44. Vodarek V.: Physical Metallurgy of Modified (9-12) % Cr Steels, VSB-TU Ostrava, 2003.
45. Masuyama F., Advanced Heat Resistant Steel for Power Generation, eds.
46. Viswanathan R.and Nutting J., The Institute of Materials, London, 1999, 33-48.
47. Viswanathan R.and Bakker W., *J. Mater. Eng. Perf.*, Vol. 10, 2001, pp. 81-95.
48. Viswanathan R.and Bakker W., *J. Mater. Eng. Perf*. Vol. 10, 2001, pp. 96-101.
49. A DOE Newsletter "A modified 9Cr-1Mo Steel shows excellent potential for steam generator applications", DOE/FE-0053/41, Dec. 1982.
50. Sikka V.K., Ward C.T., and Thomas K.C., "Modified 9Cr-1Mo Steel – An Improved Alloy for Steam Generator Application," in Ferritic Steels for High-Temperature Applications, edited by A. K. Khare, American Society for Metals, Metals Park, OH, 1983, pp. 65-84.
51. Middleton C., Metcalfe E., "A review of laboratory Type IV cracking data in high chromium ferritic steels", Paper C386/027, Published in IMechE Proceedings, London, 1990.
52. Brett S.J., Allen D.J. and Pacey J., "Failure of a modified 9Cr header endplate", Proc. Conf. on "Case Histories in Failure Investigation", Milan, Sept. 1999, pp. 873-884.
53. Allen D.J., Brett S.J., "Premature failure of a P91 header endcap weld: minimising the risks of additional failures", Proc. Conf. "Case Histories in Failure Investigation", Milan, Sept. 1999, pp.133 143.

54. Brett S.J., “Identification of weak thick section modified 9Cr forgings in service”, Published in the CD version of the Proceedings of the Swansea Creep Conference; Organised by the University of Swansea and EPRI, and held in Swansea, UK, April 2001.
55. Brett S.J., “The creep strength of weak thick section modified 9Cr forgings”, Published in the Proceedings of Baltica V, Vol. 1, June 2001.
56. Concari S., Merckling G., "Evaluation of Microstructure Evolution and Recommendations for Residual Life Assessment", ECCC Creep Conference, 12-14 September 2005, London.
57. Benvenuti A., Corti S., Ricci N., Bontempi P., “Assessment of material thermal history in elevated temperature components”, Material characterisation Elsevier science 1996.
58. Askins M., Shammas M.S., Silcock J.M., Metallographic examination of 1/2Cr1/2Mo1/4V creep specimens from ERA project 2021 CEGB confidential note 1982.
59. Brear J.M., Bruce S., Cane B.J., Slicock J.M., Summary of calculations of creep curves from coarsening equations CEGB research internal document 1982.
60. Onizawa T., Wakai T., Ando M. and Aoto K., "Effect of V and Nb Contents on Mechanical Properties of High Cr Steel", ECCC Creep Conf., September 2005, London.
61. Hald J., “Creep resistant 9-12% Cr steels - long-term testing, microstructure stability and development potentials”, Elsam/Energy E2/IPL-MPT TU Denmark.
62. Homolova' V., Janovec J., Zahumenskỳ P., Vỳrostkova' A., "Influence of thermal-deformation history on evolution of secondary phase in P91 steel", *Material Science and Engineering* A349, 2003, pp. 306-312.
63. Sklenička V., Kuchařova K., Kudrman J., Svoboda M., Kloc L., "Microstructure stability and creep behaviour of advanced high chromium ferritic steels", *Kovove Mater*., Vol. 43, 2005, pp.20-33.
64. Stabuli M., Giselbrecht K.H., Stief W., Di Gianfrancesco J., Kern A., T. U.: ibid, p. 1065.
65. Abe F., Igarasci M., Wanikawa S., Tabuchi M., Itakagi T., Kimura T., Yamaguchi K., in: Proceedings 3rd EPRI Conference on Advances in Materials Technology for Fossil Power Plants. Swansea, The Institute of Materials 2001, p. 79.
66. Straub S.: Verformungsverhalten und Mikrostruktur warmfester martensitiscer 12%- Chromstähle, VDI Forschungsberichte 5, VDI Verlag, Düsseldorf, 1995, p. 405.
67. Polcik P.: Modellierung des Verformungsverhalten der warmfesten 9-12% Cromstähle in Temperaturbereich von 550-650^{o}C, Shaker Verlag, Aachen, 1999, p. 92.
68. Magnusson H., Sandstrom R., "Dislocation climb of particles at creep conditions in 9-12% Cr steels", Work to be published, Stockholm, Sweden, 2007
69. Eliasson J., Gustafson A., Sandstrom R., "Kinetic modelling of the influence of particles on creep strength", *Key Eng. Mat*., Vol. 171, pp.277-284.
70. Hald J., VGB Power Tech, Vol. 12, 2004, p. 74.
71. Harris J.E., Tucker M.O. and Greenwood G.W., *Met. Sci*., Vol. 8, 1974, p.311.

72. Preston O. and Grant N., *Trans. Met. Soc*. *AIME*, Vol. 221, 1961, p164.
73. Zwalsy K.M. and Grant N.,*Trans. Met. Soc*. *AIME*, Vol. 221, 1961, p.371.
74. Bonis L.J. and Grant N., *Trans Met. Soc AIME*, Vol. 218, 1960, p.877.
75. Ansell G.S. and Weertman J., *Trans. Met. Soc. AIME*, Vol. 215, 1959, p.838.
76. McLean D., *Met. Review*, Vol. 7, 1962, p.481.
77. Claver A.H. and Wilcox B.A., *Met. Sci*. Vol. 1, 1967, p.86.
78. Threadgill P.L. and Wilshire B., Proc. ISI Conf. on "Creep Strength in Steel and High Temperature Alloys", Sheffield 1972, *Met. Soc*., p.8
79. Kushima H., Kimura K., Abe F., "Degradation of mod. 9Cr-1Mo steel during long term creep deformation", Tetsu-to-Hagane, Vol. 85, 1999, pp.841-847.
80. Suzuki K., Kumai S., Kushima H., Kimura K., Abe F., "Heterogeneous recovery and precipitation of Z phase during long term creep deformation of modified 9Cr-1Mo steel", Tetsu-to-Hange, Vol. 86, 2000, pp. 550-557.
81. Endo T., Masuyama F., Park K.S., "Change in hardness substructure during creep of mod. 9Cr-1Mo steel", Tetsu-to-Hange, Vol. 88, 2002, pp. 526-33.
82. Kimura K., Kushima H., Abe F., "Improvement of creep life prediction of high Cr ferritic creep resistant steel by region partitioning method of stress vs. time to rupture diagram", J*. Soc. Mater. Sci*. Jpn., Vol. 52, 2003, pp. 57-62.
83. Bodine G.C., Chakravarti C., Owens C.M., Roberts B.W., Vandergriff D.M., and Ward C.T., A Program for the Development of Advanced Ferritic Alloys for LMFBR Structural Application, ORNL/Sub-4291/1, TR-MCD-015, Oak Ridge National Laboratory, 1977.
84. Wada T., The Continuous Cooling Transformation Diagram and Tempering Response of 9Cr-1Mo-V-Nb Steels, J-4672, Climax Molybdenum Company of Michigan, Ann Arbor, MI, 1981.
85. Strum R., Jenko M., Ule B., "Accelerated test determination of creep properties for 9Cr-1Mo steel weldments at different PWHT conditions", 3rd Hida & Integrity Conference, Oeiras, Portugal 2002 – Integrity of High Temperatures Repair Welds.
86. Witwer M., Cerjak H., and Buchmayr B.: Proc. Int. Conf. on 'High temperature materials for power engineering', Liege, Belgium, Université de Liège, September 1990, pp. 751-760
87. The Ringberg Workshop 1997 on the Application of Computational Thermodynamics, Calphad 24/1, 2000, pp. 15-94.
88. Foret R., Stránský K., Krumpos J., Million B., Pilous V.: Proc.Int. Conf. on 'Integrity of High-Temperature Welds', The Institution of Mechanical Engineers, The Ipswich Book Company, Suffolk, UK, 1998, pp. 135-142.
89. Andersson J.O., Hőglund L., Jőnsson B., Ägren J., in: G. R. Purdy (ed.), Fundamentals and Applications of Ternary Diffusion, Pergamon Press, New York,1990, pp. 153-163.
90. Porter D.A., Easterling K.E.: Phase Transformations in Metals and Alloys, The Thetford Press Ltd. England, 1986.
91. Kirkaldy J.S., Young D.J.: Diffusion in the Condensed State, The Institute of Metals, London, 1985.
92. Pilous V., Stránský K., "Structural Stability of Deposits and Welded Joints in Power Engineering", Cambridge Int. Science Publ., Cambridge, 1998.
93. Purmensky J. et al., "Microstructure and creep rupture strength of welded joints in the steel P91", Proceedings of CREEP 8, Eight International

Conference on Creep and Fatigue at elevated Temperatures, July 22-26 2007, San Antonio, Texas.
94. Allen D.J.: Proc.6th Int. Conf. PARSONS 2003, Engineering Issues in Turbine Machinery, Power Plant and Renewables, Eds.A.Strang et.al., IOM-UK, 2003.
95. Dogan B.: Proc.2nd Int. Conf. Integrity of High Temperature Welds, Ed. Hyde T.H., IOM-UK, 2003.
96. Wu R., Sandstrom R., Seitisleam F., "Influence of extra coarse grains on the creep properties of 9 % CrMoV (P91) steel weldment", *J. of Engineering Materials and Technology*, Vol.126, 2004.
97. Di Gianfrancesco A., "Microstructural stability and creep data assessment of TENARIS grades 91 and 911".
98. Auerkari P. et al., "Data acceptability criteria and data generation: creep data for welds", ECCC Recommendations – Vol.3, Part II [Issue 3].
99. Letofsky E., Cerjak H., "Metallography of 9-12Cr steel power plant weld microstructure".
100. Matsui M., et al., "Degradation of creep strength in welded joint of 9% Cr steel", ISIJ International, Vol. 41, 2001, Supplement, pp.S126-S130.
101. Ceyhan U., Horstmann M. and Dogan B.: Int. Conf. WELDS 2005, “High Temperature Cross-Weld Characterisation of Steel Weldments by MicrotensileTesting”, Geesthacht, Germany, September 2005.
102. Sekhar N.C. and Reed R.C.: 6th ASM Int. – International Trends in welding Research Conference Proceedings, Pine Mountain GA, April 2002.
103. Cam G., Erim S., Yeni C. and Kocak M.: Welding Journal, Vol.78, no.6, 1999, pp.193-201.
104. Vandermeulen W., Snykers M. and Van Ashbroek Ph., “Post irradiation creep properties of cold worked 316 stainless steel as measured with small creep specimens”, Conf. “The use of small scale specimens for testing irradiated specimens”, ASTM STP 888, Ed. W.R.Corwin and G.E.Lucas, ASTM, Philadelphia, USA, 1986, pp. 252-257.
105. Ceyhan U., Horstmann M. and Dogan B., "High Temperature Cross-Weld Characterisation of Steel Weldments by Microtensile Testing", Paper presented at the Int. Conf. WELDS 2005, GKSS Research Centre, Geesthacht, Germany, 8-9 September 2005.
106. Sekhar N.C. and Reed R.C.: 6th ASM Int. – International Trends in welding Research Conference Proceedings, Pine Mountain GA, April 2002.
107. Cam G., Erim S., Yeni C. and Kocak M.: *Welding Journal*, vol.78, no.6, 1999, pp.193-201.
108. Lucon E., Bicego V., D’Angelo D. and Fossati C.: ASTM STP 1204, Philadelphia, PA, 1993.
109. Borggreen K., Storesund J., “Remnant Life Assessment by Use of Miniature Creep Test Specimens”, FORCE - Institut report 95.09.
110. Garzillo A., Guardamagna C., Moscotti L., Ranzani A., “A technique for the residual life assessment of high temperature components based on creep rupture testing on welded miniature specimens”, *Int. J. Pres. Ves.& Piping*, Vol. 66, 1996, pp.223-232.
111. McCarthy P., Brear J.M., "Successful miniature specimen testing: a case study" Proc. fifth Int. Conf. "Creep and Fracture of Engineering Materials and Structures", Swansea, 28 March-2 April 1993, pp. 661-670.

112. Hakl J.H., Vlasak T., Pecha J. and Pech R., "Creep resistance of steel weldments after long term operation", BALTICA IV, Life Management and Maintanance for Power Plants, Vol.2, VTT Symposium 247, 12-14 June,2007.
113. Roebuck B., Brown L., Banks J., Brooks R., Evans M., "Miniaturised testing", NPL Report DEPC-MPE 042, March 2007.
114. Farrell K., Byun T.S., Jones J.W., Gibson L.T., Sitterson R.G., Mashimoto N., Bailey J.L. and Gardner M.J., Small specimen procedures for determination of deformation maps, Conf. “Small Specimen Test Techniques”, ASTM STP 1418, ASTM, Philadelphia, USA, 2002, pp. 283-293.
115. Spigarelli S., Quadrini E., "Analysis of the creep behaviour of modified P91 welds", *Materials and Design*, Vol. 23, 2002, pp. 547-552.
116. Sharpe Jr. W.M., Danley D. and Lavan D.A., “Micro specimen tensile tests of A533B”, Conf. “Small Specimen Test Techniques”, ASTM STP 1329, Ed. Corwin W.R., Rosinski S. and Van Walle E., ASTM, Philadelphia, USA, 1998, pp. 497-512.
117. Kimura A., Suzuki T., Jincho M. and Matsui H., “Dependence of ductile brittle transition behaviour on the size of the Chary specimen and the location of the V notch in the HAZ of welded A533B”, Conf. “Small Specimen Test Techniques”, ASTM STP 1329, Ed. W.R.Corwin, S. Rosinski and E. Van Walle, ASTM, Philadelphia, USA, 1998, pp. 513-522.
118. Marini B., Carassou S., Wident P. and Boulat P., “Evaluation of the fracture toughness of a C-Mn steel using small notched tensile specimens”, Conf. “Small Specimen Test Techniques”, ASTM STP 1329, Ed. W.R.Corwin, S. Rosinski and E. Van Walle, ASTM, Philadelphia, USA, 1998, pp. 513-522.
119. Harling O.K., Lee M., Sohn D-S, Kohse G. and Lau C.W., “The MIT miniaturised disc bend test”, Conf. “The use of small scale specimens for testing irradiated specimens”, ASTM STP 888, Ed. W.R.Corwin and G.E.Lucas, ASTM, Philadelphia, USA, 1986, pp. 50-65.
120. Lucas G.E., Odette G.R. and Sheckward J.W., Conf. “The use of small scale specimens for testing irradiated specimens”, ASTM STP 888, Ed. W.R.Corwin and G.E.Lucas, ASTM, Philadelphia, USA, 1986, pp.112-140.
121. Hamilton M.L., Toloczko M.B. and Lucas G.E., “Miniaturised specimens for testing of irradiated materials”, IEA Int. Symp. Ed. P Jung and H. Ullmaier, Forschungs Zentrum Julich GmbH, 1995, pp. 46-58.
122. Foulds J.R., Wu M., Srivastav S. and Jewett C.W., “Fracture and tensile properties of ASTM cross comparison exercise on A533B steel by small punch testing”, Conf. “Small Specimen Test Techniques”, ASTM STP 1329, Ed. Corwin W.R., Rosinski S. and Van Walle E., ASTM, Philadelphia, USA, 1998, pp. 557-574.
123. Byun T.S., Lee E.H., Hun J.D., Farrell K. and Mansur L.K., “A method to study deformation mechanisms in ion irradiated steels using a bend test technique”, Conf. “Small Specimen Test Techniques”, ASTM STP 1418, Ed. M.A.Sokolov, J.D.Landes and G.E. Lucas, ASTM International, West Conshohocken, Pa., USA, 2002, pp. 267-282.
124. Mao X. and Takahashi H., "Development of further-miniatutized specimen of 3mm diameter for TEM disk small punch tests", *J. of Nuclear Materials*, Vol.150, 1987, pp.42-52.

125. Saucedo-Munoz M.L., "Creep property measurements of service-exposed SUS 316 austenitic stainless steel by the small-punch creep-testing technique", *J. Mater. Res*., Vol.17, no.8, 2002, pp. 1945-1953.
126. Cheon, J.S. and Kim, I.S. "Initial Deformation during Small Punch Testing", Vol.24, no.4, July 1996, pp.255-262
127. Komazai S., Hashida T., Shoji T., Suzuki K., "Development of small punch tests for creep property measurements of Tungsten-alloyed 9% Cr ferritic steels", *Journal of Testing and Evaluation*, JTEVA, Vol.28, no.4, 2000, pp. 249-256.
128. Dedov A., Klevtsov I., Lausmaa T. and Neshumayev D., “Method of small samples for assessment of properties of power plant components: sampling devices and stress concentration in dimples”.
129. Byun T.S., Lee E.H., Hun J.D., Farrell K. and Mansur L.K., "A method to study deformation mechanisms in ion irradiated steels using a bend test technique", Conf. “Small Specimen Test Techniques”, ASTM STP 1418, Ed. Sokolov M.A., Landes J.D. and Lucas G.E., ASTM International, West Conshohocken, Pa., USA, 2002, pp. 267-282.
130. Fong W.L. and Fraser C.R., "Evaluation of ductility of Zircally – 2 materials using an ellipsoidal shaped punch", Conf. “Small Specimen Test Techniques”, ASTM STP 1329, Ed. Corwin W.R., Rosinski S. and Van Walle E., ASTM, Philadelphia, USA, 1998, pp. 602-613.
131. Harling O.K., Lee M., Sohn D-S, Kohse G. and Lau C.W., "The MIT miniaturised disc bend test", Conf. “The use of small scale specimens for testing irradiated specimens”, ASTM STP 888, Ed. Corwin W.R. and Lucas G.E., ASTM, Philadelphia, USA, 1986, pp.50-65.
132. Lucas G.E., Odette G.R., Sokolov M., Spatig P., Yamamoto T. and Jung P., "Recent progress in small specimen test technology", *J. Nucl. Mats*., 307-311, 2002, pp. 1600-1608.
133. Manahan M.F., Browning M.E., Argon A.S. and Harling O.K., “Miniaturised disc bend test technique development and application”, Conf. “The use of small scale specimens for testing irradiated specimens”, ASTM STP 888, Ed. Corwin W.R. and Lucas G.E., ASTM, Philadelphia, USA, 1986, pp.17-49.
134. Mychailo B. et al., "The effect of test machine compliance on the measured shear punch yield stress as predicted using finite element analysis".
135. Osgerby S. and Banks J.P., "Experimental aspects of small punch testing at elevated temperatures", NPL Report DEPC-MPE 029, June 2006.
136. Sargent M.F., and Ashby P.M., Indentation creep, *Mats. Sci. and Technol*., 8 July 1992, pp. 591-601.
137. James C.M., 2002, Impression creep and other localised tests, *Mats. Sci. and Technol.*, A322, pp. 23-42.
138. Hyde T.H. and Sun W., “Short cylinder compression testing and its potential use in representing uniaxial behaviour of materials”, Conf. “Advances in Life Assessment and Optimisation of Fossil Power Plant”, Orlando, Fa., USA, EPRI, Palo Alto, Ca. USA, 2002.
139. Campitelli E.N., Spatig P., Bonade R., Haffelner W. and Victoria M., 2004, “Assessment of constitutive properties from small punch tests: experiment and modelling”, *J. Nucl. Mats*., Vol. 335, pp. 366-378.

140. Parker J., "Life management of creep strengthened ferritic steels in boilers and piping", BALTICA IV, Life Management and Maintanance for Power Plants, vol.1, VTT Symposium 247, 12-14 June, 2007.
141. Komazaki S., Honda T., Nakajima M. and Kohno Y., "Creep damage analysis of 9-12%Cr Ferritic steels by instrumented indentation test", Proceedings of Eighth International Conference on Creep and Fatigue at Elevated Temperatures, July 22-26, 2007, San Antonio Texas.
142. Tabor D., The hardness of metals, Clarendon Press, London, 1951.
143. Shabel B.S., Young R.F., "A new procedure for the rapid determination of yield and tensile strength from hardness tests", In J.F.Bussiere (Ed.), Non-destructive characterization of materials II. Plenum Press, New York, pp. 335-343.
144. Lai M.O., Lim K.B., "On the prediction of tensile properties from hardness tests", *J.Mater.Sci*., Vol.26, 1991, pp. 2031-2036.
145. Fischer-Crips A.C., Introduction to contact mechanics, Mechanical Engineering Series, Springer Verlag, New York, 2000.
146. Beghini M., Bertini L., Fontanari V., "Evaluation of the stress-strain curve of metallic materials by spherical indentation", *International Journal of solids and structures*, 2005.
147. Tipping Ph. and Schindler H.J., "Characterisation of complex weld material variation by instrumented indentation test using Meyer's approach".
148. Johnson K.L., Contact Mechanics, Cambridge University Press, Cambridge, 1985, pp.171-179.
149. Taljat B., Zacharia T., Kosel F., "New analytical procedure to determine stress-strain curve from spherical indentation data", *Int. J. Solids Struct*. 35(33), 1998, pp. 4411-4426.
150. Giannakopoulos A.E., Suresh S., "Determination of elastoplastic properties by instrumented sharp indentation", *Scr.Mater*. 40(10), 1999, pp. 1191-1198.
151. Nayebi A., Bartier O., Mauvoisin G., El Abdi R., "New method to determine the mechanical properties of heat treated steels", *Int. J. Mech. Sci*., Vol. 43, 2001, pp. 2679-2697.
152. Chu S. N. G. and Li J. C. M., Impression creep; a new creep test, *J. Mat. Sci*., Vol.12, 1977, pp.2200-2208.
153. Gibbs W. S., Aikin R. M., Martin P. L. and Patterson R. A., Impression creep characterisation of Ti Al weldments, Proc. 4th Int. Conf. on Creep and Fracture of Engineering Materials and Structures, Swansea, 1990, pp. 227-286.
154. Hyde T. H., Yehia K. A. and Becker A. A., “Interpretation of Impression Creep Data Using a Reference Approach”, *Int. J. Mech. Sci*., Vol. 35, no.6, 1993, pp. 451-462.
155. Hyde T. H., Sun W. and Becker A. A. “Analysis of the impression creep test method using a rectangular indenter for determining the creep properties in welds”, *Int. J. Mech. Sci*., Vol.38, no.10, 1996, pp. 1089-1102.
156. Kameda J. and Buck O., "Evaluation of the ductile to brittle transition temperature shift due to Temper Embrittlement and neutron irradiation by means of small punch test", *Materials Science and Engineering*, Vol. 83, 1986, pp.29-38.
157. Baik J.M., Kameda J., and Buck O., “Development of small punch tests for ductile-brittle transition temperature measurements of temper embrittled Ni-

Cr steels", The use of Small Scale Specimens for Testing Irradiated Materials, ASTM STP 888, W.R.Corwin and G.E.Lucas, Eds., 1986, pp.92-111.
158. Misawa T., Adachi T., Saito M. and Hamaguchi Y., "Small punch test for evaluating ductile-brittle transition behaviour of irradiated ferritic steels", *Journal of Nuclear Materials*, Vol.150, 1987, pp.194-202.
159. Kohse G., Ames M., and Harling O.K., "Progress in developing DBTT determinations from miniature disk bend tests", *Journal of Nuclear Materials*, 141-143, 1986, pp.513-517.
160. Joo Y.H., Hashida T. and Takahashi H., "Determination of ductile-brittle transition temperature (DBTT) in Dynamic small punch test", *Journal of Testing and Evaluation*, Vol.20, no.1, pp.6-14, 1992.
161. Baik J.M., Kameda J., and Buck O., "Small punch test evaluation of inter-granular embrittlement of an alloy steel", *Scr.Metall*., Vol.17, 1983, pp.1443-1447.
162. Baik J.M., Kameda J., and Buck O., "The use of small-scale specimen for testing irradiated materials, ASTM STP 888, edited by W.R.Corwin and G.E.Lucas, *Scripta Metall*. 17, 1983, p.1143.
163. Manahan M.P. et al.,"The development of a miniaturized disk bend test for the determination of postirradiation mechanical properties", *J.of Nucl.Mater*. 103 & 104, 1981, pp.1545-1550.
164. Sugimoto T., Komazaki S. and Misawa T., "Evaluation of DBTT and creep properties of aged main valve casing by using small punch specimens", *Key Engineering Materials*, Vols. 297-300, 2005, pp.1470-1476.
165. Matsushita T., Munoz M., Joo Y.H., Shoji T., "DBTT estimation of ferritic low alloy steels in service plant by means of small punch test", Proceedings of the KSME/JSME Joint conference, Fracture and strength' 90, Korean society of Mechanical Engineers, Seoul, 1990, pp.259-264.
166. Kameda J., Bloomer T.E., Gold C.R., Sugita Y., Ito M. and Sakurai S., "Examination of in-service coating degradation in gas turbine blades using small punch testing method", Material Research Society Symp. Proc. Vol.343, 1996, pp.39-44.
167. Lee W.K., Metzger D.R., Donner A., Lepik O.E., "The use of a small punch test procedure to determine mechanical properties", Small Specimen Test techniques, ASTM STP 1329, W.R.Corwin, S.T.Rosinski, and E.van Walle, 1998.
168. Bulloch J.H., "A review of the ESB small punch test data on various plant components with special emphasis on fractographic details", *Engineering Failure Analysis*, Vol. 9, 2002, pp.511-534.
169. X.Mao, T.Shoji, and H.Takahashi, "Characterisation of fracture behaviour in small punch test by combined recrystalization-etch method and rigid plastic analysis", *Journal of Testing and Evaluation*, Vol.15, no.1, 1987, pp. 30-37.
170. Mao X., Takahashi H., and Kodaira T., "Supersmall punch test to estimate fracture toughness J_{IC} and its application to radiation embrittlement of 2.25Cr-1Mo steel", *Mater.Sci. and Eng*., A150, 1992, pp.231-236.
171. Foulds J.R., Woytowitz P.J., Parnell T.K., Jewett C.W., "Fracture toughness by small punch testing", *Journal of Testing and Evaluation*, Vol.23,1995, pp.3-10.

172. Munoz M., Liu S.C., Komazaki S.I., Kwon I., Hashida T., Takahashi H., Nakajima H., "Evaluation of thermal ageing embrittlement of austenitic stainless steels JN1, JJ1, and JK2 by cryogenic small-punch testing", *J. of Materials Research*, Vol.17, no.4, April 2002, pp.852-860.
173. Munoz M., Liu S.C., Hashida T., Takahashi H., Nakajima H., "Correlationship between JIC and equivalent fracture strain determined by small-punch tests in JN1, JJ1 and JK2 austenitic stainless steels", *Cryogenics*, Vol.41, 2001, pp.713-719.
174. Shindo Y., Yamaguchi Y. and Horiguchi K., "Small punch testing for determining the cryogenic fracture properties of 304 and 316 austenitic stainless steels in a high magnetic field", *Cryogenics,* Vol. 44, 2004, pp. 789-792.
175. Mao X., Shoji T., and Takahashi H., "Characterization of fracture behaviour in small punch test by combined recrystallization–etch method and rigid plastic analysis", *J.Test. Eval.*, Vol.15, 1987, pp.30-37.
176. Komazaki S., Shoji T. and Takamura K., "Evaluation of thermal aging embrittlement in directionally solidified Ni-base superalloy by small punch test", *J. of Engineers Materials and Technology*, Vol.127, 2005, pp.476-482.
177. Abendroth M., Kuna M., "Development of ductile damage and fracture parameters from the small punch test using neural networks", *Eng. Fract. Mech.*, Vol. 73, 2006, pp.710-725.
178. Lee J.S., Kim I.S. and Kimura A., "Application of small punch test to evaluate sigma-phase embrittlement of pressure vessel cladding material", *J.of Nucl.Sci. and Techn*., Vol.40, no.9, 2003, pp.664-671.
179. Misawa T., Nagata S., Aoki N., Ishizaka J. and Hamaguchi Y., "Fracture toughness evaluation of fusion reactor structural steels at low temperatures by small punch tests", *J. of Nucl. Mater*., Vol. 169, 1989, pp.225-232.
180. Fleury E. et al., "Small punch test to estimate the mechanical properties of steels for steam power plant: II. Fracture toughness", Int.Journ. of Pressure Vessels *and Pipings,* Vol. 75, 1998, pp.707-713.
181. Isselin J., Wang S., Komazaki S. and Shoji T., "Development of small punch test for EAC Evaluation", *Key Engineering Materials*, Vols. 297-300, 2005, pp. 980-985.
182. Chakrabarty J., "A theory of strech forming over hemispherical punch heads", *Int.J. mech. Sci. Pergamon Press*, Vol.12, 1970, pp.315-325.
183. Parker J.D. and James J.D., "Creep behaviour of miniature disc specimens of low alloy steel", Development in a Progressing Technology, ASME, PVP – Vol.279, 1994, pp.167-172.
184. Lucas G.E.: "Review of Small Specimen Test Techniques for Irradiation Testing", *Met. Trans*., Vol. 21A, May 1990, s. 1105.
185. Purmenský J.: Review of Small Punch Techniques (Bend Test, Bulge Test and Shear Punch Test) Materials Dep. of University College, Swansea, May 1991
186. Okada A., Yoshie Y., Kojima S., Abe K., Kiritani M.: "The correlation among a variety of miniaturized mechanical tests and their application to D-T neutron irradiated metals", *J. of Nuclear Materials*, Vol. 133-134,1985, p.321.
187. Parker J.D., Stratford G.C., Show N., Metcalfe H., "The application of miniature disc testing for the assessment of creep damage in CrMoV rotor steel".

188. Parker J.D., Stratford G.C., Show N., Spink G. and Tate E., "Deformation and fracture processes in miniature disc tests of CrMoV rotor steel"
189. Ule B., Jenko M., Sturm R., "Accelerated small-punch creep testing", MTAEC9, 38 (ACT) 17, 2003.
190. Yang Z., Wang Z., "Relationship between strain and central deflection in small punch creep specimens", *Int. J. of Pressure Vessels and piping*, Vol.80, 2003, pp.397-404.
191. Ule B. et al., "Small punch test method assessment for the determination of the residual creep life of service exposed components: outcomes from an inter-laboratory exercise", *Nucl. Eng. And Design,* Vol. 192, 1999, pp. 1-11.
192. Dobes F., Milicka K., "On the Monkman-Grant relation for small punch test data", *Mater. Sci. and Engin*., A336, 2002, pp.245-248.
193. Klevtsov I. and Dedov A., "Assessment of ultimate tensile strength and yield strength of power plant steels by means of small punch tests"
194. Leury E., Ha J.S., "Small punch test to estimate the mechanical properties of steels for steam power plant: I. Mechanical strength", *Int.Journ. of Pressure Vessels and Pipings*, Vol.75, 1998, pp.699-706.
195. Campitelli E.N. et.al, "Assessment of the constitutive properties from small ball punch test: experiment and modelling", J.*of Nucl.Mater*., Vol.335, 2004, pp.366-378.
196. Eskner M. and Sandstrom R., "Mechanical property evaluation using the small punch test", *J. of Testing and Evaluation*, Vol.32, no.4, 2004.
197. Shan J., Ling X., Qian Z., "Residual life assessment of in-service high temperature components by small punch creep test", Proceedings of Eighth International Conference on Creep and Fatigue at Elevated Temperatures, 22-26 July 2007, San Antonio Texas.
198. Hurst R., Bicego V. and Foulds J., "Small punch testing for creep – progress in Europe", Proceedings of CREEP8 – Eight International Conference on Creep and Fatigue at Elevated Temperatures, 22-26 July 2007, San Antonio, Texas.
199. Crudeli R., Tettamanti S.: "Small Punch Creep Test: a Promising Methodology for High Temperature Plant Components Life Evaluation", BALTICA IV Plant Maintenance for Managing Life & Performance, Vol. 2, 1998, pp. 501-509.
200. Li Y. and Sturm R., "Determination of Norton creep law and rupture time dependence from small punch test", 3rd International Conference on Integrity of High Temperature Welds, Conference Proceedings ISBN 1-86125-166-1, 24-26 April 2007, London.
201. Milicka K., Dobes F., "Small Punch testing of P91 steel", *International Journal of Pressure Vessels and Piping*, Vol. 83, 2006, pp.625-634.
202. Jang-Bog Ju, Jae-il Jang, Dongil Kwon, "Evaluation of fracture toughness by small-punch testing techniques using sharp notched specimens", *International Journal of Pressure Vessels and Piping*, Vol. 80, 2003, pp.221-228.
203. Mao X., Saito M., Takahashi H., "Small punch test to predict ductile fracture toughness J_{IC} and brittle fracture toughness K_{IC}", *Scripta Metallurgica et Materialia*, Vol.25, 1991, pp.2481-2485.

204. Ritchie R.O., Knott J.F. and Rice J.R., “On the relationship between critical tensile stress and fracture tougness in mild steel”, *J. Mech. Phys. Solids*, Vol.21, 1973, pp.395-410.
205. Bayoumi M.R. and Bassim M.N., “Study on relationship between fracture toughness (J_{IC}) and bulge ductility”, *Int.Journal of Fracture*, Vol.23, 1983, pp.71-79.
206. Mao X., Takahashi H., Kodaira T., “Estimation of mechanical properties of irradiated nuclear pressure vessel steel by use of subsize CT specimen and small punch specimen”, *Scripta Metallurgica et Materialia*, Vol.25, 1991, pp.2487-2490.
207. Li Y., "An analytical Approach for Interpreting Creep Curves from Small Punch Test", Proceedings of the 9th International Conference on Creep & Fracture of Engineering Materials & Structures, University of Wales Swansea, 589-600. Or Proceedings of the 3rd Conference on Advances in Material Technology for Fossil Power Plants, University of Wales Swansea, 2001, pp.473–488.
208. Li Y., Sturm R.: "Small Punch Test for Weld Heat Affected Zones", WELDS 2005 conference, GKSS, September 2005.
209. Dobes F., Milicka K.: "Small Punch Testing in Creep Conditions", *Journal of Testing and Evaluation*, Vol.29, no.1, 2001, pp.31-35.
210. Dobes F. et al.: "Miniaturised Disk-bend Creep Test of Heat Resistant Steels at elevated Temperatures", *Engineering Mechanics*, ISSN 1210-2717, Vol.5, no.3, 1998, pp.157-160.
211. Timoshenko S.: “Strength of Material”, Mc-Graw-Hill, 1957, p.104.
212. Di Persio F., “Small Punch Test for Assessing H_2 Induced Damage in Steel for Pressurized Equipment Operating at High Temperature", PhD thesis, EC, JRC-Institute for Energy, NL 2004.
213. Hurst R., Di Persio F., Stratford G.C., "Small Punch Test for Assessing H_2 Induced Damage in Steel for Pressurized Equipment", High Temperature Plant Integrity & Life Extension, Cambridge University, UK, 14-16 April 2004.
214. Bicego V., Hurst R., Di Persio F., Stratford G.C., "Comparability of Results via the Miniaturised Small Punch Creep Test Method and Traditional Uniaxial Creep Testing", 11th International Conference on Fracture, Turin (Italy), 20-25 March 2005.
215. Maile K. et al., "COPERNICUS – SP Test Method Assessment for the Determination of the Residual Creep Life of Service Exposed Components", Final report, EU Project ERB CIPA CT94 0103, 1998.
216. Mao X., and Takahashi H., “Development of a Further Miniaturized Specimen of 3mm Diameter for TEM Disk Small Punch Tests”, *J. of Nucl. Mat*., Vol. 150, North Holland Publ. Co., 1987, pp 42-52.
217. Auerkari P., Bendick W., Coussement C., Hack R., Holdsworth S., Hurst R., Rantala J. H., "Predicting Long Term Creep Behaviour Using the LICON Methodology", Proc. Third Conf. on Advances in Material Technology for Fossil Power Plants, University of Wales Swansea, April 2001.
218. INTEGRITY Growth Project GRD 1/10886, P91 feature test nr.1: 4PB test under internal pressure and 4PB of the repair-welded P91 pipe with service-exposed and virgin pipes. Final report, JRC, September 2005.

219. Bicego V., Di Persio F., Rantala H., "Small Punch Creep Test Method: Results from a Round Robin Carried out within EPERC TTF5" EPERC Technical Report Nr.2, European Commission, JRC, T.N.P.03.112, 2003.
220. Li Y., Šturm R., “Determination of creep properties from small punch test”, Proceedings of the 2008 ASME Pressure Vessels & Piping Conference, PVP2008, 27-31 July 2008, Chicago, Illinois, USA.
221. Boquest P. et al., “Manufacturing experience of thicker plates for pressure vessels”, Proc. of an ECSC Information day on the Manufacturer and properties of steel 91 for the Power Plant and Process Industries, Germany, Nov.1992.
222. Saikala G., Ray S.K., “Evaluation of quasistatic fracture toughness of a modified 9Cr-1Mo (P91) steel”, *Mater. Science and Eng*., A 479, 2008, pp.105-111.
223. Taylor N., Bicego V., Tettamanti S., “Manuale ingeneristico su P/T91”, rapporto topico CISE-SMS-96-79, 1996.
224. Milicka K. and Dobes F., Steel and Materials for Power Plants. EUROMAT 99 – Vol.7; Eds. P.Neumann et al., FRG 2000, p.372.
225. Milicka K. and Dobes F.: Proc. of Int. Conf. Advanced Metallic Materials. Eds. Jerz J. et al. Inst. Mat. & Machine Mech. SAS, Bratislava 2003, p.202.
226. Saito M. and Takahashi H., Proceedings: 1st Inter. Symp. on Functionally Gradient Material, Sendai, Japan, Functionally Gradient Material Forum, Oct. 1990, p.297.
227. Foulds J.R. and Viswanathan R., ”Nondisruptive material sampling and mechanical testing”, *Journ. of Non-Destructive Evaluation*, Vol.15, nos. 3-4, 1996, pp.151-162.
228. Hamilton M.L. and Huang F.H.,”Use of the disk bend test to assess irradiation performance of structural alloys”, The Use of Small Scale Specimens for Testing Irradiated Material, ASTM STP 888, Corwin W.R. and Lucas G.E., eds. ASTM, Philadelphia, PA, 1986.
229. Foulds J.R. and Viswanathan R., “Accelerated stress rupture testing for creep life prediction – its value and limitations”, *Jouranl of Pressure Vessel Technology*, Vol. 120, 1998, pp.105-115.
230. Stephens R.L., Foulds J.R. and Andrew S.P., S.P.Unpublished data from measurements using SSam-2, Exponent, Inc., California, USA, 2002.
231. Roberts P., Dane I., “Scoop sampling for small punch test method”, Rolls-Royce Naval Marine, Presentation to CEN/WS21- UNI, Milan, Nov 2004.
232. Suzuki M. et al.,” Estimation of toughness degradation by microhardness and small punch test” in Small specimen test techniques applied to nuclear reactor vessel thermal annealing and plant life estimation, ASTM STP 1204, Philadelphia, 1993, pp. 217-227.
233. Foulds J.R. and Viswanathan R., “Small punch testing for determining the material toughness of low alloy steel components in service”, *Journ. of Engineering Mater. and Thecnology*, Vol.116, 1994, pp.457-464.
234. Masushita T. et al., “DBTT estimation of ferritic low alloy steels in service plant by means of small punch test, fracture and strength -1990, Key engineering materials. Trans. Tech. Zurich, Switzerland, Vol.51,1991.
235. Lucon E. et al., “Impact Characterization of Sub-Size Charpy V-Notch Specimens Prepared from Full-Size Certified Reference Charpy V-Notch

Test Pieces", *Journal of ASTM International* (JAI), Vol. 2, Issue 7, July/August 2005.
236. RAPHAEL, Specification of Test Programmes for Vessel Material Features Tests, Project co-funded by the European Commission under the Euratom Research and Training Programme on Nuclear Energy within the Sixth Framework Programme, 2002-2006.